Development of Small Molecule Inhibitors of PDZ Domains

Dissertation zur Erlangung des akademischen Grades des

Doktors der Naturwissenschaften (Dr. rer. nat)

eingereicht im Fachbereich Biologie, Chemie, Pharmazie

der Freien Universität Berlin

Vorgelegt von

Nestor kamdem

Mai 2012

This Ph.D thesis describes the work done between April 2007 and April 2012 at the Leibniz-Institut für Molekulare Pharmakologie (FMP), under the supervision of Prof. Dr. Hartmut Oschkinat

I hereby certify that all the work described in this thesis was done by me, unless specified otherwise in the text. This thesis has not been submitted in whole or in part for my degree or diploma at this or any university

Nestor Kamdem

Berlin, May 2012

Dedicated to my family

1. Reviewer: Prof. Dr. Hartmut Oschkinat
2. Reviewer: Prof. Dr. Rainer Haag

Date of defense: 08.08.2012

Acknowledgements

It is a great pleasure to express my sincere gratitude to the people who supported me during this work at the Leibniz-Institut für Molekulare Pharmakologie (FMP).

I am deeply indebted to **Prof. Dr. Hartmut Oschkinat** who gave me the unique opportunity to work on this interesting project. I also owe him thanks for supervision, guidance and encouragement.

I would like to thank **Prof. Dr. Rainer Haag** for being my second reviewer

Dr. Annette Diehl and coworkers: **Martina Leidert** ; **Bich Thao Nguyen**; **Natalja Erdmann**; **Nils Cremer** and **Kristina Rehbein**. This work would have never been possible without you expressing proteins. Many thanks.

I owe **Dr. Peter Schmieder** and team: **Monika Beerbaum**; **Brigitte Schlegel**. I have learned a lot about NMR because of your devotion to support me.

Dr. Gerd Krause and team: **Dipl. Bioinf. Christian Schillinger** and **Dipl. Bioinf. Annika Kreuchwig**; for modeling, very interesting discussions and guidance.

Dr. Carolyn Vargas for introducing me to this research project and for fruitful discussion about the synthesis

My sincere thanks to **Dr. Yvette Roske** from the MDC who solved the crystal structures of the protein in complex with compounds

I am grateful to **M.sc Liang Fang** from the MDC for performing cell-biological assays

Thank you to **Dr. Michael Lisurek** and **Dr. Bernd Rupp** for being great support with software

Thank you to **Dr. Frank Eisenmenger** and **Mr. Alexander Heyne** for their great support with computer systems

Thank you to **Dr. Jörn Saupe** for fruitful discussions in the course of this work.

Many thanks to **Dr. Trent Franks** and **Dr. Andrew Nieuwkoop** for reading and corrections

Thank you to **Frau. Andrea Steuer** for helping about administration

I would like to thank present and past members of AG Oschkinat, for their support and encouragement while undertaking this work.

I acknowledge the financial support from the German Science Foundation (DFG) within the ”Forschergruppe 806”

I would like to thank many friends who supported me day-to-day

My work is dedicated to my family. Thank you for everything you did for me. Thank you to you mother and to you father.

To my wife Annette kamdem, my daughters Solyne kamdem and Marylove kamdem. To you my son Simo Kamdem.

AF-6 ALL-1	*fused gene from chromosome 6*
AChR	*acetylcholine receptor*
CSP	*chemical shift perturbation*
(ClogP)	*octanol-water partition*
Da	*dalton*
DIL	*dilute domain*
DMSO	*dimethyl sulfoxide*
Dlg	*disc-large tumor suppressor*
Dvl	*dishevelled*
EMT	*epithelial-mesenchynal transition*
FHA	*forkhead-associated domain*
FBDD	*fragment-base drug design*
GST	*glutathione s-transferase*
GSK3ß	*glycogen synthase kinase 3 beta*
HTS	*high-throughput screening*
HSQC	*heteronuclear single quantum correlation*
HMQC	*heteronuclear multiple quantum correlation*
INEPT	*insensitive nuclei enhanced by polarization transfer*
ITC	*isothermal titration calorimetry*
ICAM	*intercellular adhesion molecule*
JAM	*junctional adhesion molecule*
JNK	*c-Jun N-terminal kinases*
LRP	*low density lipoprotein receptor-related proteins*
LFA1	*lymphocyte function-association antigen-1*
LEF	*lymphoid enhancer factor*
MAGI	*membrane-associated guanylate kinase*
NMDA	*N-methyl-D-aspartate*
NMJ	*neuromuscular junctions*
nNOS	*nitric-oxide synthase*
NMR	*nuclear magnetic resonance*
NOE	*nuclear overhauser effect*
PDZ	*PSD-95, Dlg, ZO-1*
PPI	*protein-protein interaction*

PSD	*postsynaptic density*
PTEN	*phosphatase and tensin homolog*
PBM	*pdz-binding motif*
PI3K	*phosphoinositide 3-kinase*
PCP	*planar cell polarity*
Ret9	*receptor tyrosine kinase subtype 9*
RA	*ras-associated*
STD	*saturation transfer difference*
SAM	*steriel alpha motif*
SAR	*structure activity relationship*
SH2	*scr homology 2*
SH3	*scr homology 3*
SAR	*structure activity relationship*
Tiam1	*t-cell lymphoma invasion and metastasis 1*
TRPC1	*transient receptor potential channel 1*
TCF	*t-cell Factor-1*
TROSY	*transverse relaxation-optimised spectroscopy*
TFA	*trifluoro acetic acid*
TLC	*thin layer chromatoography*
UNIPROT	*universal protein resource*
WaterLOGSY	*water-ligand observed via gradient spectroscopy*
ZO	*zona occluden*

Most biological processes depend on finely tuned protein-protein interactions (PPI) that are mediated by small modular protein domains. PDZ (PSD95/Disc large/Zonula occludens-1) domains interact with small mostly C-terminal peptide sequences of interactions partners. PDZ-mediated interactions are implicated in several diseases, including many types of cancers. Therefore, small molecules that block these interactions represent a potential therapeutic approach. In this work, small molecule inhibitors of Dvl PDZ and AF-6 PDZ with an affinity of up to 2.4 µM and 62.2 µM are reported respectively. “Hits” for Shank-3 PDZ and PSD95-2 PDZ are also reported.

Dishevelled (Dvl) proteins are important regulators of the Wnt signaling pathway that is implicated in human cancers. In the Wnt signaling pathway, Dvl PDZ interacts with Frizzled receptors to facilitate the propagation of the Wnt signal leading eventually to turmorigenesis. Small molecules that disrupted interactions between Dvl PDZ and Frizzled are reported in the first part of this work, where a specially designed library of 212 compounds for PDZ was screened against Dvl-3 PDZ by two-dimensional ^{1}H - ^{15}N-HSQC. The first round of screening resulted in the identification of two series of scaffold compounds, the adamantane scaffold and the sulfonamide scaffold. To optimize the binding affinity of the adamantane scaffold, further extensions were designed to facilitate the creation of new interactions with the carboxylate binding loop region of Dvl-3 PDZ. The binding improved from K_D = 190 µM for the initial hit to K_D = 45 µM for compound **11** (2-((1S,3R,5S)-adamantan-1yl)-2-(2-(furan-2-carboxamido)-3-methylbutamid)acetic acid).

A crystal structure of Dvl-3 PDZ in complex with compound **11** was solved. It revealed the importance of the adamantane moiety that points to the hydrophobic pocket of Dvl-3 PDZ.

Compound **19** (4-methyl-2-(5,6,7,8-tetrahydronaphthalene-2- sulfonamido)hexanoic acid) was identified as the best among the tested sulfonamide scaffolds. Modifications to compound **19** resulted in compounds **36** with K_D = 81 µM and **37** with K_D = 84 µM. The x-ray structure of Dvl-3 PDZ in complex with compounds **36** and **37** were solved with a resolution of 1.43 Å for **36** and 1.6 Å for **37**, respectively.

Optimizations were undertaken yielding a new series of compounds. The binding constant of these compounds ranged from 9.4 µM to 59.5 µM. Compounds **61**, **64** and **76** were the best binders for Dvl-3 PDZ and bind more tightly to Dvl-1 PDZ with the binding constants down to 2.4 µM. Competition assays revealed that the most tightly binding compound **61** and the Dpr peptide compete for the same site on the surface of Dvl PDZ domain. Compounds **61**, **64** and **76** inhibit the Wnt signaling pathway as demonstrated by cell based assays.

The second part of the work concerns the AF-6 PDZ domain. The structure of AF-6 PDZ in complex with compound **81** (5-(4-trifluoromethylbenzyl)-2-thioxo-4-thiazoline) resulted in the synthesis of new derivatives with an improved binding constant down to 62.2 µM.

Five other PDZ domains including Shank-3 PDZ, PSD95-1 PDZ, PSD95-2 PDZ PSD95-3 PDZ and α-Syn PDZ were further explored with our library of small molecules created in the course of this work. Compound **101h** was detected as a “hit” scaffold for Shank-3 PDZ and compound **101j** as “hit” scaffold for PSD95-2 PDZ.

Eine Vielzahl biologischer Prozesse ist abhängig von fein abgestimmten Protein-Protein Interaktionen (PPIs), welche durch kleine modulare Proteindomänen vermittelt werden. PDZ (*PSD95/Disc large/Zonula occludens-1*)-Domänen interagieren mit kurzen, meist Carboxy-terminalen (C-terminalen) Peptidsequenzen bestimmter Proteine. PDZ vermittelte Wechselwirkungen sind bei mehreren Krankheiten, einschließlich zahlreicher Krebsarten, beteiligt. Aus diesem Grund stellen kleine Moleküle, die diese Interaktionen verhindern einen potenziellen therapeutischen Ansatz darf. In dieser Arbeit werden niedermolekulare Inhibitoren für die Dvl und AF-6 PDZ-Domänen mit einer Affinität von 2,4 µM beziehungsweise 62,2 µM vorgestellt. Kandidaten für die PDZ-Domänen von Shank-3 sowie PSD95-2 die im verlauf von selektivität untersuchungen gefunden werden, werden ebenfalls diskutiert.

Dishevelled (Dvl) Proteine sind wichtig für die Regulation des Wnt-Signalweges. Dieser Signalweg ist in diversen humanen Krebserkrankungen involviert. Im Wnt-Signalweg interagiert die Dvl PDZ-Domäne mit Frizzled-Rezeptoren um die Übertragung des Wnt-Signals zu ermöglichen. Im ersten Teil dieser Arbeit werden kleine Moleküle vorgestellt, die in der Lage sind, die Interaktion zwischen der Dvl-PDZ-Domäne und dem Frizzled-Rezeptor zu stören. Für die Betrachtung dieses Aspekts wurde eine spezielle Bibliothek mit 212 Verbindungen für PDZ-Domänen konzipiert und die wechselwirkung dieser Substanzen mit der Dvl-3 PDZ-Domäne untersucht. Das erste Screening ermöglichte die Identifizierung von zwei Serien von Verbindungen, die jeweils ein einheitliches Grundgerüst aufweisen, und entweder eine Adamantan- oder Sulfonamid-Gruppe enthalten. Für die Optimierung der Bindungsaffinität der Adamantan-Verbindungen wurde das Grundgerüst so erweitert, dass neue Interaktionen mit der Carboxylatbindungsstelle der Dvl-3 PDZ-Domäne ermöglicht werden. Die Bindungsaffinität der beschriebenen Liganden verbesserte sich von K_D = 190 µM für den ersten Hit auf K_D = 45 µM für die Verbindung **11**(2 - ((1S, 3R, 5S)-Adamantan-1-yl) -2 - (2 - (Furan-2-carboxamido)-3-methylbutamid) essigsäure Für diese Verbindung im Komplex mit der PDZ-Domäne von Dvl-3 wurde eine Kristallstruktur gelöst. Mit Hilfe dieser Kristallstruktur konnte gezeigt werden,

dass die Adamantan-Gruppe die hydrophobe Bindungstasche der Dvl-3 PDZ Domäne ausfüllt.

Aus der Sulfonamid-Serie konnte Verbindung **19** (4-Methyl-2-(5,6,7,8-Tetrahydronaphthalin-2-sulfonamido) Hexansäure) als beste Substanz identifiziert werden. Modifikationen dieser Verbindung führten zu Verbindung **36** mit K_D = 81 µM und **37** mit K_D = 84 µM. Die Kristallstrukturen der Dvl-3 PDZ-Domäne im Komplex mit den Verbindungen **36** beziehungsweise **37**. Optimierungsschritte nahe die zu einer weitere Reihe von Verbindungen Fürhten. Die Bindungskonstanten dieser Verbindungen bewegen sich zwischen 9,4 µM und 59,5 µM. Die Verbindungen **61**, **64** und **74** zeigten die beste Affinität für die Dvl-3 PDZ-Domäne und binden noch stärker an die Dvl-1 PDZ-Domäne mit Bindungskonstanten bis zu 2,4 µM. Kompetitionsassays zeigten, dass die bestbindende Verbindung **61** mit dem Dpr Peptid um dieselbe Bindungsstelle auf der Oberfläche der Dvl PDZ-Domäne konkurriert. Mittels eines zellbasierten Assays konnte gezeigt werden, dass die Verbindungen **61**, **64** und **76** den Wnt-Signalweg inhibieren.

Der zweite Teil der Arbeit beschäftigt sich mit der AF-6 PDZ-Domäne. Die Struktur der AF-6 PDZ Domäne im Komplex mit Verbindung **81** (5 - (4-trifluormethylbenzyl)-2-thioxo-4-Thiazolin) führte zur Synthese neuer Derivate mit verbesserten Bindungskonstanten bis zu 62,2 µM.

Im Zuge dieser Arbeit wurden fünf weitere PDZ-Domänen, darunter Shank-3 PDZ, PSD95-1 PDZ, PSD95-2 PDZ, PSD95-3 PDZ und α-Syntrophin PDZ mit der Bibliothek der niedermolekularen Substanzen untersucht. Dabei konnten die Verbindung an **101h** für die Shank-3 PDZ-Domäne sowie **101j** für die PSD95-2 PDZ-Domäne als gute Kandidaten für weitere Optimierungen ermittelt werden.

Knowledge of protein-protein interactions (PPIs) is important to understand how proteins function in biological systems. In this work, a small molecule approach is initiated to study the function of PDZ domains-mediated PPI. Nuclear magnetic resonance (NMR) techniques are the method used to identify and refine small molecules. This introductory chapter provides general informations about the proteins investigated and the major pathway targeted in this work. Furthermore, the different NMR techniques used in drug discovery are briefly introduced.

1.1 Protein-protein interactions (PPIs)

There is not a class of macromolecular interactions known that rivals the complexity, diversity and regulatory impact of interactions between proteins.[1] Knowledge of PPIs is important to understand how proteins function in biological systems. Muscle contraction, allosteric changes in multimers, structural connection between cells, and signaling between cells are mediated by PPIs.

PPIs can modify the kinetic properties of proteins such as the binding of substrates and catalysis. [2,3] Well known examples are the interaction of succinate thiokinase and α- ketoglutarate dehydrogenase that lowers the K_m for succinyl coenzyme-A by 30-fold.[4] PPIs can allow substrate channelling, and often result in the formation of new binding sites, change of the specificity of a protein for its substrate and also inactivate proteins.[4,5, 6, 7,8]

Often, PPIs are mediated by small protein domains that bind certain classes of peptide sequences. These include WW domains that mediate PPIs through recognition of proline-rich peptide motifs and phosphorilated serine/threonine-proline sites,[9] Scr homology 2 (SH2) domains which bind tighly to phosphorilated tyrosine residues,[10] and Scr homology 3 (SH3) domains which mediate PPIs through recognition of specific proline-rich sequences.[11]

PDZ (PSD95/Disc large/Zonula occludens-1) domains often recognize short amino acid motifs at the C-termini of target proteins.[12,13,14]

Many PPIs influence signal transduction pathways relevant for the progression of cancer. For example, in the Wnt signaling pathway the involved proteins are often mutated in cancer. Dishevelled (Dvl) protein is known to be an essential protein in the Wnt signaling pathway, because it transduces Wnt signals from the membrane

receptor Frizzled to downstream components using its PDZ. Therefore, by blocking the PDZ domain of Dvl with small molecule, Wnt signaling can be inhibited.

PPIs represent a highly populated class of targets for drug discovery.[15] Discovering small molecule drugs that disrupt protein-protein interactions is an enormous challenge.

1.2 Small-molecule inhibitors of protein-protein interactions

Protein-protein interaction interfaces exhibit an overall match between polar residues through a large hydrogen bond network, often mediated by water molecules, and hydrophobic interactions between aromatic and aliphatic patches.[16] Developing small molecules that modulate protein-protein interactions is difficult, owing to issues such as the lack of well-defined binding pockets.[17] The contact surface involved in protein-small molecule interactions are often smaller (~ 300-1000Å^2)[18, 19] compared with those involved in protein-protein interactions (~ 1500-3000Å^2).[16, 20] For example, the complex of ß-catenin with Tcf3 or Tcf4 is characterized by an unusually large binding interface, with a binding constant of Kd ~ 10 nM.[21,22] The inhibition of such interaction with a small organic molecule is a real challenge.

However, Small molecules do not need to cover the entire protein-binding surface, because the subset of interactions that contribute to high-affinity binding is often smaller.[23] These specific interactions are commonly referred to as “hot-spots” which consist of essential residues that hamper the interaction upon mutation. It was shown in the complex between human-growth hormone and the human growth hormone receptor, that a far greater loss in affinity was seen when two tryptophan residues were mutated to alanine as compared to other mutations made in the interface.[24] “Hot-spot” residues are usually found in the centre of the interface and are surrounded by residues that have lesser effect on stability.

Often, it is difficult to find starting points for the design of PPIs inhibitors. Natural small molecules known to bind at protein-protein interfaces are rare, whereas drug-friendly enzymes often have small molecule substrates that can serve as templates for designing antagonists.[25] The first attempts to inhibit protein-protein interactions are often mimics of short peptides.[26] This approach has been successful for discovering inhibitors of protein complex formation in the case of LFA1/ICAM[27], IL-2/IL-2[28] receptor, and P53/MDM2.[29]

Small molecules that target protein-protein interfaces are too large to be drugs. For good bioavailability, most orally active drugs should fulfil key properties defined by Lipinski.[30, 31] These properties, known as “Lipinski rule of 5” are: molecular mass smaller than 500 Da; number of hydrogen-bond donors less than 5; number of hydrogen-bond acceptors less than 10; the calculated octanol-water partition (ClogP) less than 5.

1.3 PDZ Domains

PDZ domains are abundant protein-protein interaction modules of approximately 90 residues found in bacteria, yeast, plants and animals.[32,33,34] PDZ domains were first identified as regions of sequence homology found in diverse signaling proteins. The name PDZ [postsynaptic density 95 (PSD-95), disc large (Dlg), and Zonula occludens 1 (ZO-1)] derives from the first three proteins in which these repeats were identified.[35] PSD-95 is a 95 kDa protein involved in signaling at the post-synaptic density, DLG is the *Drosophila melanogaster* Discs Large protein and ZO-1 which is the zonula occludens-1 protein involved in maintenance of epithelial cell polarity. PDZ domains have also been referred to as Discs large Homology Repeat (DHR) domains or GLGF repeats due to the highly conserved four-residues GLGF sequence within the domain. There are over 440 PDZ domains occurring in more than 260 proteins in the H. *Sapiens* genome,[36] most of them serve as scaffolding functions. PDZ mediated protein-protein interactions are now drawing more attention because of the critical role they play in cell-cell junctions, signaling pathways, and subcellular membrane trafficking.[37,38,39] They are also involved in human congenital diseases and in regulating aspects of cytoarchitecture in mice.[40] They recognize important drug targets, including G protein-coupled receptors (GPCRs) and ion channels.[41, 42]

1.3.1 Structures of PDZ Domains

The PDZ fold consist of six β-strands (βA - βF), flanked by two α - helices (αA- αB).[43] The N- and the C- termini of canonical PDZ domains are in proximity to each other on the opposite side from the peptide-binding groove between the αB-helix and the βB-strand. The peptide binding mechanism is referred to as β-strand addition. In this way, the peptide ligand backbone participates in the extensive hydrogen-bonding

pattern of the such extended β-sheet structure.[44, 45] The conserved Gly-Leu-Gly-Phe (GLGF) sequence of the PDZ domain is found within the βA - βB connecting loop and is important for hydrogen bond coordination of the ligand´s C-terminal carboxylate (COO^-) group.[46] There are approximately 20 PDZ-peptide complex structures determined.[47,48,49] The structure of of the NHERF PDZ 1 domain bound to the QDTRL peptide is shown in Figure 1.1

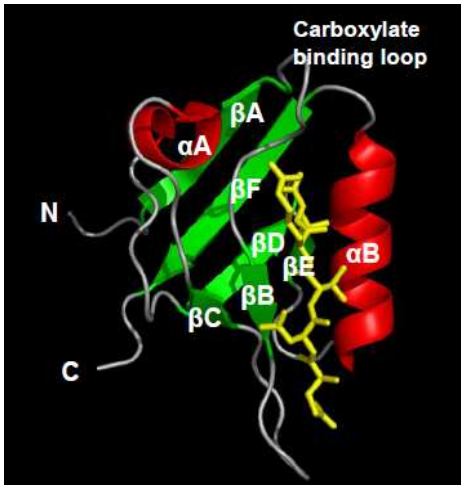

Figure 1.1: Ribbon diagram of the NHERF PDZ1 domain bound to the QDTRL peptide [48]
The strands βA–βF is shown in green, and the helices αA and αB are shown in red. The peptide ligand QDTRL is shown in yellow.

1.3.2 Binding mechanism of PDZ domain

PDZ domains recognize specific C-terminal sequences of PDZ-binding motifs (PBM). In the respective complexes, the C-terminal residue of the ligand is referred to as P_0; subsequent residues towards the N-terminus are termed P_{-1}, P_{-2}, and P_{-3} etc… Previous studies revealed that P_0 and P_{-2} residues are most critical for recognition.[50, 51] PDZ domains are divided into at least three main classes on the basis of their preferences for residues at these two sites: Class I PDZ domains recognize the motif S/T-X-Φ-COOH; (Φ is hydrophobic residue and X any amino acid). Class II PDZ domains recognize the motif Φ -X-Φ-COOH whereas class III PDZ domains recognize the motif X -X-C-COOH. However, there are still a few PDZ domains that do not fall into any of these specific classes. The mechanism of peptide recognition is well described in Figure1.2. In fact, structures of PDZ-peptide

complexes reveal that at the end of the peptide-binding groove is the GLGF loop also termed “carboxylate-binding loop”. In the complex, the ligand terminal carboxylate is coordinated by a network of hydrogen bonds to main-chain amide groups of the GLGF loop, as well as by an ordered water molecule that is coordinated by the side chain of an often conserved arginine/lysine residue.[45]

In the structure shown in Figure 1.2, hydrogen bonds are present between the amide nitrogen of Val (P_0) and the carbonyl of Phe-325, as well as between the carbonyl oxygen of Thr (P_{-2}) and the amide nitrogen of Ile-327. In fact, these main chain interactions with βB are responsible for stabilizing an extended peptide in the binding groove and probably increase the affinity of the interaction.

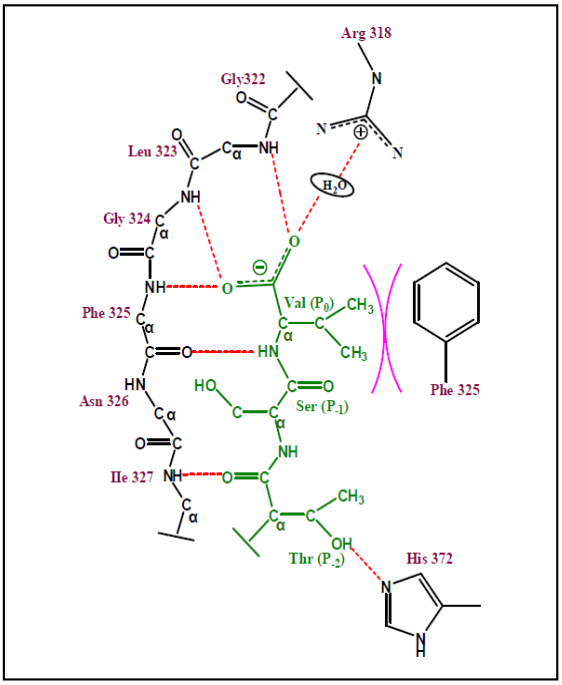

Figure 1.2: Diagram of PSD-95 PDZ domain 3 (residues 306-394) with a bound peptide (NH_2-KQTSV-COOH, shown in green). Adapted from [45, 47] Residues in the PDZ-domain-binding pocket are shown in black; the peptide is shown in green. Hydrogen bonds are drawn as red dotted lines, and hydrophobic packing is indicated by pink arcs.

In the structure of a canonical PDZ-domain as described in section 1.3.1, the loops connecting the βA to the βB sheets and the αB helix with the βF strand retain their flexibility in solution, whereas the rest of the structure is relatively rigid.[52] Due to this flexibility, a movement of βA is facilitated upon insertion of the binding ligand. It was demonstrated that mutations in the carboxylate binding loop region can affect binding

of compounds. The Figure 1.3 indicates the case of interaction between PSD95 and nNOS. The PSD95-2 PDZ which interacts with the PDZ domain of nNOS has a Lys residue at position 318 in the carboxylate-binding loop. The PSD95-1 PDZ and the PSD95-3 PDZ contain an Arg-318.[53] Therefore, the first and the third PDZ domains of PSD95 which do not bind nNOS contain an Arg residue at the position of a Lys in PSD95-2 PDZ which bind nNOS.

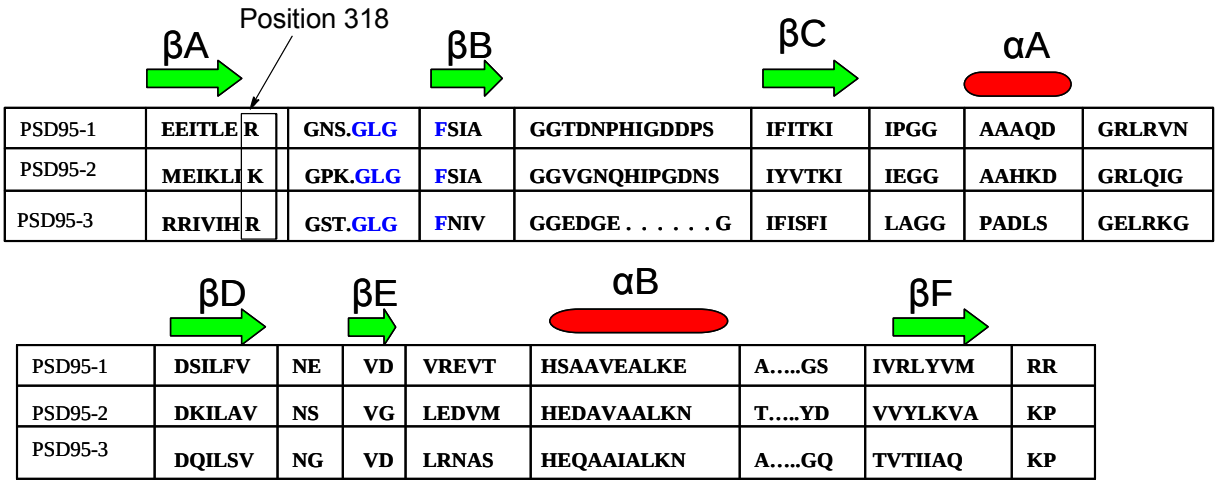

Figure 1.3: Structure based-alignment of the Amino Acid sequences of PSD95-(1,2,3) PDZ domains indicating the carboxylate loop region

The **GLGF** motif can vary quite significantly amongst PDZ as shown in Table 1.1

	PDB code	X- Φ -G-Φ motif
1- ErbinPDZ (Erb-B2)	1MFG	**GLGF**
2- GRIP1PDZ6	1N7F	**PLGI**
3- AF6PDZ	2AIN	**GMGL**
4- MAGI-1PDZ1	2I04	**GFGF**
5- ZO-1PDZ1	2H2B	**GFGI**
6- NHERF-2 PDZ	2HE4	**GYGF**
7- Par-6 PDZ	1RZX	**PLGF**
8- Tamalin PDZ	2EGK	**TFGF**
9- PSD95-PDZ1	1RGR	**GLGF**
10-SYNTROPHIN PDZ	2PDZ	**GLGI**

Table 1.1: Residues of GLGF loop of some PDZ domain [54]

In canonical PDZ domains, the replacement of the first glycine residue by some other residue like serine, threonine or phenylanine has been observed. The hydrophobic residues in the second and the fourth position of the motif are, in general constituted of residues like valine, isoleucine, leucine or phenylanine.

The hydrophobic binding pocket of canonical PDZ domains is created by the side chain of these residues. The variation of the **GLGF** loop contributes to the specificity of PDZ domains.

1.3.3 Dimerization of PDZ domains

Dimerization is another mode of PDZ-PDZ interaction involving recognition of internal motifs. Shank-1 PDZ and GRIP-1 PDZ 6 form a homodimer via the conserved βB/βC loop and N-terminal βA strands, with an antiparallel orientation between the βA strands of the proteins.[55,56] However, the formation of this kind of PDZ dimer does not affect the peptide-binding sites of both PDZ domains.

Another novel dimerization mode of PDZ domains was reported previously in NMR and X-ray crystallographic studies.[54,57,58,59,60] It was shown that PDZ2 of ZO protein forms a dimer through an extensive domain swap invloving *β*- strands. The N- and the C-termini of ZO-1-PDZ2 are not close to each other.

In this arrangement, the canonical peptide-binding groove remains intact in both subunits of the PDZ2 dimer and is created by elements contributed from both monomers.

1.3.4 Interaction with internal motifs of target proteins

Some PDZ domains can also bind to internal sequences of target proteins. A well-characterized example is the PDZ domain of neuronal nitric oxide synthase (nNOS), the neuron- and muscle-specific isoform of the enzyme that produces the second messenger nitric oxide (NO). The PDZ domain of nNOS specifically heterodimerizes with PDZ domains from PSD95 and syntrophin in neuron and muscle cells respectively. [60, 61]

1.3.5 PDZ domains involved in the regulation of cancer relevant pathways

PDZ domains play a crucial role in different pathways including EMT (Epithelial-Mesenchymal Transition) and Wnt. It is well known that abnormal activation of these pathways lead to many diseases including different types of cancer.

Some examples of the PDZ domains interactions with the PBM can be clearly observed in the regulation of EMT and Wnt pathways as shown in Figure 1.4.

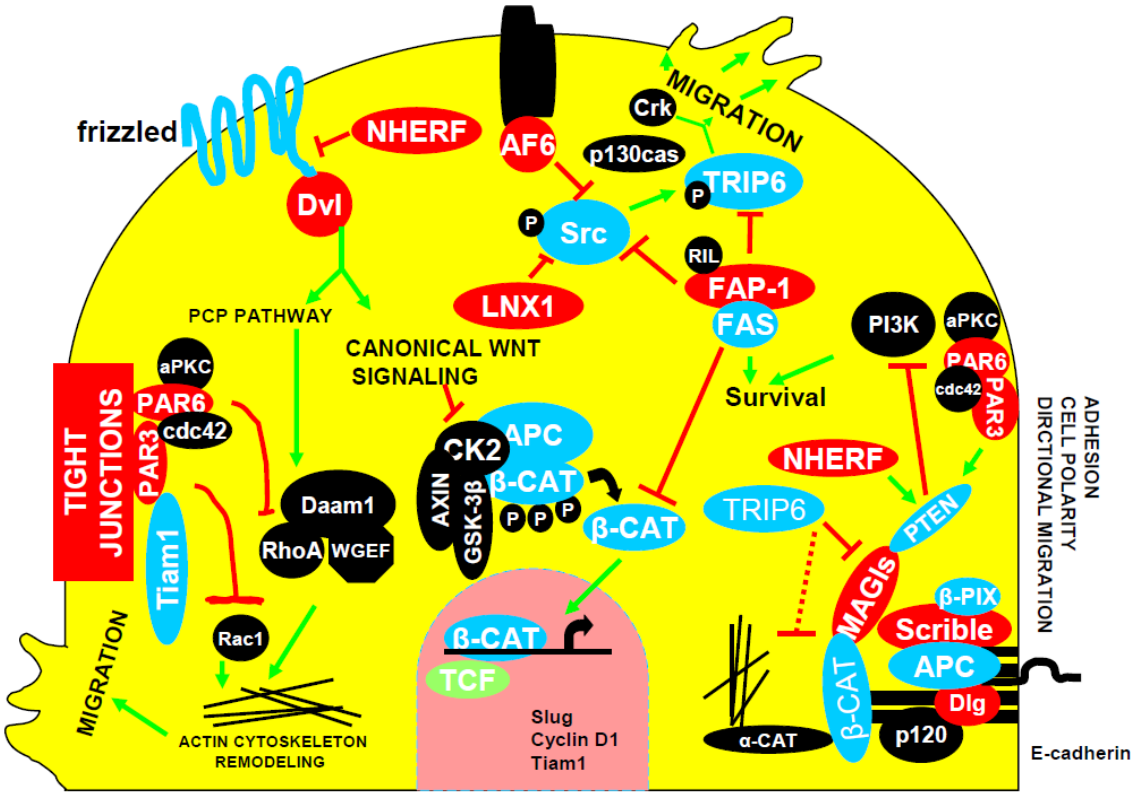

Figure 1.4: PDZ domain interactions in the regulation of EMT and Wnt signalling. Proteins possessing PDZ domains are shown in red and those possessing PDZ binding motifs are shown in blue. Figure adapted from V.K. Subbaiah.[62]

Both β-catenin and PTEN have PBM that enables them to interact with MAGI PDZ domain 5 to create the β-catenin-MAGI-PTEN complex. It was demonstrated that membrane-bound PTEN down-regulates the PI3K signalling pathway, inhibiting several process related to tumour formation and cancer progression, including cell growth and migration.[63] Par-3 PDZ interacts with T-cell lymphoma invasion and metastasis 1 (Tiam1) that has a PBM, whose interaction is essential for tight junction assembly and which contributes to the control of polarized cell migration.[64] The

interaction between the PBM of Frizzled receptors and NHERF-1 PDZ down-regulates β-catenin.[65] Dishevelled-PDZ (Dvl PDZ) binds directly to Frizzled receptors through an internal PBM, and the canonical or non canonical pathway is then activated, leading to β-catenin stimulation and hence cell proliferation. Dvl is frequently overexpressed in human cancers.

1.4 Dishevelled protein (Dvl)

The cytoplasmic protein dishevelled is a key protein of the Wnt signaling pathway which controls numerous cell fate decisions during animal development. The dishevelled gene was first identified in *Drosophila* mutants.[66] It was later discovered that the key role played by this gene is the regeneration of segment polarity in the early embryo.[67] Dishevelled is also involved in the Frizzled-dependent signaling cascade governing Planar cell polarity (PCP) in the wing, legs, and abdomen. It is positioned at the branchpoint between the canonical Wnt and PCP signaling pathways.[68,69,70,71] Three Dvl genes, Dvl-1, Dvl-2, and Dvl-3 have been identified in genome of mammals. Dvl homologs are conserved in Drosophila melanogaster (dishevelled[dsh] and Xenopus laevis [Xdsh]).[72] The three homologs identified in humans are expressed in both embryonic and adult tissues, including brain, heart, lung, kidney, skeletal muscle, and others.[73] Breast, colon, prostate, mesothelium, and lung cancers are involved in upregulation and over-expression of Dvl proteins. [74,75,76,77]

1.4.1 Structure of dishevelled proteins

Dishevelled are modular proteins comprising 500 to 600 amino acids containing three conserved domains: an N-terminal DIX domain, a central PDZ domain, and a C-terminal DEP domain.[78] (Figure 1.5).

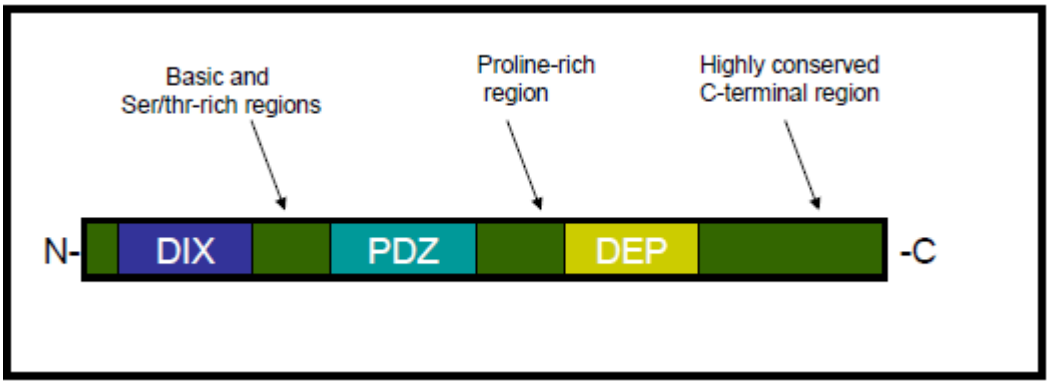

Figure 1.5: The schematic structure of dishevelled proteins

The overall structure of dishevelled is not yet known, however, structural descriptions of each of the three major domains are known. The DIX (Dishevelled/Axin) domain is largely α-helical in structure.[79] The PDZ (PSD-95, DLG, ZO1) domain, which consists of six β-sheets and 2 α-helices, forms a hydrophobic cleft that facilitates binding to other proteins. The DEP domain consists of a bundle of three α-helices.

Beside the three highly conserved domains of dishevelled, several additional conserved regions are observed. A basic region and scattered serine/threonine-rich segment strech between the DIX and PDZ domain. A proline rich region with an SH3 protein-binding motif is located downstream of the PDZ.[80,81] The extreme C terminus is very highly conserved across species, However it's function remains unclear.[82]

1.4.2 Dishevelled protein in Wnt signaling pathway

The Wnt signaling pathway not only plays a key role in embryonic development and maintenance of homeostasis in mature tissues, but it is also implicated in tumorigenesis. Dishevelled protein works downstream of the Frizzled receptor but upstream of β-catenin.[83] The Wnt pathway is initiated by Wnt molecules interacting with the transmembrane Frizzled receptors on the cell surface through binding to an amino-terminal cysteine-rich-domain to the dishevelled. Dishevelled protein then transduces the Wnt signal to downstream components. Two distinct pathways have been observed: The Canonical Wnt signaling pathway, and the non-canonical Wnt signaling pathway.[84] The canonical Wnt signalling pathway (Wnt/β-catenin pathway) involves the inhibition of GSK3β activity and stabilization of β-catenin in the cytoplasm. It is essential for cell fate in *Drosophila* and *Xenopus*. In this pathway,

dishevelled functions downstream of the Frizzled/LRP complex via the inhibition of Axin function. The mechanism of the canonical pathway is depicted in (Figure 1.6 A and B). The non-canonical pathways are β-catenin-independent. They are known as Wnt/calcium and Wnt/JNK in vertebrates, or Wnt/ PCP in flies.

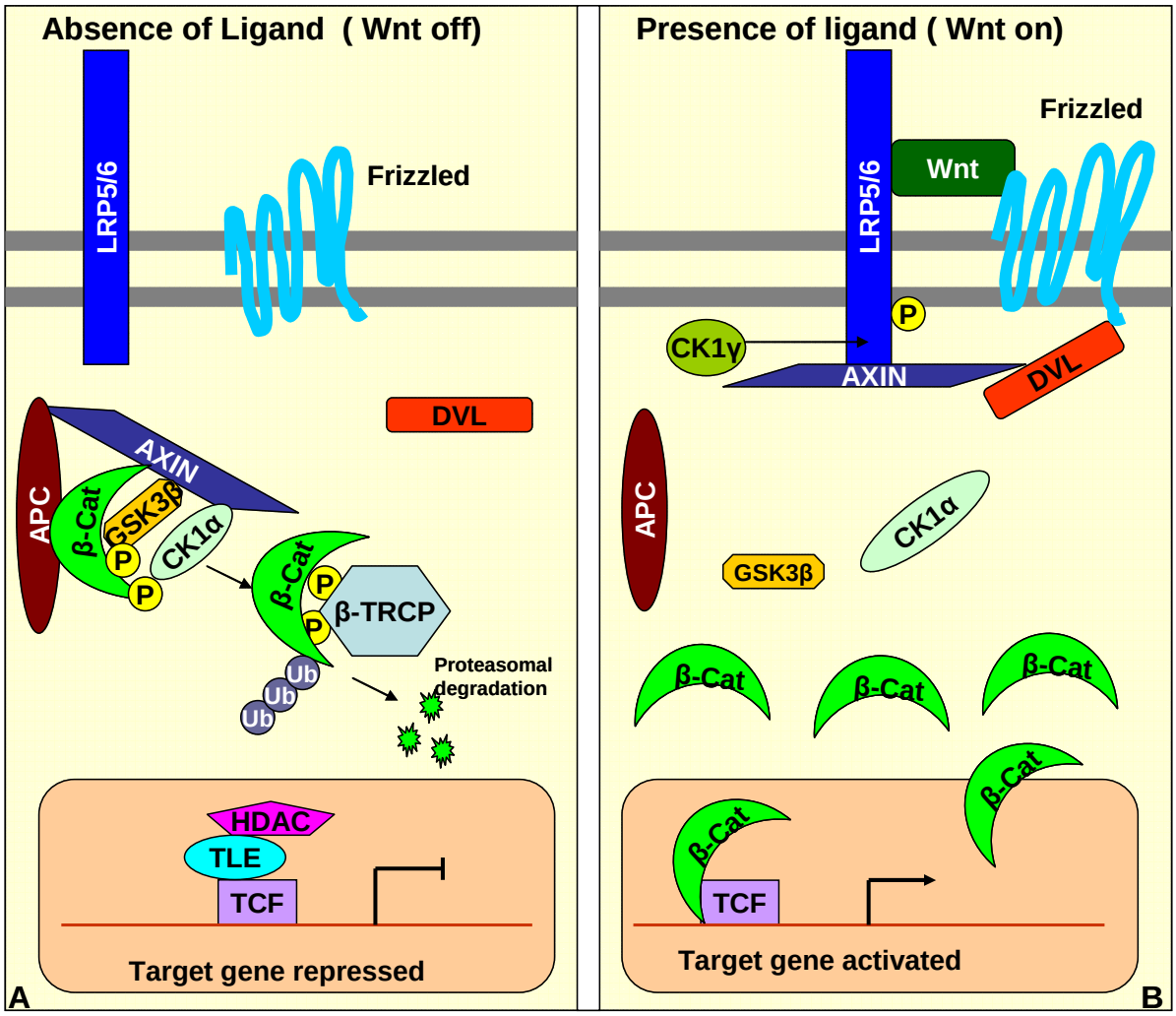

Figure 1.6: Overview of canonical Wnt signalling pathway Wnt/β-Catenin Signaling

(A) In the absence of Wnt, cytoplasmic β-catenin forms a complex with Axin, APC, GSK3, and CK1, and is phosphorylated by CK1 and subsequently by GSK3. Phosphorylated β-catenin is recognized by the E3 ubiquitin ligase β-Trcp, which targets β-catenin for proteosomal degradation. Wnt target genes are repressed by TCF-TLE/Groucho and histone deacetylases (HDAC).

(B) In the presence of Wnt ligand, a receptor complex forms between Fz and LRP5/6. Dvl recruitment by Fz leads to LRP5/6 phosphorylation and Axin recruitment. This disrupts Axin-mediated phosphorylation/degradation of β-catenin, allowing β-catenin to accumulate in the nucleus where it serves as a co activator for TCF to activate Wnt-responsive genes.

The canonical signaling pathway is implicated in tumorigenesis by enhancing proliferation and *in loco* tumour formation.[85] The non-canonical signaling pathway is also implicated in tumorigenesis by contributing to the invasion and cancer progression.[86] In the frequent overexpression of Dvl in human cancer, the role of Dvl PDZ interactions in tumorigenesis have been confirmed by using mutagenesis, peptidic and inhibitory compounds. That is why the Dvl PDZ domain has been identified as a potential target for drug discovery and development.[87,88]

1.5 Dishevelled PDZ (Dvl PDZ)

1.5.1 The central role of the PDZ domain in the interaction with dishevelled-binding proteins

The PDZ domain of the Dvl is used to transduce the Wnt signals from the membrane receptor Frizzled to the downstream components.[87]

Three Dvl homologs Dvl-1, Dvl-2, Dvl-3 have been identified in humans. Their PDZ domains are highly conserved (Figure 1.7). The high degree of sequence conservation is an indication that specificity is conserved among the three forms. Therefore, ligands that bind Dvl-2 PDZ are expected to bind Dvl-1 PDZ and Dvl-3 PDZ.

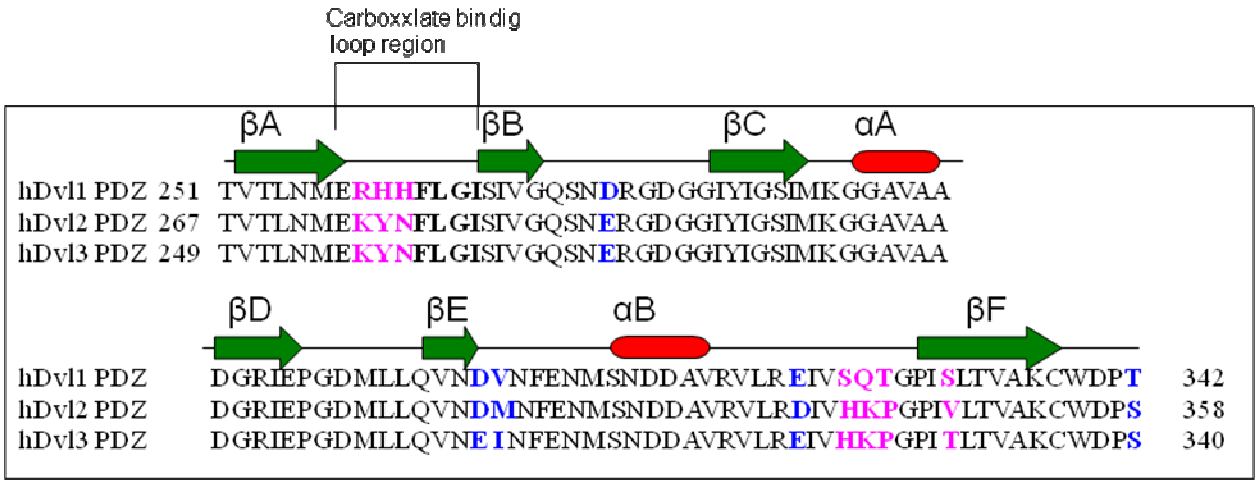

Figure: 1.7: structure based-alignment of the amino acid sequences of Dvl1,2 and 3 PDZ. Identities are highlight in pink and similarities are highlight in blue. UNIPROT Code: O14640 (Dvl-1 PDZ); O14641 (Dvl-2 PDZ); Q92297 (Dvl-3 PDZ).

Several Dvl-binding proteins partners have been identified. The region of Dvl that is mainly responsible for the interaction with binding proteins is the PDZ domain. Some Dvl PDZ binding partners are depicted in (Figure 1.8).

Research conducted in *Xenopus* have shown that Dvl binding peptides of Frizzled and Dpr/Fredo inhibited canonical Wnt signaling and blocked Wnt-induced secondary axis formation in a dose dependent manner. The relatively weak (kd ~ 10 µM) interaction presents an opportunity to block Wnt signaling at the Dvl PDZ level by using small molecules inhibitors. Several studies to identify peptides mimic that can bind to the Dvl PDZ domain have been undertaken.[88]

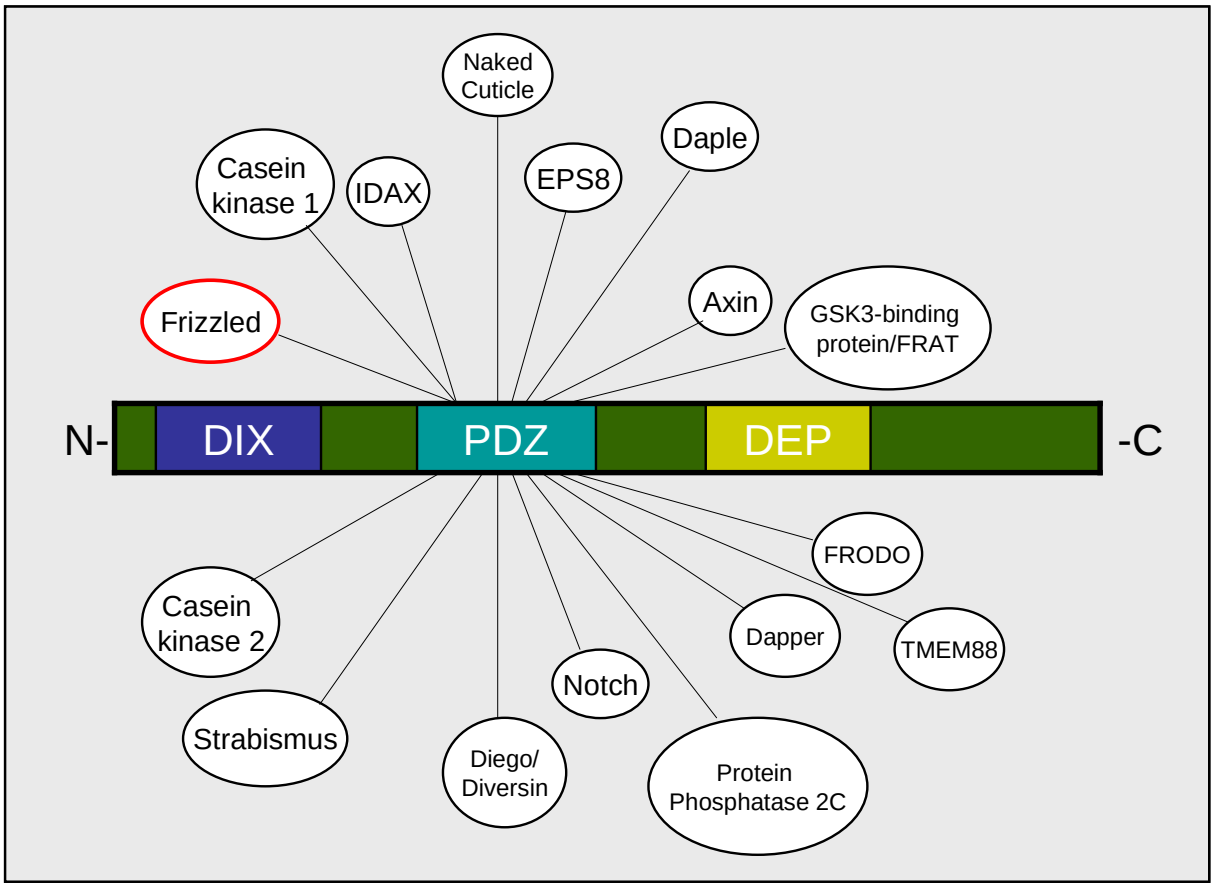

Figure 1.8: Binding partner of Dvl-PDZ (blocking of Frizzled signaling leads to cancer treatment)

1.5.2 Interactions between the Dvl PDZ domain and Frizzled

The Dvl PDZ domain recognizes an internal sequence and an extreme C-terminal tail of target proteins through a binding groove form between αB-helix and βB strand.[88,89] The direct interaction between the Frizzled-7 and Dvl PDZ occurs through the conserved motif KTXXXW (GKTLQSWRRFYH). This internal sequence

of Frizzled peptide bind to the conventional C-terminal peptide binding groove between αB and βB. This was demonstrated by mutating the three conserved residues in the Frizzled-7, which leads to the abolishment of the binding. Therefore the three residues in Frizzled-7 are essential for binding to Dvl PDZ in contrast to the C-terminus of the Frizzled-7, which does not bind to the PDZ domain. In order to verify that an internal motif is involved in the Frizzled-PDZ interaction, four peptides comprising one C-terminal peptide (WKWYGF-COOH) and three internal sequences (WKDYGWIDGK, SGNEVWIDGP, EIVLWSDIP) [88] were selected to study their interaction with hDvl-2 PDZ. These studies revealed that the binding cleft of Dvl PDZ is more flexible than those of canonical PDZ domains and facilitates recognition of both C-terminal and internal peptides.

The Frizzled (KTXXXW) motif alone is insufficient for high affinity interaction between Frizzled and Dvl PDZ; other residues within the KTXXXW motif greatly enhance the affinity of the interaction.[89] The work of Cheyette et al.[90] also indicates that the C-terminal residues of Dpr/Frodo bind to the Dvl PDZ domain with the relatively weak binding affinity (kd ~ 16 μM).[87] The three -dimensional structures of the Dvl PDZ domain in complex with the last 8 residues (SLKLMTTV) of the Dapper peptide revealed that the P_{-3} residues adopts the right α-helix conformation. P_{-4} and P_{-5} adopt the β-strand extended conformation.[90] Single modifications at the P_{-1} site in the binding peptide of Dvl-1 PDZ can increase the binding affinity through a hydrophobic interaction contribution. In this regards, tripeptides VVV and VWV were identified as Dvl-1 PDZ binding partners.[91] The VWV peptide binds tighter (K_D = 2 μM) than the VVV (K_D = 71 μM). Based on these results, short peptides containing the motif VWV can be considered as potential Dvl PDZ competitors.

1.6 AF- 6 PDZ Domains

AF-6 is a scaffolding protein that links cell membrane-associated proteins and the actin cytoskeleton.[92] AF-6 is a multidomain protein that contains two Ras-binding domains within its N terminus [93], a forkhead-associated domain (FHA) [94], a class V myosin homology region known as dilute domain (DIL), [95] a proline rich region in the C-terminal area and a PDZ domain that may function as a docking site for other molecules.[96] AF-6 PDZ binds Bcr, leading to the activation of Ras via its Ras-binding

domain. This in turn results to the formation of an AF-6-Bcr-Ras ternary complex that downregulates the Ras-mediated signal transduction pathway.[97] Furthermore, the AF-6 PDZ is involved in interactions with the junctional adhesion molecule (JAM),[98] the poliovirus receptors related protein,[99] several members of the Eph receptor family of receptor tyrosine kinases, and neuroxins.[100] It was demonstrated by Wiedemann et al[101] that the class II AF-6 PDZ domain binds target peptides with affinities in the 20 – 150 µM range. Nonpeptidic small molecule inhibitors of AF-6 PDZ domain have recently been reported.[102]

Figure 1.9 Schematic description of AF-6 protein. RA: Ras-associated domains; FHA: Forkhead-associated domain; DIL: dilute domain; PDZ: PSD-95-Dlg-ZO-1 domain; P: proline-rich regions

```
                2         10        20        30        40
AF-6 PDZ  KEPEIITVTLKKQNGMGLSIVAAKGAGQDKLGIYVKSVVKGGAADVDG
                50        60        70        80        90
          RLAAGDQLLSVDGRSLVGLSQERAAELMTRTSSVVTLEVAKQGA
```

Figure 1.10 Amino acid sequence alignment of the AF-6 PDZ domain (Protein Data Bank entry: 1T2M)

AF-6 PDZ interacts for example with Bcr where the C-terminal peptide of Bcr forms intermolecular hydrogen bonds with the backbone amide of residues Gly and Leu of the GMGL loop for AF-6 PDZ. As usual, the peptide binds to the PDZ domain by fitting into a hydrophobic groove between the second β-strand (βB) and the second α-helix (αB). These informations concerning the interaction between AF-6 PDZ domain and the Bcr peptide gave some insight into the mechanism, which might be useful for drug discovery.

1.7 PDZ domains used to investigate selectivity

Five other PDZ domains were investigated for selectivity: the first, the second and the third PDZ domain of PSD95 which belongs to class I PDZ, the shank-3 PDZ, a member of class II PDZ and the α-syntrophin PDZ.

1.7.1 PSD95 PDZ domain

Known as an abundant postsynaptic scaffolding protein, PSD95 is implicated in signaling in glutaminergic neurons by acting as molecular scaffold for the formation of protein complexes localized at the postsynaptic density of dendritic spines.[103] Furthermore, PSD95 directly interacts with actin-regulatory proteins such as Kalirin-7, and indirectly interacts through the postsynaptic scaffold Shank with actin-regulatory proteins such as β-Pix.[47,103] PSD95 belongs to a family of related proteins that includes PSD93, SAP97 and SAP102. PSD95 proteins comprise three tandem PDZ domains, an SH3 domain and a guanylate-kinase-like domain.[104] The three PDZ domains of PSD95 (PDZ1, PDZ2, PDZ3) share high sequence homology and have similar three-dimensional structures consisting of an antiparallel β-sandwich formed by two α helices and six β strands.[104] The C-terminal peptide of CRIPT binds to PDZ1 of PSD95 with a dissociation constant of 10 µM.[105] PSD95 PDZ1 and PSD95 PDZ2 domains interact with the C termini of NR2A and NR2B subunits of NMDA receptors.[106] These interactions lead to increased production of nitric oxide (NO) by neuronal nitric oxide synthase in the cell. An overstimulation of the NMDA receptor is observed during brain ischemia leading to toxic levels of NO and to the death of the cell.[109] A heterodimeric PDZ-PDZ interaction is also observed between the PDZ domain of PSD95 and the PDZ domain of neuronal nitric-oxide synthase (nNOS).[107] PSD95 is implicated in many diseases, therefore any inhibitor of the many interactions in which it is involved is a promising candidates for drug development.[108, 109]

1.7.2 Shank- 3 PDZ

Shank proteins are scaffolding proteins that are major components of the postsynaptic density. The Shank family consists of three family members, Shank-1,

Shank-2 and Shank-3.[110] The Shank proteins vary in molecular mass, but share a common domain organization that is constituted of seven N-terminal ankyrin repeats, an SH3 domain, a PDZ Domain, a proline-rich region, and a sterile alpha motif (SAM) domain. It was suggested that Shank may cross-link homer and PSD95 complexes in the Post synaptic density, to play a role in the signaling mechanisms of both mGluRs and NMDA receptors.[111] The N-terminal ankyrin repeats of Shank-1 and Shank-3 binds to spectrin.[112] The PDZ domain of Shank-3 was also found to interact with the PBM of the receptor tyrosine kinase, which is bound in the Ret9 but not in the Ret51 isoform.[113] The PDZ domain of Shank recognizes the consensus C-terminal sequence X-T/S-X-L in which X represents any amino acid.[114] The crystal structure of the Shank-1 PDZ in complex with the C-terminal hexapeptide (EAQTRL) of GKAP was determined.[52] It was observed that Shank-1 interacts directly with the P_{-1} position of the ligand via hydrogen-bonds with Asp634 located at the end of the βC strand. Interestingly, Asp634 is conserved among all the Shank-(1,3) proteins in rat and Shank-(1,2) in human. It was also shown that the shank-1 PDZ domain has the ability to form a dimer. These findings suggest that the dimer may represent the functional state of the Shank PDZ domain. Saupe et al.[115] have recently developed small molecules inhibitors of Shank-3 PDZ.

1.7.3 α1-Syntrophin PDZ

The Syntrophins are key components of the destrophin protein complex at the neuromuscular junctions (NMJ) which organize acetylcholine receptor (AChR) clusters.[116] Syntrophins connect a variety of signaling proteins and ion channels to the dystrophin protein complex. They exist in two forms, acidic (α) or basic (β) that display distinct tissue distribution. Syntrophins are modular proteins that are constituted of one PDZ domain, two pleckstrin homology (PH) domains and a syntrophin-unique domain apparently responsible for the binding to dystrophin/utrophin.[117, 118,119] The PDZ domain of α-syntrophin has been reported to bind several proteins including neuronal nitric oxide synthase (nNOS),[120] voltage-gated sodium channels,[121] and ATP-binding cassette (ABC) transporters.[122] It was also found that syntrophins regulate α1-D-adrenergic receptors through a PDZ domain-mediated interaction. These findings suggest that syntrophins play an

important role maintaining receptor stability by directly interacting with the receptor PDZ-interacting motif.[123] Through a glutathione S-transferase (GST) pull-down assay, it was demonstrated that the transient receptor potential channel 1 (TRPC1) binds to the PDZ domain of α-syntrophin.[124] The PDZ domain and the PH1 domain of α-syntrophin works in concert to facilitate the localization of AChRs as concluded by Adams et al.[125] The PDZ domain of syntrophin recognizes a ligand motif of R/K/Q-E-S/T-X-V-COOH.[126]

1.8 NMR spectroscopy as tool for drug discovery

Nuclear magnetic resonance (NMR) spectroscopy is powerful tool in drug discovery. NMR is unique in its ability to provide information on the structural, thermodynamic and kinetic aspects of ligand binding. Identification of small organic compounds that modulate the activity of a particular biological target is a very important step in the drug discovery process. Identification requires the screening of a very large number of compounds, often more than a million. The ability of NMR to detect weak intermolecular interactions (μM < K_D < mM) make it an ideal screening tool for initial "hits", to be optimized with chemical modification for consecutive hit-to-lead development. In NMR binding assays, binding is indicated by chemical-shift changes, changes in diffusion constants, NOEs relaxation times or exchange of saturation.[127]

1.8.1 NMR screening methods

The advantage of NMR –based screening technology is that both the interaction and the binding site of the compound can be detected. NMR tolerates a certain level of compound mixing, and generally pools of 5 to 100 compounds can be interrogated for binding. The development of cryo-probes has made this NMR screens more Sensitive.[128] SAR by NMR[129], RAMPED-UP NMR[130], and NMR-SOLVE[131] were the first NMR screening methods developed to identify ligands that bind a therapeutic target in a biologically relevant manner. These methods observe chemical shift changes in two-dimensional 2D ^{1}H-^{15}N HSQC. Multistep NMR screening has been developed, [132] to minimize resource usage. For the multistep NMR technique,

one-dimensional 1D ^{1}H NMR line-broadening experiments and 2D ^{1}H-^{15}N HSQC chemical shift perturbation experiments are combined to identify “hit” compounds from a library of small molecules. Ligand base NMR screening techniques are an effective post-screening tool for validating the results of high-throughput (HTS) screens. ^{1}H-^{15}N HSQC NMR screening techniques then reveal the binding site. Isotope-flitered NOESY experiments supply information that enables precise docking of the ligand into the protein binding pocket. The conformation of the bound ligand can be determined by transfer NOE. NMR screening provides a natural connection between combinatorial and medicinal chemistry, HTS, structure-based drug design and genomics. [133] An alternative to HTS is the fragment-based drug design (FBDD) where NMR plays an important role. [134,135] Of particular importance is the ability of to identify possible targets classified as “undruggable” after HTS. Also, NMR-FBDD approaches could be extended to in-cell NMR experiments to provide, mapping information from chemical shift perturbations for serially expressed protein systems.[136]

Methods	Definition	Description
HSQC/ HMQC	Heteronuclear Single Quantum Correlation / Heteronuclear Multiple Quantum Correlation	2D experiments, central to the chemical shift perturbation method. Most commonly used to generate ^{1}H-^{15}N correlations of large deuterated proteins
TROSY	Transverse Relaxation-Optimised Spectroscopy	Taking advantage of the interference of different relaxation mechanisms. Leading to an improvement of ^{1}H-^{15}N correlation of large deuterated proteins
INEPT	Insensitive Nuclei Enhanced by Polarization Transfer	Technique which uses heteronuclear coupling constants to transfer magnetization to insensitive nuclei, allowing their detection
CRIPT	Cross Relaxation-Induced Polarization Transfer	Alternative to the INEPT where magnetization is transferred using cross-correlated relaxation
NOE/ NOESY	Nuclear Overhauser Effect	NOEs are main NMR parameter used for conformational analysis and protein structure determination by NMR. NOEs are in general measured using a 2-D NMR experiment termed NOESY.
STD	Saturation Transfer Difference	Technique that allows the identification of ligands from a mixture of low molecular weight compounds by transferring saturation from the macromolecular target to the ligands.
Water-LOGSY	Water-ligand observed *via* gradient spectroscopy	Technique which uses water molecules to mediate the transfer of magnetization from the macromolecular target to the ligand

Table 1.1: Some NMR methods and keywords relevant for screening

1.8.2 WaterLOGSY

Water-ligand observed via gradient spectroscopy (WaterLOGSY) is a powerful screening NMR technique. [137,138] The experiment selectively transfers magnetization from the bulk water via the protein-ligand complex to the free ligand. Structures of protein-ligand complexes show that water molecules are important for the interaction of the protein and the ligand.[139]

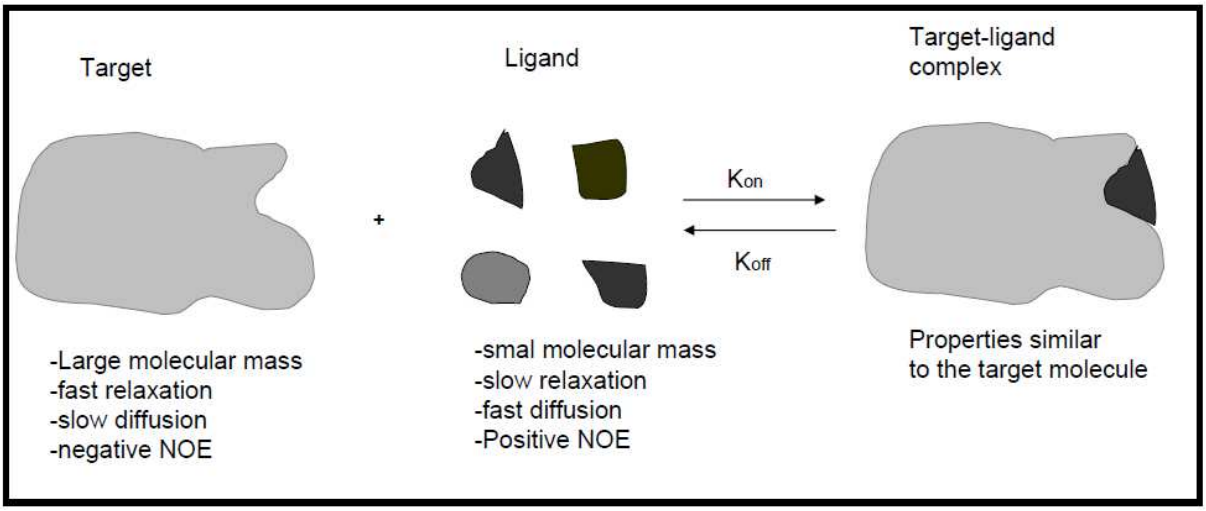

Figure 1.10: Alteration of the physicochemical properties during the process of binding. upon binding, the ligand adopts the properties of the large target molecule due to drastic increase in the effective molecular mass.[140]

The observed intermolecular water-ligand NOE is negative indicates that the residence time of the water molecules in protein cavities range between a few ns to a few hundred µs.[141,142] The detection of NOEs, even at short mixing times, could be explained either by bound water squeezed between ligand and protein or by an extensive network of hydrogen-bonded water molecules with a long residence time surrounding the free ligand.

1.8.3 Saturation Transfer Difference

The STD experiment transfers magnetization from the macromolecular target to the ligand or vice versa.[143] The magnetization is transferred via spin diffusion to the bound ligand. In the case of the dissociation of the ligand from the target protein into the solution, the magnetization change in the bound state is retained in the free ligand. The experiment is carried out by subtracting the spectrum obtained while

irradiating the target protein resonances from the spectrum obtained when irradiation is off resonance.

1.8.4 Heteronuclear Single Quantum Correlation (HSQC)

^{1}H-^{15}N HSQC experiments detect the binding of ligand to the receptor, but also at the same time help to identify the amino acids involved in the binding. The technique can detect chemical shifts changes in the backbone and side chain resonances amide proton and nitrogen. This technique requires acquisition of an ^{1}H-^{15}N HSQC spectrum of the receptor as a reference spectrum. A second spectrum is acquired in the presence of one or more potential ligands. Binding is deduced if the resonance position of a cross-peak is significantly shifted compared to the reference spectrum. Strong chemical shift perturbations (CSPs) are observed usually in the vicinity of ligand binding site. In general, perturbations are considered significant if the chemical shift perturbation difference (ΔCSP) is greater than 0.05 ppm for at least two residues in the spectrum.[144] In the case where mixtures of compounds have been used, the active compound is obtained through successive deconvolution. The HSQC technique is also used to estimate the strength, stoichiometry, specificity and the kinetics aspects of the interactions. The binding constant can be obtained by monitoring chemical shifts changes as a function of ligand concentrations.

The ^{1}H-^{15}N HSQC technique is mainly applied to soluble 30 - 40 kDa proteins that are suitable for stable isotope labelling. ^{1}H-^{13}C HSQC yields information on chemical shift changes in all side chains. ^{1}H- ^{13}C HSQC spectra are more complex than ^{1}H-^{15}N HSQC spectra; hence they have not been widely employed to test for binding. Also, ^{15}N-labelling is less expensive.

1.8.5 Determination of chemical shift perturbation

Chemical shift perturbations give valuable informations concerning the binding situation of the ligand with the protein.

Chemical shift perturbations (CSP, Δδ) are obtained by comparing the ^{1}HN-^{15}N backbone resonances of a protein alone to those of protein-ligand complex. In general, the mean shift difference (Δδ in ppm) is calculated according the equation 1.

$$\Delta\delta = \sqrt{\left[\frac{1}{2}(\Delta\delta H)^2 + \frac{1}{25}(\Delta\delta N)^2\right]} \quad \text{(Eq.1)}$$

Here $\Delta\delta N$ and $\Delta\delta H$ are the amide nitrogen and amide proton chemical shift differences respectively between the free and the bound states of the protein. The equation 1 is applied for each cross peak showing chemical shift changes.

The average values of chemical shifts changes (ΔCSP) for N cross peaks (equivalent to N residues in the case of correlations is calculated according to equation 2.

$$\Delta CSP = \frac{\Sigma \Delta\delta_n}{n} \quad \text{(Eq.2)}$$

where N is the number of cross peaks selected

The ΔCSP gives an indication about the strength of the interaction involved in the complex when comparing similar systems, or at best when investigating a series of complexes involving the same protein, and binding partners interacting *via* the same mechanism. In such cases, it may be helpful to interpret its value as follows:

(i): $\Delta CSP < 0.02$ (no interaction); (ii): $0.02 \leq \Delta CSP \leq 0.05$ (very weak interactions)

(iii): $0.05 < \Delta CSP \leq 0.1$ (weak interactions) (iv): $0.1 < \Delta CSP \leq 0.2$ (intermediate interactions) (v): $0.2 < \Delta CSP \leq 0.5$ (strong interactions) and (vi): $\Delta CSP > 0.5$ (very strong interactions).

1.9 Strategy used to identify and to develop inhibitors of protein-protein interactions

In the course of this work, small molecule modulators of PDZ-mediated protein-protein interactions were developed by starting from weakly binding compounds identified by NMR. In the first step, NMR was used to validate a library of 212 small molecules identified *via* virtual screening by Dmytro Kovalskyy of the company Enamine in Kiew. The molecules were selected after docking into the binding site of PDZ domains. As a powerful tool in the discovery of small molecules that target protein-protein interactions, the particularity of NMR, its ability to identify small molecules that bind to the target protein with upper micromolar range, was exploited at this stage. ^{1}H-^{15}N HSQC was the NMR technique used to detect the hits.

In a second stage, they were improved by step-wise addition of further groups, again supported by chemical shift assays. In individual cases, calorimetry was applied to determine binding constants. Then, based on X-ray crystallography data, they were further improved by structure-based design and larger molecules synthesized which showed binding constants in low micromolar range and that were able to compete with the endogenous ligands. These molecules were then tested in a biological assay using a reporter cell line.

.

Schematically, the strategy presented here includes the following steps

1. Design of Library by virtual screening
2. Hit identification by NMR
3. First round of refinement by screening derivatives
4. Co-crystallization of best compounds, structure-based design of competitive binders
5. Biological assays test

1.10 Aim of the work

The aim of this work is to develop small molecule inhibitors of protein-protein interactions (PPIs). PDZ domains are important small modules among many others that often mediate PPIs leading to the regulation of many cellular processes. It was the domain of choice to study the function of PPIs. There are more than 440 PDZ domains in human genome occurring in 250 proteins; hence the importance of this domain. The Dvl PDZ and the AF-6 PDZ are the two representative domains used in this work. All small molecules obtained were tested on a selected panel of other PDZ domains for selectivity.

To achieve our objectives, we followed and tested the strategy described in section 1.9 to identify inhibitors of Dvl PDZ.
For the AF-6 PDZ, we started from 5-(4-trifluoromethylbenzyl)-2-thioxo-4-thiazolidine, a known scaffold previously detected by NMR, and developed new potent inhibitors by chemical synthesis.

2.1 Dvl-3 PDZ

2.1.1 "Hit" identification

A two-dimensional ^{1}H-^{15}N HSQC NMR-assisted virtual ligand screening approach was used to identify, small molecules inhibitors of Dvl PDZ followed by subsequent modification to improve binding affinity. 212 small molecules specifically designed for PDZ domain inhibition by company Enamine were first screened against the Dvl-3 PDZ domain. Binding was detected by comparing 2D ^{1}H-^{15}N HSQC spectra of Dvl PDZ in the absence and presence of ligand to elucidate ligand-induced changes of chemical shifts. Chemical shift perturbation differences (ΔCSPs) were calculated for compounds in which at least two amino acid residues were showing shifts. Compounds were classified into different categories depending on ΔCSPs values. (i):inactive compounds (ΔCSP < 0.02); (ii): very weak interactions (0.02 ≤ ΔCSP ≤ 0.05); (iii): weak interactions (0.05 < ΔCSP ≤ 0.1); (iv): intermediate interactions (0.1 < ΔCSP ≤ 0.2); (v): strong interactions (0.2 < ΔCSP ≤ 0.5) and (vi): very strong interactions (ΔCSP> 0.5). As results of the first round of screening, 23 compounds with ΔCSPs values between 0.01 and 0.12 ppm were obtained. A closer analysis of these compounds revealed two different scaffolds. The first group contained an adamantane moiety while the second group contained a sulfonamide moiety. The two scaffolds share a carboxylic acid function COO^{-} and an amide function.

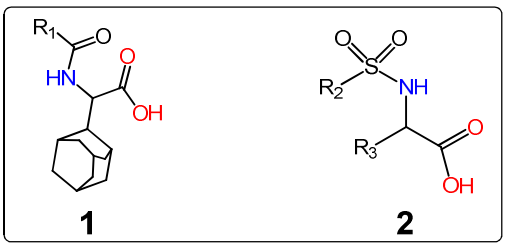

Figure 2.1: Scaffolds obtained from the first round of the screening: 1) Adamantane scaffold; 2) Sulfonamide scaffold

2.1.2 Preliminary SAR analysis of adamantane compounds

Adamantane derivatives are known for diverse biological properties, mainly as antiviral, antibacterial, antifungal and anti inflammatory agents. Adamantane is a highly lipophilic compound. Therefore, the incorporation of an adamantane group into

several molecules results in compounds with relatively high lipophilicity. Since the discovery of adamantine[145] as antiviral and antiparkinson drug, several research projects investigated adamantane derivatives as chemotherapeutic agents. Nowadays, several drugs containing the adamantane moiety are available on the market. Three compounds containing adamantane were obtained as results of our screening. They all exhibited the same value of ΔCSPs which was 0.1 ppm indicating weak interactions. The interaction of these compounds with the Dvl-3 PDZ seems to be driven by the presence of the COO^- group which might interact with the carboxylate binding loop of the Dvl-3 PDZ on the one hand, and on the other hand the adamantane moiety which might interact with its hydrophobic binding pocket.

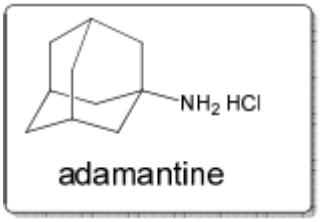

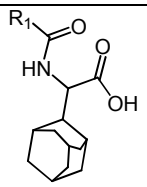	
Compound Nr	ΔCSP (ppm)
3 R_1 = 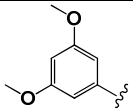	0.1
4 R_1 = 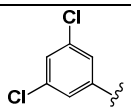	0.1
5 R_1 = 	0.1

Table 2.1: "Hits" identified for the Dvl-3 PDZ domain by NMR-based screening. ΔCSP is the mean value of 5 amino acid residues showing chemical shift perturbation. **3)** 2-(adamantan-2-yl)-2-(3,5-dimethoxybenzamido)acetic acid; **4)** 2-(adamantan-2-yl)-2-(3,5-dichlorobenzamido)acetic acid; **5)** 2-(adamantan-2-yl)-2-benzamidoacetic acid

To further assess the binding characteristics of the adamantane scaffold, we performed NMR titrations to measure the binding affinities of compound **3** (2-(adamantan-2-yl)-2-(3,5-dimethoxybenzamido)acetic acid)**.** The dissociation constant

was then derived by monitoring the protein HN chemical shift change as a function of the ligand concentration. Three residues those are located in the binding pocket of Dvl-3 PDZ were considered for K_D determination. These residues included R322, V289 and S265. (Figure 2.2).

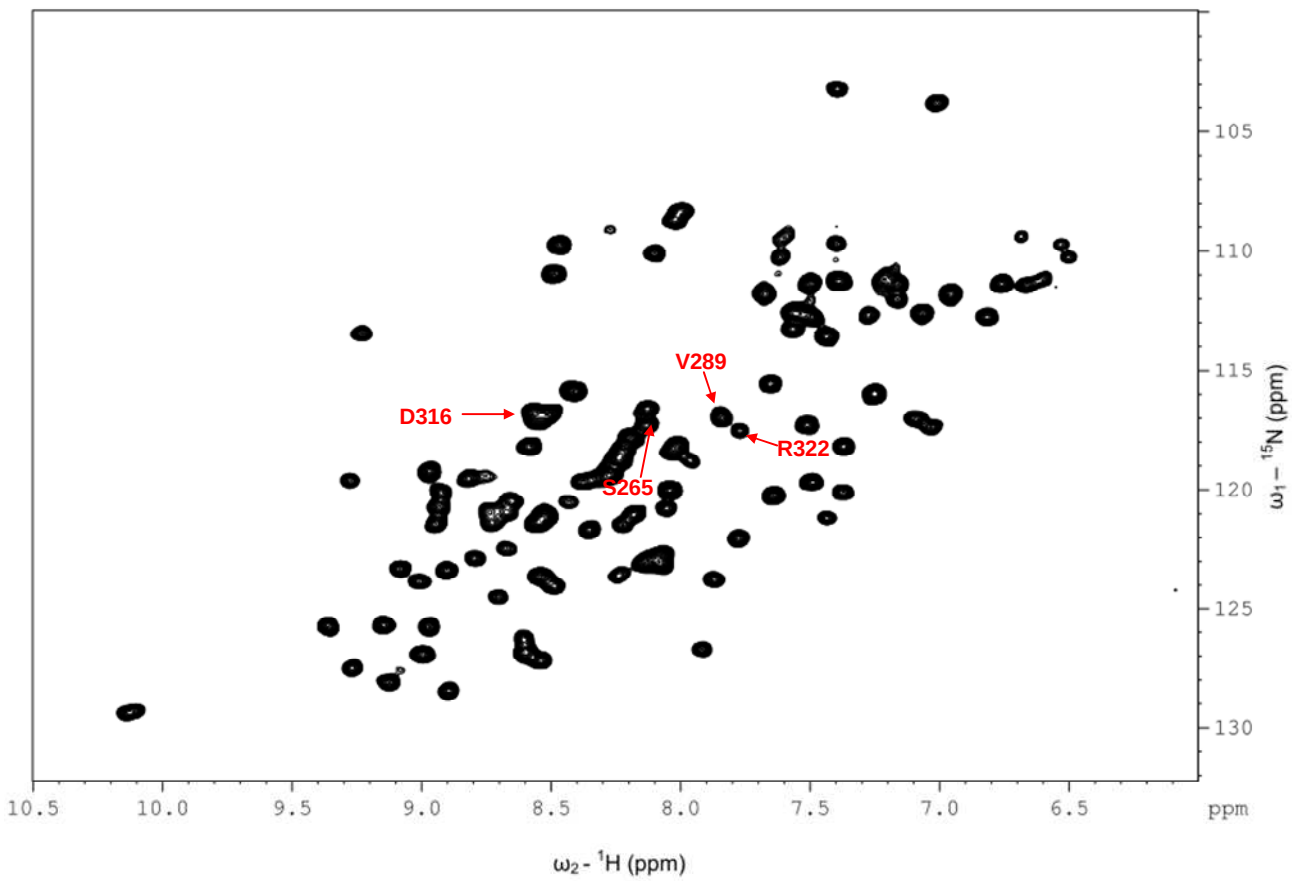

Figure 2.2: ^{1}H-^{15}N-HSQC spectra of Dvl-3 PDZ domain. Residues R322, V289, S265 are important residues of the binding groove of Dvl-3 PDZ

The ^{1}H-^{15}N HSQC titration experiment (Figure 2.3) of scaffold compound **3** with the Dvl-3 PDZ showed that residues that are affected are those surrounding the binding groove, amongst them S265, V289 and R322. The largest chemical shift perturbations were observed for Ser 265 in the βB-strand and Arg 322 in the αB-helix structure of Dvl-3 PDZ. The gradual change of chemical shifts means that Dvl-3 PDZ domain and compound **3** are in fast exchange. The amino acids that showed stronger shifts with our compound were also those that showed stronger shifts with the tripeptide VWV,[91] indicating that the conserved binding site of the Dvl-3 PDZ is being targeted.

The binding constant derived from the titration experiment was 189.4 ± 11.2 µM. This was seen as a promising binding constant opening voice for possible fast improvement.

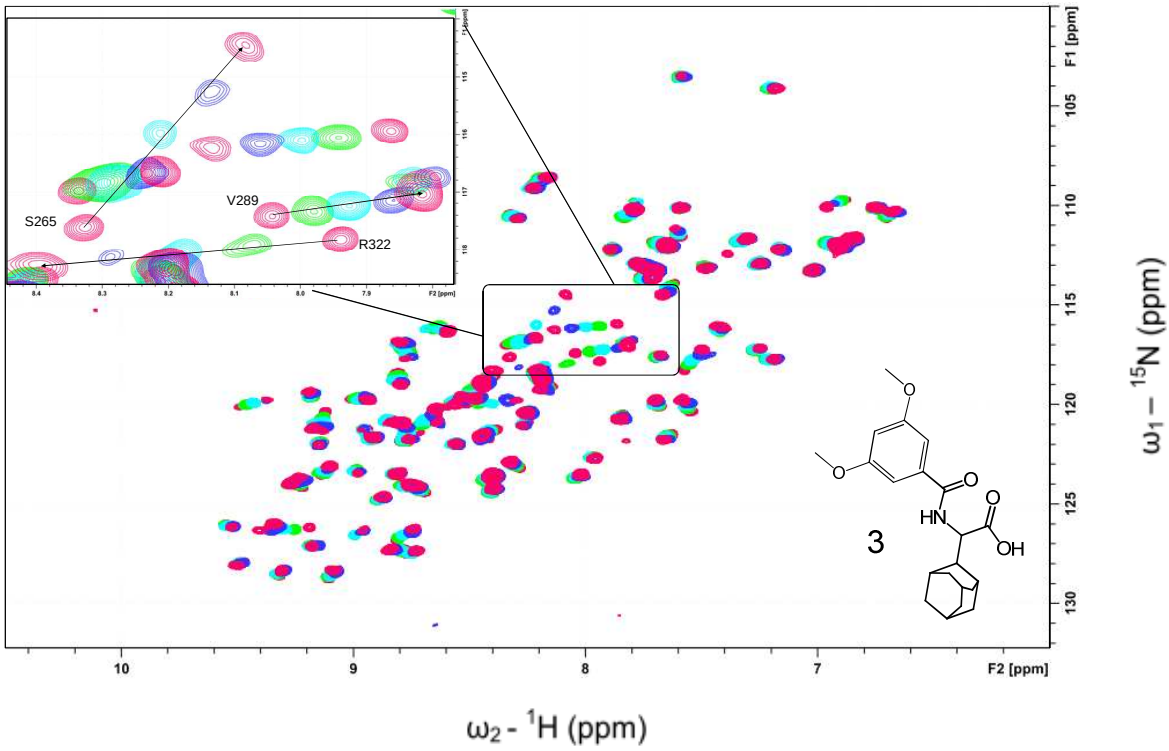

Figure 2.3: ^{1}H-^{15}N HSQC spectra of Dvl-3 PDZ domain alone and varying concentrations of compound 3. The zoom shows the gradual increasing of shifts with residues surrounding the binding pocket of Dvl-3 PDZ

2.1.3 Modifications of adamantane scaffolds

In order to achieve a comprehensive SAR and also to obtain a better binder, new series of molecules were designed. Taking into account the fact that the adamantane moiety is large enough to occupy completely the hydrophobic pocket of the Dvl-3 PDZ, no changes were made to this part of the compound. The SAR studies were focused on the substitution of the scaffold at the R_1-position. New R_1 moieties containing more heteroatoms were designed. (Table 2.3). We also combined the adamantane moiety with the sulfonamide moiety. (Figure 2.4). To achieve our goal, a series of 12 compounds were obtained from our cooperation partner from Enamine.

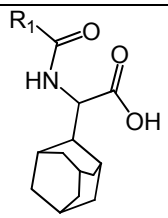

6-15

Compound Nr	R_1	Compound Nr	R_1
6	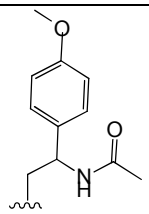	**11**	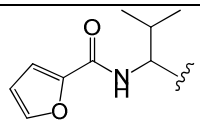
7	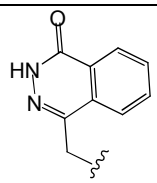	**12**	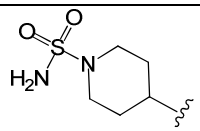
8	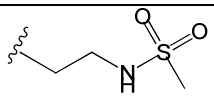	**13**	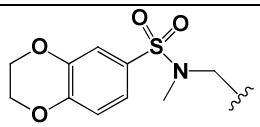
9	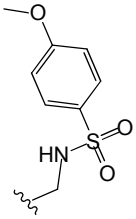	**14**	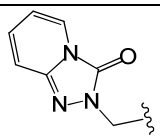
10	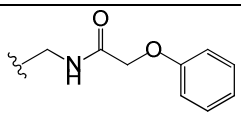	**15**	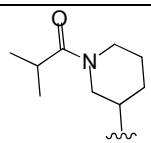

Table 2.2: Structure of compounds series 6-15

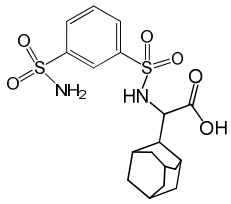

16

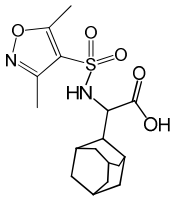

17

Figure 2.4: Compounds containing adamantane and sulfonamide moieties

A total of 12 compounds **6-17** containing the adamantane moiety and different substituents were further investigated.

Compound Nr	ΔCSP (ppm)	Compound Nr	ΔCSP (ppm)
6	0.08	**12**	0.12
7	0.06	**13**	0.23
8	0.09	**14**	0.1
9	0.15	**15**	0.08
10	0.09	**16**	0.15
11	0.19	**17**	0.12

Table 2.3: Chemical shift perturbation values of Dvl-3 PDZ resonances for compounds (6 – 17)

According to the ΔCSP values obtained (Table 2.3), six compounds **6**, **7, 8,10,14,15** were classified as weak binders, and four compounds **9**,**11**,**12**,**13** as intermediate binders. The ΔCSP value of two compounds respectively **11** (ΔCSP = 0.19 ppm) and **13** (ΔCSP = 0.23 ppm) considerably increased. The particularity of these two compounds is that they bear a heterocyclic moiety with one and two oxygen atoms respectively. The combination of adamantane and sulfonamide moiety also led to the increasing ΔCSP values for **16** (ΔCSP = 0.15 ppm). The ^{1}H-^{15}N HSQC revealed that compound **11** bind to the amino acid residues surrounding the hydrophobic binding pocket. A binding constant of 45 µM was obtained. Higher values of chemical shift perturbation were observed for residues S265, V289, and R322. To further investigate the interaction mechanisms, the x-ray crystal structure (figure 2.5) of Dvl-3 PDZ in complex with compound **11** was solved by Dr. Yvette Roske from the Max Delbrück Center for Molecular Medicine (MDC) in Berlin-Buch. Our temptation to solve the crystal structure of the Dvl-3 PDZ in complex with compound **13** failed.

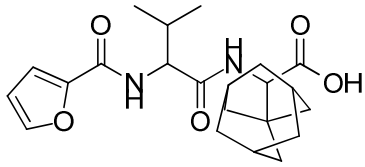

11

2-((1S,3R,5S)-adamantan-1yl)-2-(2-(furan-2-carboxamido)-3-methylbutamid)acetic acid

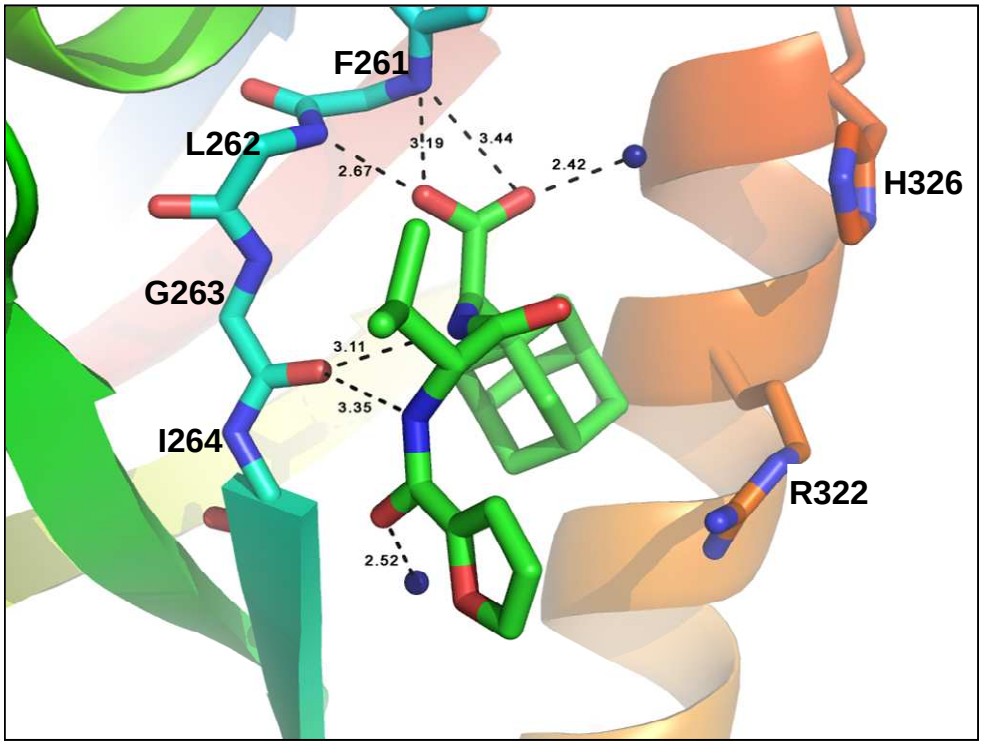

Figure 2.5: X-ray crystal structure of Dvl-3 PDZ in complex with **11** showing the hydrogen bonding interactions

These structures show that compound **11** binds between the βB-strand and the αB-helix. The carboxylate part of compound **11** interacts with the carboxylate binding loop region. Also, the two amine groups of compound **11** form hydrogen bonds to a water molecule. The adamantane part is pointing into the hydrophobic binding pocket. These interactions revealed by the X-ray crystal structure are in agreement with the results derived from ^{1}H-^{15}N HSQC spectra.

2.1.4: Preliminary SAR analysis of Sulfonamide containing amino acid like compounds

A comprehensive structure activity relationship was derived to understand the contribution of different substitution on R_2 as well as R_3 position for compounds **18 – 35** (Table 2.4)

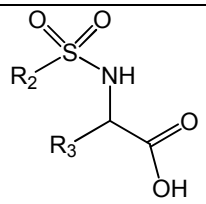

Compounds 18 - 35

Compound Nr	R_2	R_3	ΔCSP (ppm)
18	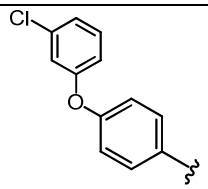	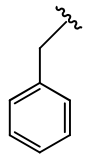	0.12
19	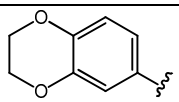	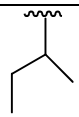	0.12
20	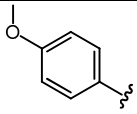	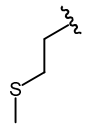	0.08
21	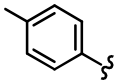		0.07
22	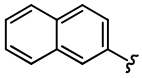	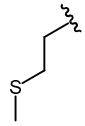	0.06
23	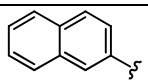		0.06
24	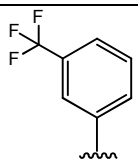		0.06

Compound Nr	R_2	R_3	ΔCSP (ppm)
25	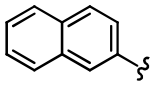	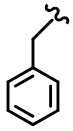	0.05
26	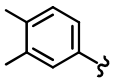		0.05
27	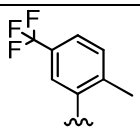	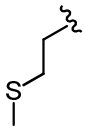	0.05
28	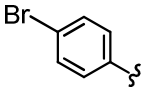	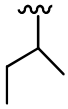	0.04
29	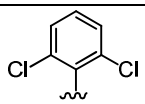	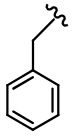	0.04
30	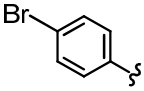		0.03
31	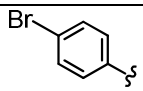	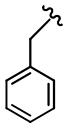	0.03
32	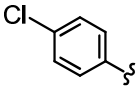	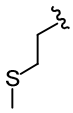	0.01
33	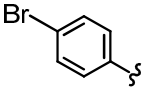	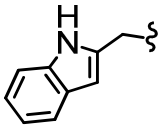	0.01
34	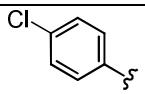	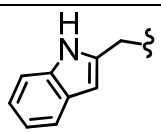	0.01
35	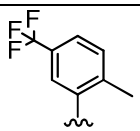	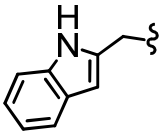	0.01

Table 2.4: Chemical shift perturbation values of Dvl-3 PDZ resonances for compounds (18-35) ΔCSP is the mean value of 4 amino acid residues showing chemical shift perturbations.

The R_3 group was only constituted of different amino acid side chain residues. The side chains of phenylanine, valine, leucine and methionine were supporting binding while the side chain of tryptophan was completely in disfavor of activities. All compounds containing the tryptophan side chain at the R_3 position were completely inactive. This was the case observed for compound **35** with tryptophan side chain as R_3 compare to compound **27** with methionine side chain as R_3. Both compounds have common R_2. However, the ΔCSP value of compound **27** was 0.05 ppm while the ΔCSP value for **35** was 0.01 ppm. Substituents at the R_2 position that were in favor for interactions are those containing aromatic rings with heteroatoms as substituents. This case was observed for compounds **18** (ΔCSP = 0.12 ppm) and **19** (ΔCSP = 0.12 ppm). The five compounds of sulfonamide scaffold that fall into the category of weak binders contains as R_3 methionine or valine side chain. All these series of weak binders have in common at the R_2 position the substituted benzene ring. Halogenated substituents on the aromatic ring of R_2 renders compounds very weak. This was the case of compounds **28**, **29**, **30** and **31** that fall into the category of very weak binders. The combination of a tryptophan side chain at the R_3 position and an R_2 moiety in which there is a halogen substituent at the aromatic ring render the compounds completely inactive as seen for compounds **33**, **34**, and **35** with the ΔCSP values of 0.01 ppm. At this stage, it was precarious to draw a conclusion concerning the influence of the nature of substituent at the R_2-position on the interactions. This situation might be due to the fact that the substituent at the R_2-position could not easily create a hydrogen bond with the carboxylate loop region. In our desire to really understand the contribution of each part of our compound to the interaction, we attempted to solve the x-ray crystal structure of Dvl-3 PDZ in complex with compound **19**. Unfortunately, it was not successful.

The binding constant of compound **19** was evaluated by NMR titration. (Figure 2.6) The titration experiment showed that residues that belong to the binding loop of the Dvl-3 PDZ domain are clearly involved in the interactions. The binding constant derived from the titration experiment was (505.7± 84.8 µM) which was weaker compared to the adamantane containing compound **3** (K_D = 189.4 ± 11.2 µM)

The similarity between these two compounds concerned the carboxyl group and the hydrogen bond donor NH which should target the carboxylate binding region of Dvl-3 PDZ. The different K_D of both compounds is eventually due to the part which was

supposed to be directed to the hydrophobic pocket of the Dvl-3 PDZ. The occupancy of this hydrophobic binding pocket seems to be optimal for the adamantane containing compound **3** but not for sulfonamide containing compound **19**.

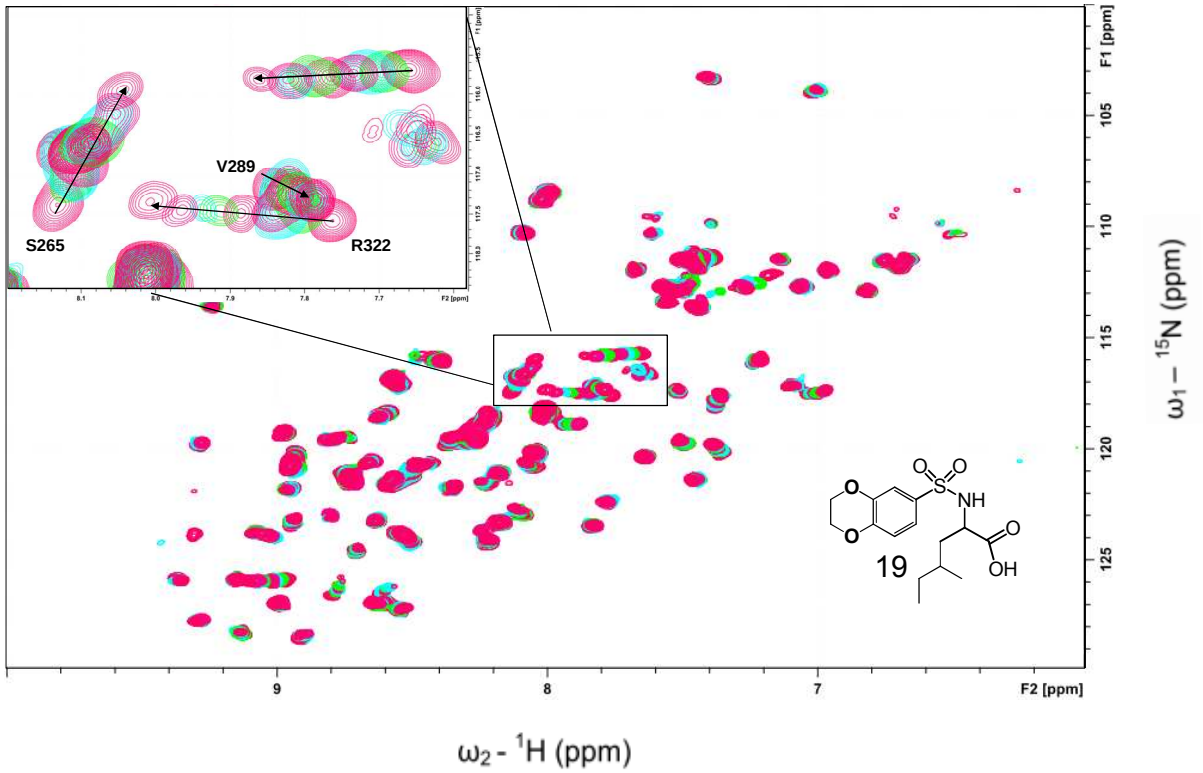

Figure 2.6: ^{1}H-^{15}N HSQC spectra of Dvl-3 PDZ domain alone and varying concentrations of compound 19. The zoom shows the gradual increasing of shifts with residues surrounding the binding pocket of Dvl-3 PDZ

.

2.1.5 Modifications of sulfonamides scaffolds

An analysis of the results on the sulfonamide scaffolds **18** and **19** suggested to explore the hydrophobic pocket of Dvl-3 PDZ by introducing different small substituents at the 5-position and to use also cycloalkane group at the 6-position. (Figure 2.7)

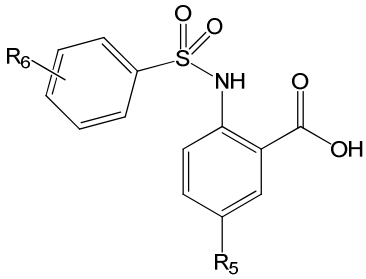

Figure 2.7: compound series 36 - 41

Compound **18** (ΔCSP = 0.12 ppm) contains at the 5-position a benzene ring which might have significantly contributed to the interaction with the protein. Compound **19** (ΔCSP = 0.12 ppm) contains a heterocyclic moiety at its 6-position. The combination of these two features might enhance affinity. Thus, a series of six compounds (**36 - 41**, Table 2.5) were further design and found in the library of small molecules of the company Enamine.

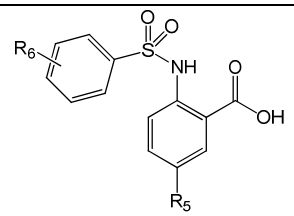

Compound Nr	R_5	R_6	ΔCSP (ppm)
36	F	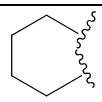	0.27
37	F	(2,3)-CH_3—	0.23
38	F	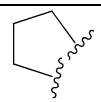	0.26
39	F	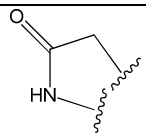	0.18
40	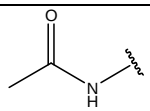	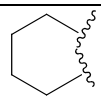	0.04
41			0.09

Table 2.5: Chemical shift perturbation values of Dvl-3 PDZ resonances for compounds (36 - 41) ΔCSP is the mean value of 4 amino acid residues showing chemical shift perturbations

The new compounds showed a 2-fold increase in chemical shift perturbations with respect to compound **19**. Compounds **36 - 38** have shown chemical shift perturbation values ranging from 0.23 to 0.27 ppm and were therefore classified as strong binders. The three compounds have in common the fluorine group at the 5-position which might have significantly contributed to the interaction. When the fluorine at the

5-position was replaced by dimethylamine and isopropyl groups respectively, the values of chemical shift perturbation decreased as observed for compounds **40** (ΔCSP = 0.04 ppm) and **41** (ΔCSP = 0.09 ppm). However, compound **41** was more active than compound **40**, which was explained by the fact that the isopropyl group is more hydrophobic than a dimethylamine group since both moieties are considered to be directed inside the hydrophobic binding pocket.

Compound Nr	Compound structure	K_D (µM)
36	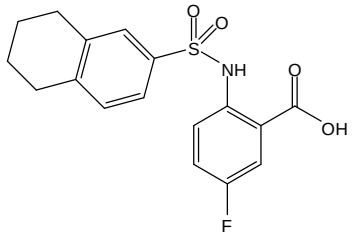	80.6 ± 6.1
37	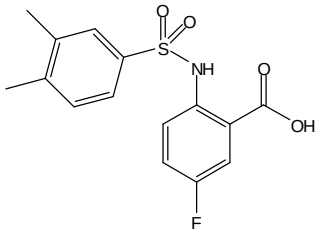	140.6 ± 14.1
38	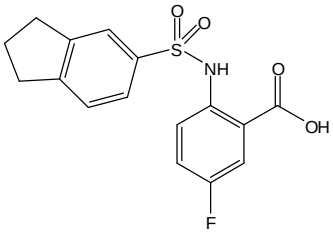	83.9 ± 7.8

Table 2.6: Dissociation constant derived from NMR methods for compounds 36-38 against Dvl-3 PDZ

The binding constant of compounds **36 - 38** were evaluated by NMR titrations. (Table 2.6) Compounds **36** (K_D = 80.6 ± 6.1) µM and **38** (K_D = 83.9 ± 7.8 µM) have shown the best values while compound **37** (K_D = 140.6 ± 14.1 µM) was less effective. These differences are mainly due to the nature of the substituent at the 6-position. Compounds **36** and **38** that bear respectively cyclohexane and cyclopentane at their 6-position yielded better K_D values than compound **37** that bears a methyl group at the 6-position.

2.1.5.1 X-ray crystal structure

To further investigate the interactions between our compounds and Dvl-3 PDZ, an x-ray structure of Dvl-3 PDZ in complex with compound **36** was determined with a resolution of 1.43 Å (Figure 2.8 A and B) while a structure of 1.6 Å resolution was obtained for Dvl-3 PDZ in complex with compound **37** (Figure 2.9 A and B)

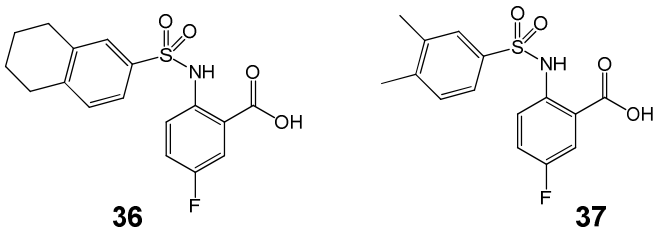

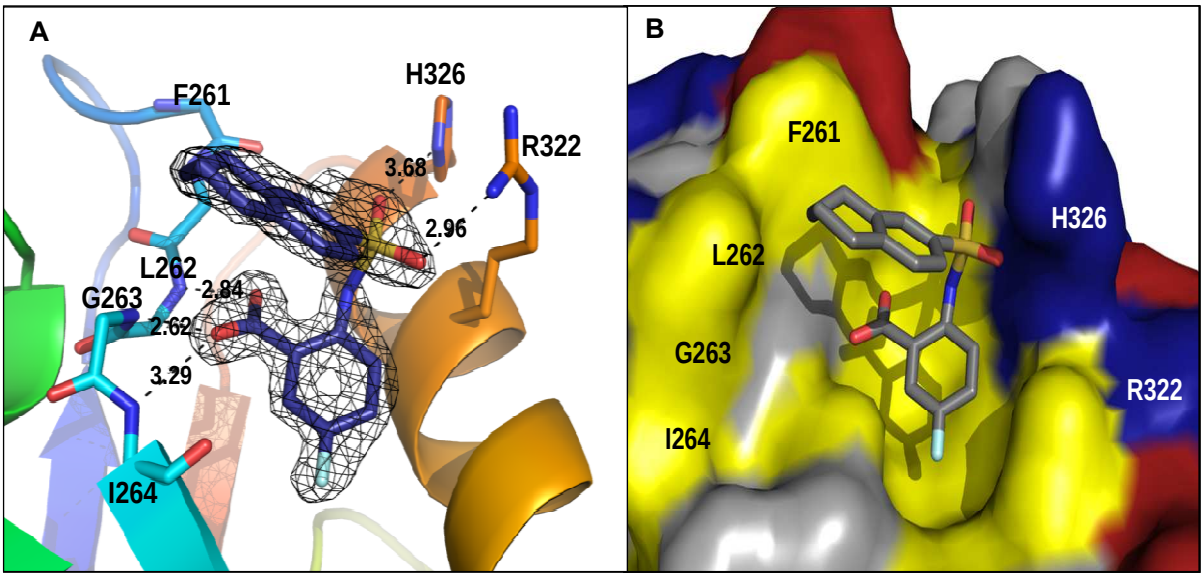

Figure 2.8: A) Dvl-3 PDZ in complex with compound **36** showing hydrogen bonding interactions with carboxylate binding loop region. B) Surface representation of Dvl-3 PDZ in complex with compound **36.** Positively charged amino acid are highlight in blue and negatively charged amino acid are highlight in red

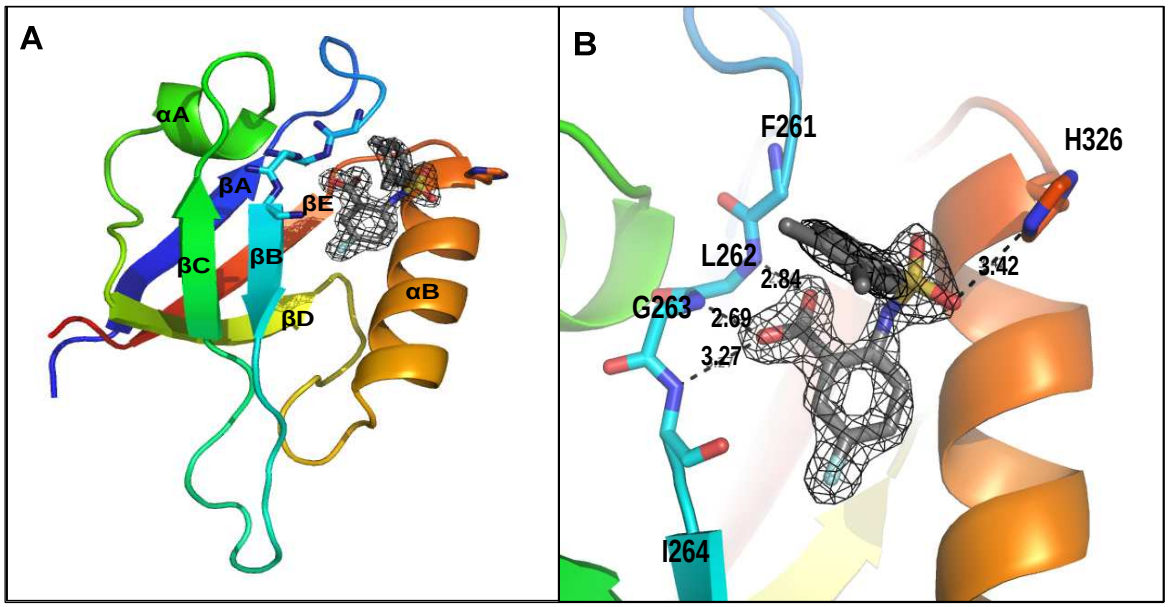

Figure 2.9: A) Dvl-3 PDZ in complex with **37.** B) Dvl-3 PDZ in complex with **37** showing hydrogen bonding interactions with carboxylate binding loop region

The Dvl-3 PDZ **36** complex structure shows the aromatic ring of the antranilic acid pointing into the hydrophobic binding pocket while the carboxylic acid is forming hydrogen bonding with the carboxylate binding loop region and the two oxygen atoms of the sulfonamide form hydrogen bonds with the side chains of histidine and arginine. There are a total of 5 hydrogen bonding interactions. (Figure 2.8 A)

The same observations were made on the Dvl-3 PDZ-**37** complex structure, however, with some differences concerning the number of hydrogen bonding interactions which was 4. (Figure 2.9 B) Only one oxygen atom of the sulfonamide was found to form a hydrogen bond with the side chain of histidine and no hydrogen bond was observed involving the side chain of arginine.

2.1.5.2 Further modifications

In our desire to further explore the importance of fluorine inside the hydrophobic pocket, it was replaced by bromine, chlorine and a methyl group, yielding compounds **42- 44.** (Table 2.7)

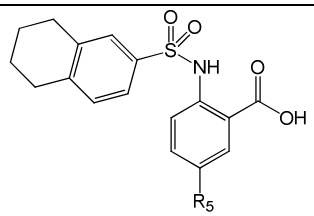

Compound Nr	R_5	ΔCSP (ppm)	K_D (µM)
42	Br	0.23	20.6 ± 2.4
43	Cl	0.28	41.2 ± 3.1
44	CH_3	0.26	62.5 ± 4.7

Table 2.7: Chemical shift perturbation values of Dvl-3 PDZ resonances and dissociation constant derived from NMR methods for compounds (36 – 41)

This resulted in increased values of chemical shift perturbations and we then categorized as strong binders. The binding constant was improved in comparison with compound **36** by a factor of 4 when substituting with bromine, 2-fold with chlorine and 1.5-fold with methyl. These results could be explained in terms of occupancy of the hydrophobic pocket. Fluorine which is the most electronegative atom is smaller than chlorine and bromine. So in terms of hydrophobic pocket occupancy the classification could be seen as follows: Br > Cl > F. In fact according to Biffinger [147], the concept of polar hydrophobicity was used to describe the phenomenon in which fluorinated fragments are less able to engage in dispersion-based interactions with aqueous solvent than alkyl or aryl groups. Fluorine is considered as bioisoster of methyl groups, therefore the K_D obtained with methyl group as replacement of fluorine could explain the better value obtained with the methyl. Chlorine is a moderate halogen bond acceptor, besides being larger in size than fluorine. The introduction of bromine at the 5-position yielded compound **42** (K_D = 20.6 ± 2.4 µM) with the best value of binding constant. Therefore, bromine which is electronically weaker, but larger in size and also more lipophilic resulted in an increase of binding constant.

To further explore the hydrophobic binding pocket, three other substituents such as 1,4-dioxepane ,1,3-dioxolane and a difluoro methoxy group were explored.

(Figure 2.10) These compounds (**45**, **46** and **47**) showed a decrease of chemical shift perturbations, indicating that they are not substitutions supporting interaction.

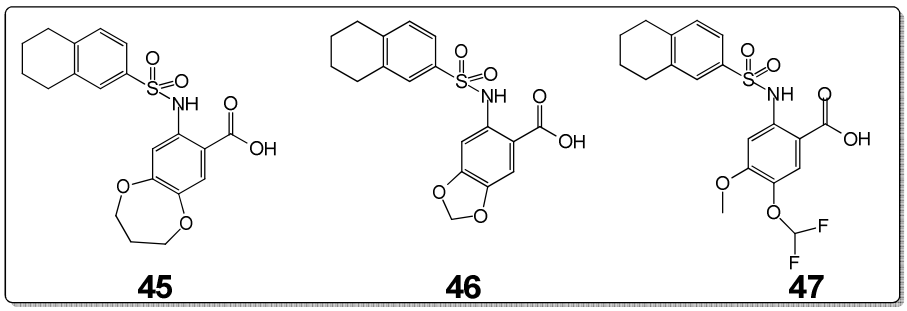

Figure 2.10: Compounds containing substituents with heteroatoms at the R_5-position

In summary, the hydrophobic pocket was able to accommodate a CH_3 group, but not 1,4-dioxepane, or 1,3-dioxolane. This obviously due to steric hindrance.

Since the replacement of fluorine by chlorine and bromine led to an improvement of binding affinity, we synthesized new compounds (**48 – 55**) with bromine and also with a trifluoromethyl group in the 5-position. (Table 2.8).

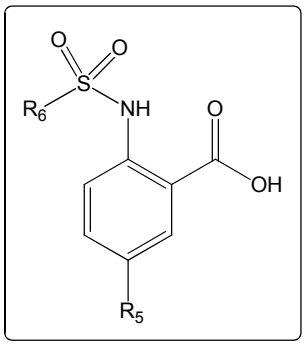

Compounds 48 - 55

Compound Nr	R_5	R_6	ΔCSP (ppm)	K_D (µM)
48	Br	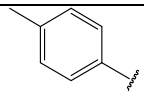	0.35	-
49	Br	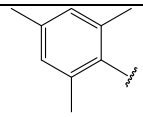	0.31	58.1 ± 2.1
50	CF_3	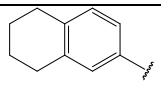	0.38	17.4 ± 0.5
51	CF_3	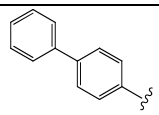	0.18	-
52	CF_3	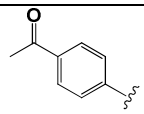	0.28	52.9 ± 1.7
53	CF_3	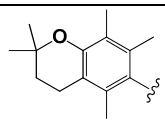	0.09	-
54	CF_3	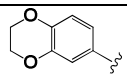	0.36	59.1 ± 1.5
55	CF_3	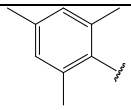	0.21	176.1 ± 8.5

Table 2.8 Chemical shift perturbation values of Dvl-3 PDZ resonances for compounds (48 – 55) and dissociation constant for compounds (49, 50, 52, 54 and 55)

On the whole new compounds, Six **(48**, **49**, **50**, **52**, **54** and **55)** showed stronger chemical shift perturbations. Compound **51** was a moderate binder and compound **53** a weak binder. The binding constants of five of these highly relevant binders were determined by ITC methods as described in 2.4. The best K_D value was obtained for compound **50** (K_D = 17.4 ± 0.5 µM) which in terms of molecular structure is similar to compound **36** with the only difference that the fluorine was replaced by the trifluomethyl. From these new and previous results, we derived the conclusion that the nature of substituent at the R_5-position contributes to the affinity in the following order: CF_3 > Br > CH_3 > Cl > F

2.1.5.3 Cell Proliferation Assay

At this stage of the work, we evaluated the cytotoxicity of our best compounds before synthesizing further derivatives. This was done in collaboration with Liang Fang from the research group of Prof. Dr. Walter Birchmeier (MDC). The effect of compounds **36**, **42**, **43**, **44** and **50** were examined by using the MTT cell proliferation assay. In this experiment, HEK293 cells were plated on 96-well plates and treated with different concentrations of compounds. After 24 h of treatment, 20 µl of MTT solution (5 mg/ml) were added into each well. After 2 h of incubation, cell culture medium was replaced with 50 µl DMSO, and the signal of the purple formazan, produced by living cells, was measured using the plate reader. Three sets of independent experiments were performed and each data point was normalized against the controls.(Figure 2.13 and Table 2.9)

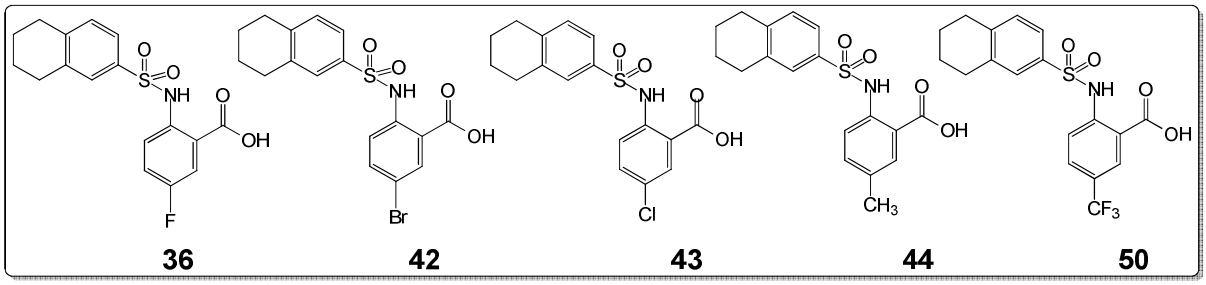

Figure 2.12: Compounds used for cell proliferation

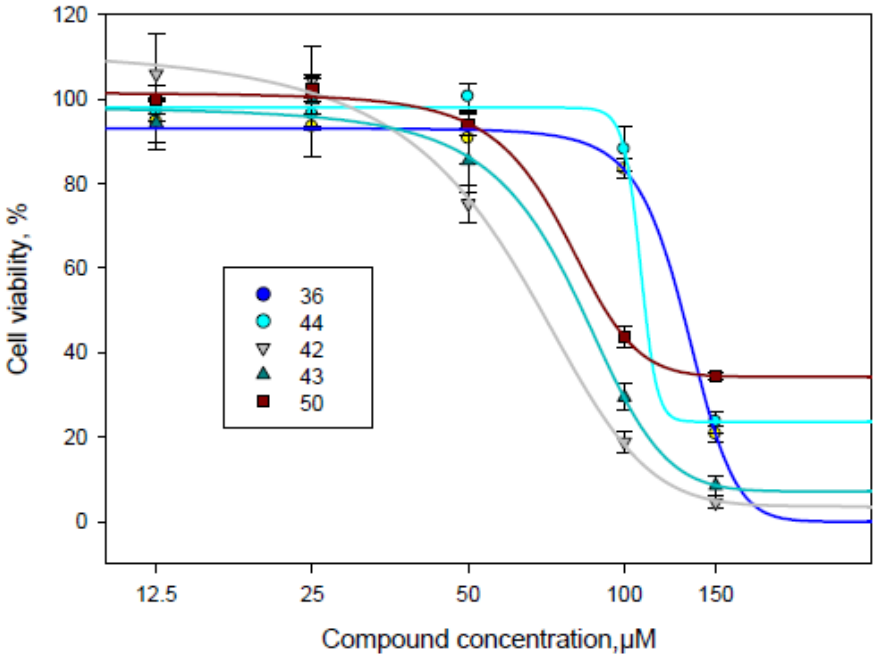

Figure 2.13: cell viability assays of compounds 36, 44, 42, 43, 50

Compound Nr	EC_{50} (µM)
36	131.5 ± 9.1
42	61.7 ± 4.8
43	80.7 ± 6.7
44	107.3 ± 7.1
50	101.7 ± 8.1

Table 2.9: Half-maximal effective concentration (EC_{50}) of compounds 36, 42, 43, 44 and 50

It appears that compounds **36**, **42**, **43**, **44** and **50** exhibited EC_{50} values in the range of 61 -131 µM, Compounds **36** (EC_{50} = 131.5 ± 9.1 µM) and **44** (EC_{50} = 107.3 ± 7.1 µM) are the least toxic. With the EC_{50} value of 61.7± 4.8 µM, compound **42** that bears the bromine group at the 5-position was the most toxic. Since the difference between the five compounds resides in the nature of substituent of the 5-position, we derived the conclusion that the substituent at the 5-postion is very relevant to the cytotoxicity, and therefore the toxicity of the compounds shown in Figure 2.12 decreases in this order: Br > Cl > CF_3 > CH_3 > F

2.1.5.4 Exploration of compounds containing a methyl group at the 5-position

The cytotoxicity results dictated us to further explore new molecules containing a methyl group or trifluoromethyl group at the 5-position. This was done in collaboration with Annika Kreuchwig and Dr. Gerd Krause of the Structural Bioinformatics and Protein design group of the Leibniz-Institut für Molekulare Pharmakologie (FMP). By choosing a methyl group at the 5-position, our expectation was to improve the binding constant and to reduce also the cytotoxicity. To achieve our aim, a series of 21 compounds (**56** – **76,** Table 2.10) were obtained from the company Enamine.

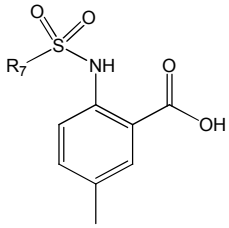

Nr	R_7	ΔCSP (ppm)	Nr	R_7	ΔCSP (ppm)
56	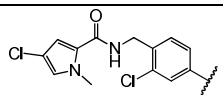	0.38	**67**	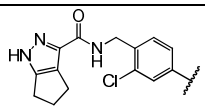	0.35
57	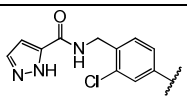	0.28	**68**	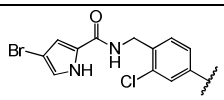	0.36
58	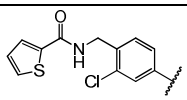	0.33	**69**	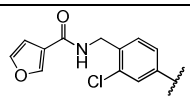	0.35
59	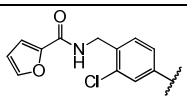	0.36	**70**	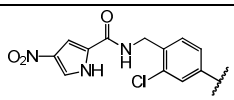	0.35
60	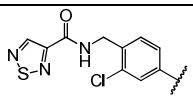	0.35	**71**	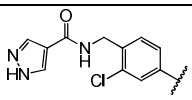	0.34
61	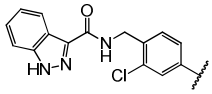	0.30	**72**	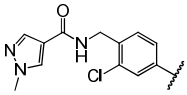	0.34
62	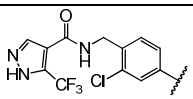	0.36	**73**	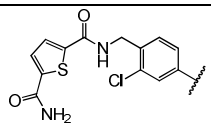	0.37
63	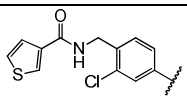	0.35	**74**	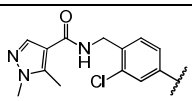	0.35
64	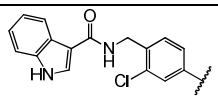	0.36	**75**	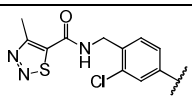	0.28
65	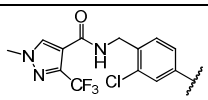	0.39	**76**	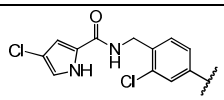	0.36
66	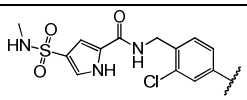	0.38			

Table 2.10: Compounds series 56-76 Chemical shift perturbation values of Dvl-3 PDZ resonances for compounds (56 – 76). ΔCSP is the mean value of 2 amino acid residues showing strong chemical shift perturbations

Analysis of the chemical shift perturbations revealed these compounds **56 - 76** to be strongly active. The effect of heterocyclic moiety attached at R_8-position was analyzed (Figure 2.14).

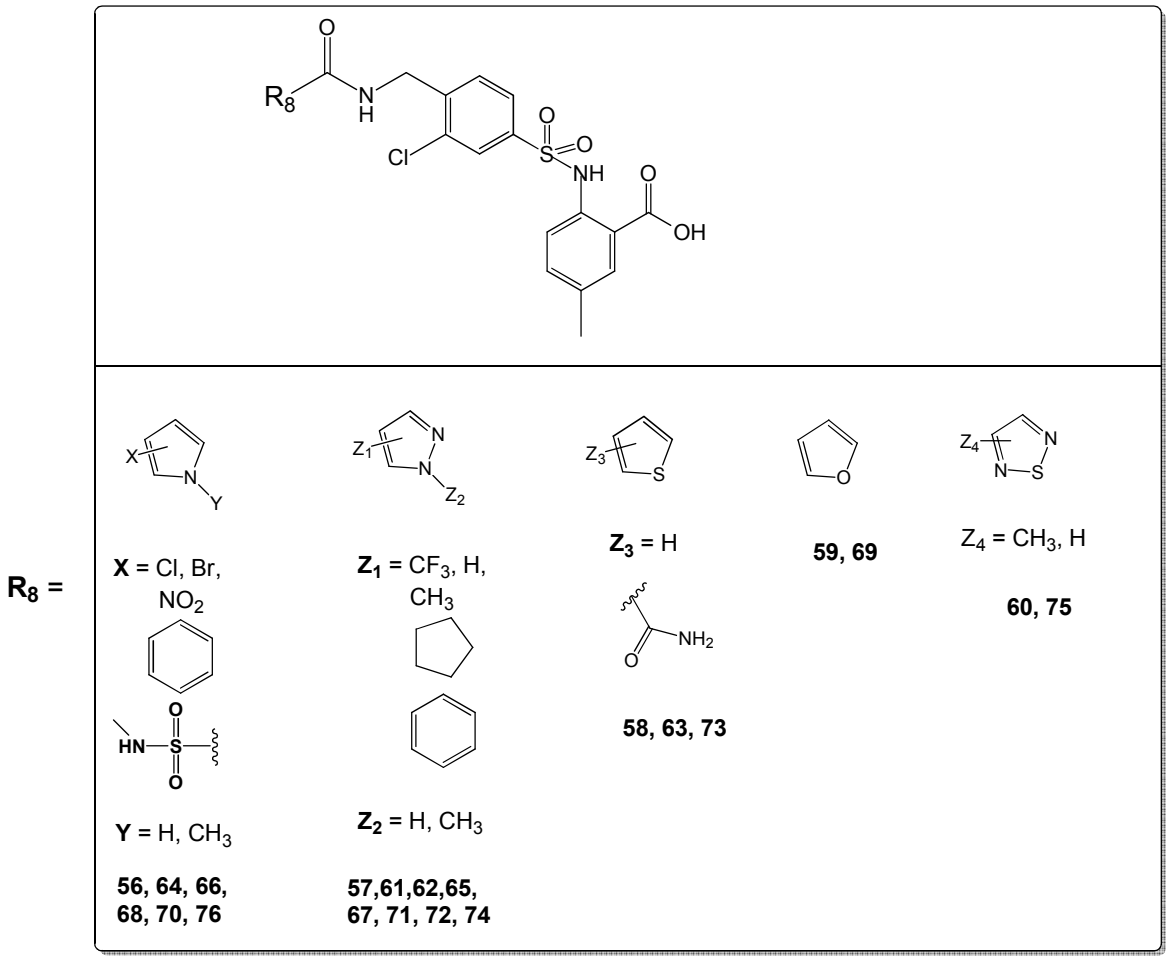

Figure 2.14 Structure of compounds series 56-76

R_8 is constituted of 5 different heterocyclic ring system including furane, thiophene, thiadiazol, pyrole and pyrazole, bearing different substituents. Therefore, compounds series **56-76** were classified into five groups: (i) pyrrole group of compounds (**56**, **64**, **66**, **68**, **70**, **76**); (ii) pyrazole group of compounds (**57**,**61**,**62**,**65**,**67**,**71**,**72**, and **74**); (iii) thiophene group of compounds (**58**,**63**,**73**); (iv) furane group of compounds (**59**, **69**) and (v) thiadiazole group of compounds (**60**, **75**). All these series of compounds have ΔCSP values in the same range. Ten compounds from these series comprising at least one from each group were selected for ITC measurements.

The values of the binding constants were in the range of 9.4 - 59.5 µM. (Table 2.11) The highest value arises from compound **59** (K_D = 59.5 ± 1.1 µM) containing a non

substituted furane moiety. Compound **60** (K_D = 32.8 ± 1.1 µM) containing the non substituted thiadiazole ring bound slightly better. Compounds **57**, **61** and **62** contain substituted pyrazole ring. Compounds **62** (K_D = 47.2 ± 1.2 µM) that contains a trifluoromethyl moiety as substituent at the pyrazole moiety shows the lower affinity of the pyrazole series.

Compound Nr	K_D (µM)
57	19.5 ± 1.2
59	59.5 ± 1.1
60	32.8 ± 1.1
61	9.4 ± 0.6
62	47.2 ± 1.2
64	21.8 ± 1.7
68	9.8 ± 0.3
70	43.8 ± 3.1
73	29.7 ± 1.9
76	12.5 ± 0.5

Table 2.11: Binding constants of compounds series 49-55 for Dvl-3 PDZ derived from ITC methods

The substitution of the trifluoromethyl group which is an electron withdrawing by electron donating group like methyl leading to **57** (K_D = 19.5 ± 1.2 µM) results in an enhancement of the binding constant by a factor of 2.5. The substitution by a phenyl ring leading to **61** (K_D = 9.4 ± 0.6 µM) further improved the binding constant 5 fold Compounds **64**, **68**, **70** and **76** contain pyrrole ring systems. Compound **70** (K_D = 43.8 ± 3.1 µM), the least active of this group, contains as substituent on the pyrrole ring an electron withdrawing group. Viewed together with the results on compound **62** containing pyrazole ring, we could derive a conclusion that an electron withdrawing group attached to the 5-heterocyclic membered-ring does not improve binding. The difference between compounds **64** (K_D = 21.8 ± 1.7 µM) and **61** (K_D = 9.4 ± 0.6) µM resides in the number of heteroatoms in the heterocyclic moiety. Compound **61** containing two heteroatoms has a better K_D value than compound **64** that contains only one heteroatom. The binding constant is further improved if

bromine or chlorine substituents are present on the pyrrole ring as observed for **68** (K_D = 9.8 ± 0.3) µM and **76** (K_D = 12.5 ± 0.5) µM

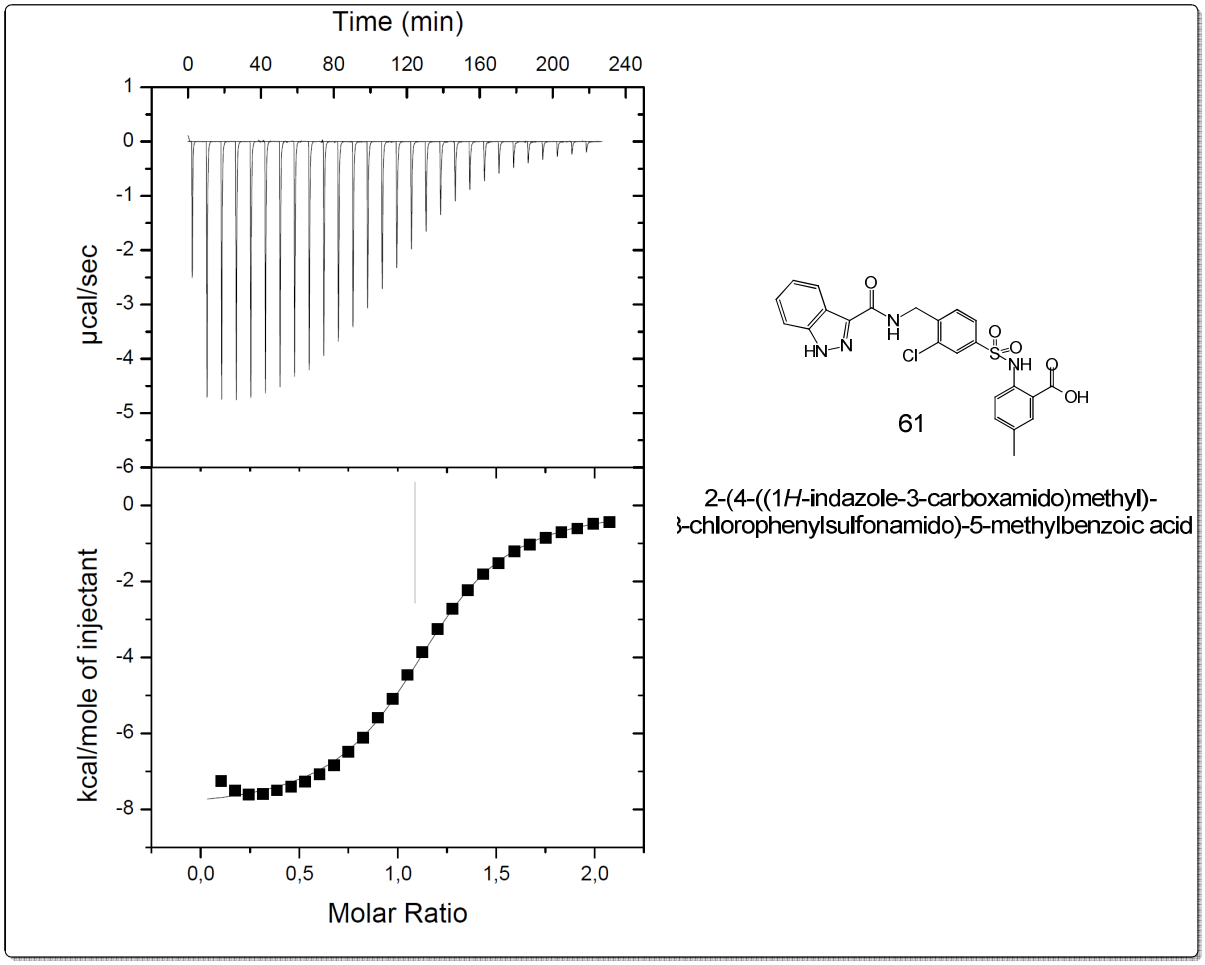

Figure 2.15: ITC data of compound 61 with Dvl-3 PDZ. A 200 µM ligand solution containing 2% DMSO was injected 30 times in 10 µL aliquots at 120 s intervals with a stirring speed of 1000 rpm into 1.4 mL sample cell containing Dvl PDZ domain at a concentration of 20 µM and 2% DMSO

2.1.5.5 Studies of compounds with Dvl-1 PDZ

The best compounds (**38, 42, 43, 44, 50, 61, 64, 68** and **76**) were evaluated for binding to the Dvl-1 PDZ. (Table 2.12) The analysis of these results revealed that our compound that binds tighly to DVL-3 PDZ also binds tighly to Dvl-1 PDZ.

Compound Nr	K_D (µM) Dvl-3 PDZ	K_D (µM) Dvl-1 PDZ	Selectivity factor $K_{D\ (DVL\ -1\ PDZ/DVL-3\ PDZ)}$
38	83.9 ± 7.8	114.4 ± 9.8	1.4
42	20.6 ± 2.4	18.2 ± 2.4	0.9
43	41.2 ± 3.1	45.6 ± 4.5	1.1
44	62.5 ± 4.7	60.5 ± 5.3	0.9
50	17.4 ± 0.5	24.5 ± 1.5	1.4
61	9.4 ± 0.6	2.4 ± 0.2	0.25
64	21.8 ± 1.7	8.0 ± 0.5	0.4
68	9.8 ± 0.3	4.7 ± 0.3	0.5
76	12.5 ± 0.5	4.7 ± 0.2	0.4

Table 2.12: Binding affinities of compounds (37, 42, 43, 44, 50, 61, 64, 68, and 76) for Dvl-3 PDZ and Dvl-1 PDZ. Selectivity of ligand to Dvl-3 PDZ over Dvl-1 PDZ as given by the K_D ratio of Dvl-1 PDZ over Dvl-3 PDZ, $K_{D\ (DVL\ 1PDZ/DVL3PDZ)}$

On the whole, the analysis of these results revealed that our compounds that bind tithly to Dvl-3 PDZ also bind tighly to Dvl-1 PDZ. Compounds **61**, **68** and **76** bind tighter to Dvl-1 PDZ than Dvl-3 PDZ. However, the K_D obtained are of same order of magnitude. The ITC data of compound **61** with Dvl-1 PDZ is shown in Figure 2.16

2.1.5.6 Competitive Binding of compound 68 with the Dpr/Frodo peptide

To obtain further insight into the binding mechanism of compound **61,** a competition assay was performed using the Dpr/Frodo peptide ($_{H2N}$-SGSLKLMTTV-$_{COOH}$)
1D ^{1}H spectra were recorded in the presence of compound **61** and the Dpr/Frodo peptide. Changes in the 1D spectra were observed when adding compound **61**.

The observed changes were simply due to the displacement of Dpr/Frodo peptide from the Dvl PDZ binding groove in the presence of compound **61.** Therefore, compound **61** inhibited interactions between Dpr peptide and the Dvl PDZ, hence inhibited interaction between Frizzled-7 and Dvl PDZ

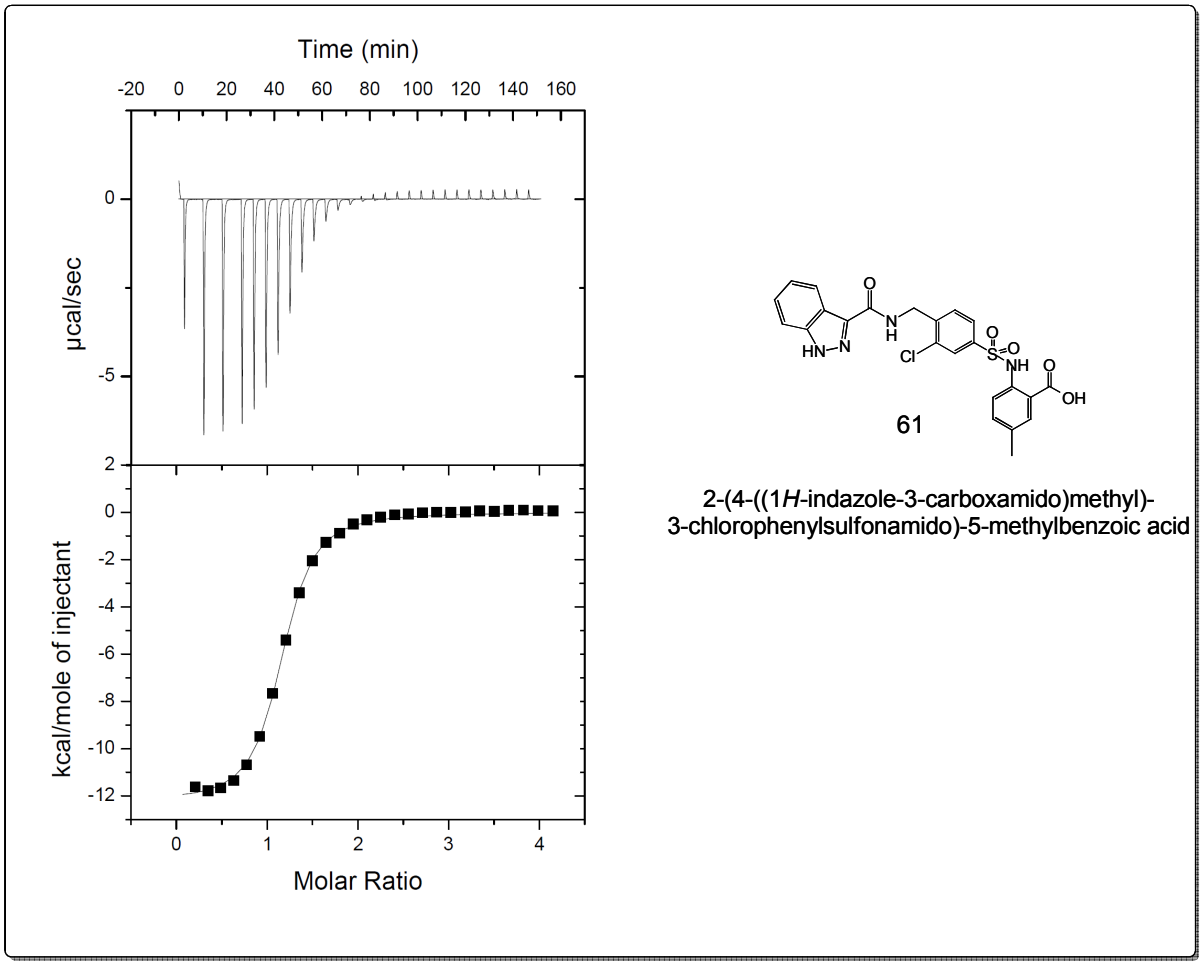

Figure 2.16: ITC data of compound 61 with Dvl-1 PDZ. A 200 µM ligand solution containing 2% DMSO was injected 30 times in 10 µL aliquots at 120 s intervals with a stirring speed of 1000 rpm into 1.4 mL sample cell containing Dvl PDZ domain at a concentration of 20 µM and 2% DMSO

2.1.5.7 Inhibition of Wnt signaling pathway

The direct interaction between the PDZ domain of Dvl and the conserved sequence C-terminal of the seventh transmembrane helix of the Wnt receptors has been described earlier. Therefore, Wnt signaling can be inhibited by blocking this interaction. In our desire to know wether our compounds inhibit Wnt signaling in the cell, the abilities of compounds **61**, **68** and **76** (Figure 2.17) to block the canonical Wnt pathway were evaluated using HEK293 cells. Prior to the evaluation in the Wnt signaling pathway, the cytotoxicity of these compounds were first evaluated, yielding to EC_{50} values in the range 139 - 200 µM. (Figure 2.18)

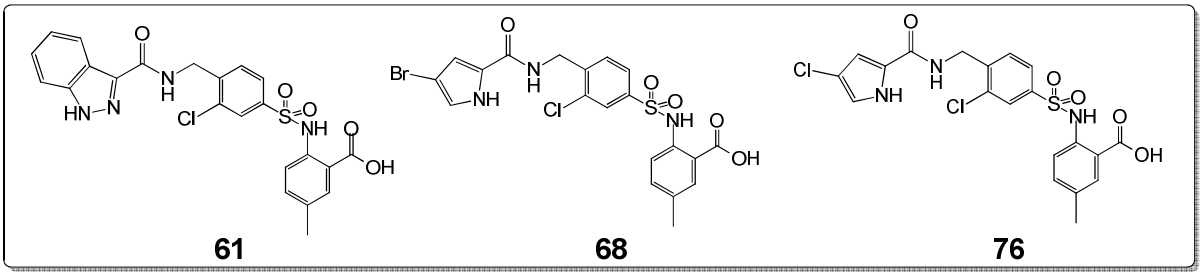

Figure 2.17: compounds 61, 68 and 76 used for the evaluation in wnt signalling pathway

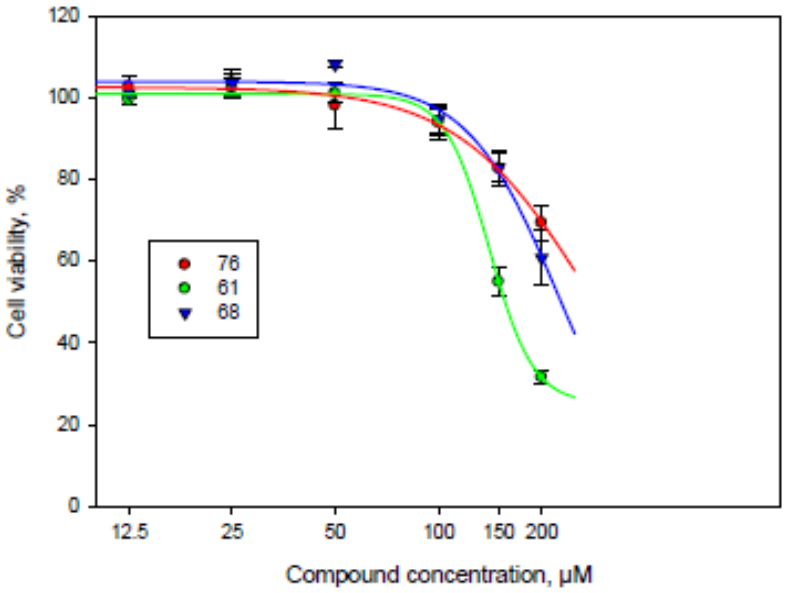

Figure 2.18: cell viability assays of compounds 61, 68 and 76

Wnt signaling in the HEK293 reporter cells, which express green fluorescent protein (GFP) in a Wnt-dependent manner, was stimulated by recombinant mouse Wnt3a (100 ng/ml) in the presence of compounds. After 24 h of treatment, the GFP signal was measured by flow cytometry. Figure 2.19 shows the level of Wnt signaling after treatment of our compounds at different concentrations. The level of Wnt signaling decreases with increasing concentration of compounds.

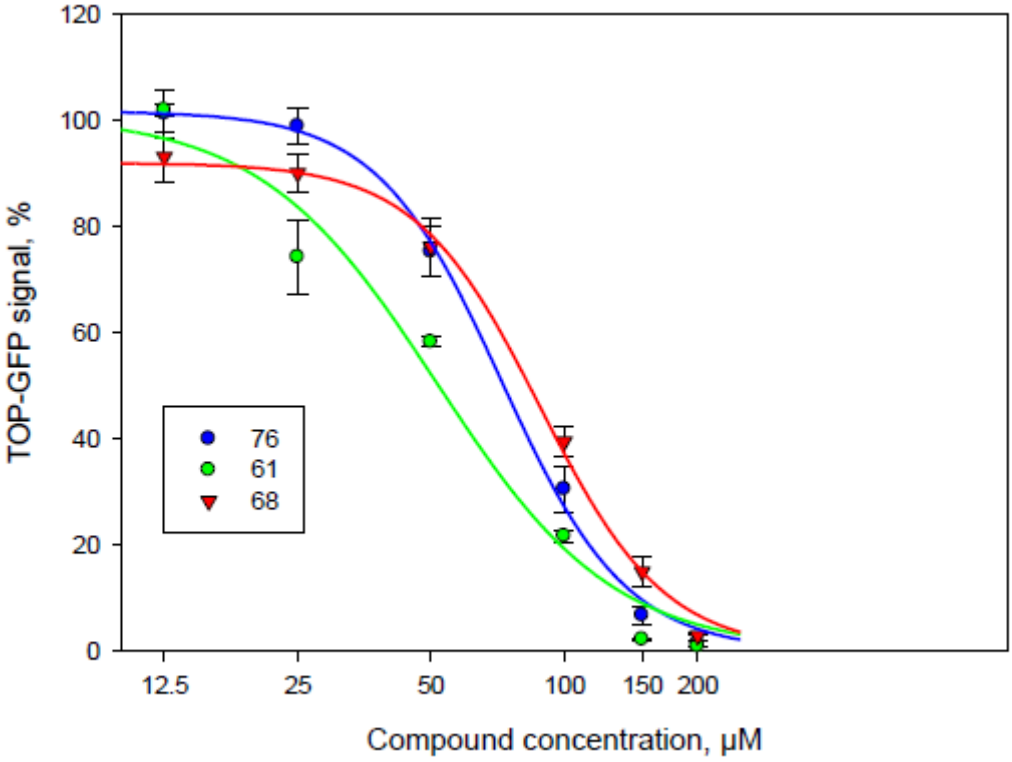

Figure 2.19: TOP- GFP (Tcf optimal promoter) reporter assay showing inhibition for compounds 61, 68 and 76. The three compounds effectively inhibit Wnt signaling pathway in a dose-dependent manner

The best inhibition was achieved with compound **61** with the half-maximal inhibitory concentration IC_{50} = 51.5 ± 1 µM. Compounds **68** (IC_{50} = 88.2 ± 4 µM) and **76** (IC_{50} = 72.2 ± 4 µM) inhibits less. These findings follow the trend of binding constants derived by ITC, **61** appearing to be the best.

2.1.5.8: Western blot experiment

To further characterize the behaviour of our compounds in the Wnt signaling pathway, western blot assays were undertaken. Cells were treated with Wnt3a (100ng/mg) for 24 h in the presence of the indicated compounds, lysed and processed for western blot. Protein level of β-catenin was detected by anti-β-catenin antibody. α-tubulin was served as loading control.

The analysis of the western blots (Figure 2.20) clearly revealed that compounds **61**, **68** and **76** inhibit accumulation of β-catenin in Hela cells treated with Wnt3a.

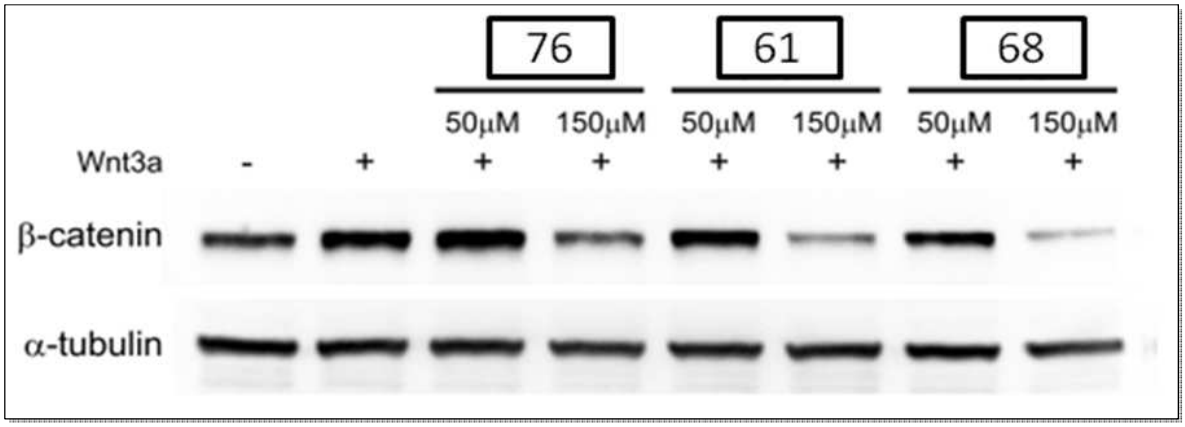

Figure 2.20: Compounds (76,61,68) inhibit accumulation of β-catenin in Hela cells treated with Wnt3a. Cells were treated with Wnt3a (100ng/mg) for 24 h in the presence of the indicated compounds, lysed and processed for western blots. The antibody β-catenin. α-tubulin served as loading control

Taken together, these results suggest that compounds **61**, **68** and **76** inhibit the transcriptional activity of TCF by directly suppressing Dvl PDZ mediated nuclear translocation of β-catenin.

2.1.6 Selectivity testing using a set of selected PDZ domains

Six other PDZ domains were tested for selectivity: the first, the second and the third PDZ domain of PSD95 which belongs to class I, the Shank-3 PDZ, a member of class II, the AF-6 PDZ, a member of class II, and the α-syntrophin PDZ. Chemical shift perturbation values are reported in Table 2.13.

	ΔCSP (ppm)					
Compound Nr	PSD95-1 PDZ	PSD95-2 PDZ	PSD95-3 PDZ	AF-6 PDZ	Shank-3 PDZ	α-1 Syn PDZ
3	0	0	0.03	0	0	-
11	0.01	0.01	0.01	0.01	0.01	0.04
13	0.01	0.01	0.01	0.01	0.01	0.08
19	0	0	0	0	0	0
36	0.09	0.06	0.01	0	0	0.05
37	0.07	0.08	0	0	0	0.07
38	0.05	0	0	0	0.01	0.05
42	0.01	0.01	0	**0.05**	0.01	0.01
43	0.01	0	0	**0.05**	0.01	0.01
44	0.01	0.01	0	**0.08**	0.01	0.01
49	0.01	0.05	0.06	0.04	0.05	0.04
50	0.01	0.05	0.02	-	0.04	-
52	0.02	0.04	0.01	0.04	0.05	0.06
54	0.02	0.05	0.01	0.04	0.05	0.08
57	0.03	0.08	0.03	0.01	0.05	0.08
60	0.04	0.08	0.05	0.01	0.05	0.08
61	**0.05**	**0.1**	**0.05**	**0.01**	**0.05**	**0.08**
62	0.03	0.06	0.04	0.01	0.05	0.06
64	0.03	0.02	0.04	0.01	0.05	0.08
68	**0.06**	**0.09**	**0.06**	**0.01**	**0.05**	**0.07**
69	0.02	0.06	0.01	0.01	0.03	0.07
70	0.06	0.09	0.05	0.01	0.05	0.08
73	0.04	0.1	0.03	0.01	0.06	0.09
76	0.07	0.09	0.1	0.01	0.05	0.08

Table 2.13: Selectivity of ligands derived from chemical shift perturbation of compounds other PDZ domains. The PDZ domain set includes PSD95-1, PSD95-2, PSD95-3, Shank-3, α-1 Syn and AF-6. ΔCSP is the mean value of 03 amino acid residues showing chemical shift perturbation.

Binding assays involving our compounds and PSD95-1 PDZ, PSD95-2 PDZ, PSD95-3 PDZ, shank-3 PDZ, AF-6 PDZ and α-1-Syn PDZ have revealed strong preference for Dvl PDZ. According to the determined chemical shift perturbations, most of the compounds bound only in negligible manner these PDZ domains. However, a few compounds have shown weak interactions (0.05 < ΔCSP ≤ 0.1) with these PDZ domains as depicted in Figure 2.21. Remarkably, α-Syn PDZ interacted with thirteen compounds weakly, followed by PSD95-2 PDZ showing weak interactions with ten compounds. Among those are compounds **61** and **68** which are the best compounds with respect to Dvl-1 PDZ binding. The binding constants for the interactions with PSD95-2 PDZ are 482.7 ± 65.2 μM for compound **61** and 446.8 ± 35.1 μM for compound **68**.

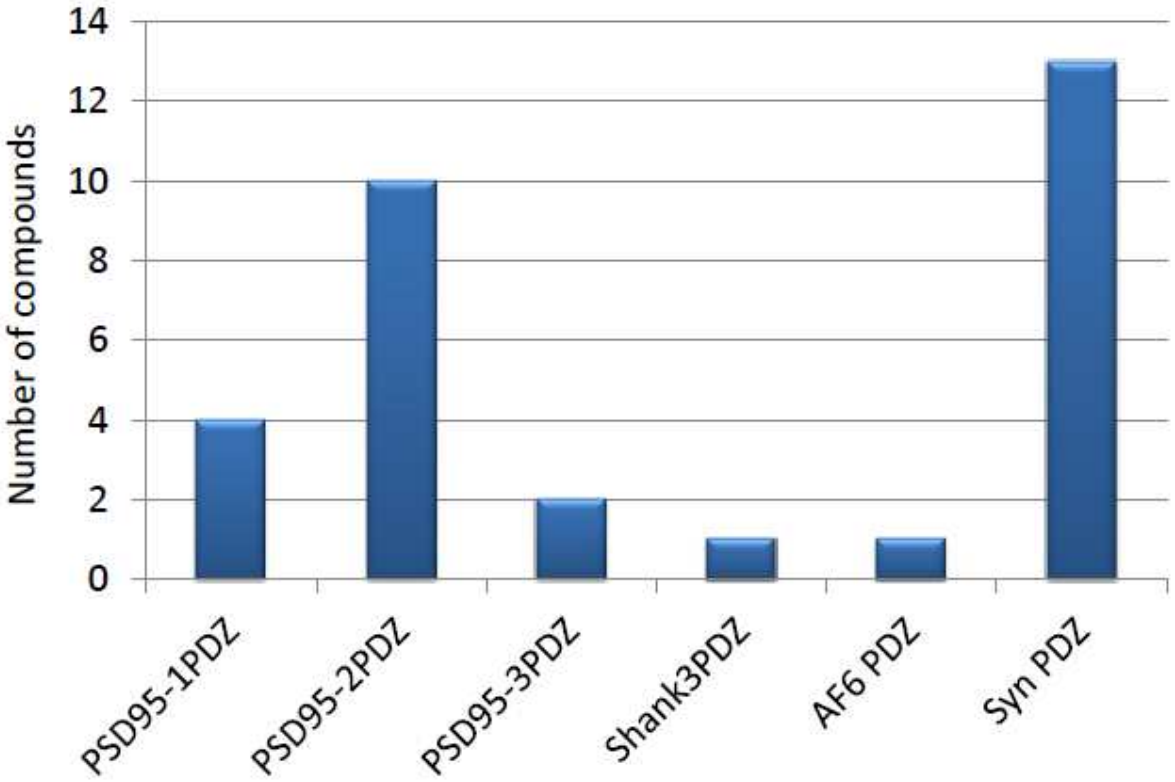

Figure 2.21: Number of compounds showing weak interactions with PDZ domains other than Dvl-1/3 PDZ. (0.05 < ΔCSP ≤ 0.1).

Compounds **42**, **43** and **44** that are extremely selective also have shown weak interaction with AF-6 PDZ. We see the reasons for this in the contribution of the substituent at the 5-position that is pointing into the hydrophobic pocket of AF-6 PDZ.

These findings led to the conclusion that our compounds were selective for Dvl PDZ. This might be due to a unique feature of the domain. Arg322 was crucial for interactions with Dvl PDZ and explained the selectivity obtained with respect to other PDZ domains. (Figure 2.22). Also, this might be due to the larger hydrophobic cavitiy for the side chain of the C-terminal residue of the interacting peptide.

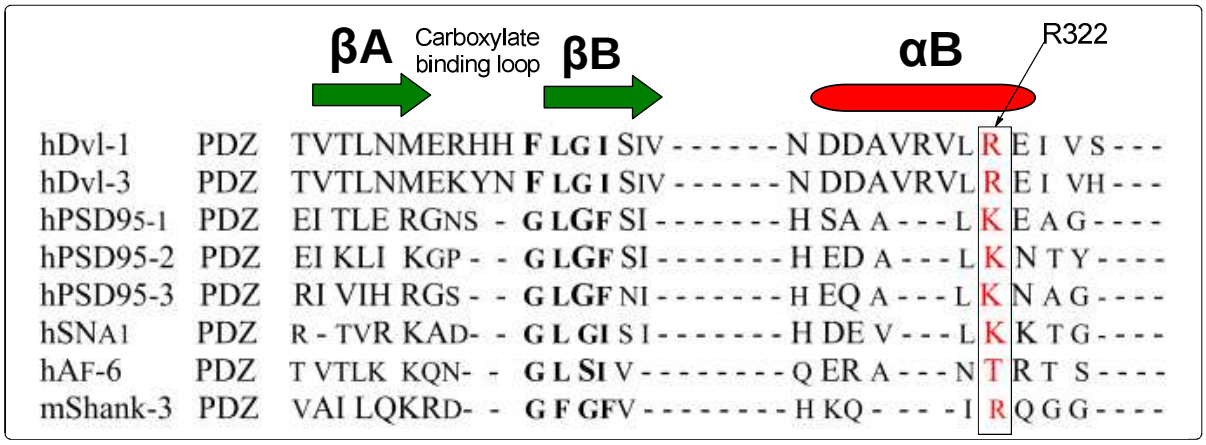

Figure 2.22 Structure-based alignment of the amino acid sequences of Dvl-1/3 PDZ; PSD95-1,2,3 PDZ; Shank-3 PDZ; AF-6 PDZ and α-1-Syn PDZ. Bold black are residues of the peptide binding groove. Arg322, (red) was crucial for interactions with Dvl PDZ and explained the selectivity obtained with respect to other PDZ domains.

2.2 AF- 6 PDZ

Small molecules inhibitors of AF-6 PDZ were synthesized based on compound **81** (5-(4-trifluoromethylbenzyl)-2-thioxo-4-thiazolidinone), a previous scaffold developed by Joshi et al.[102] The above-mentioned compound was identified as a reversible, efficient binder to the AF-6 PDZ domain, with a binding constant of 100 µM. The solution structure of AF-6 PDZ in complex with compound **81** is shown in Figure 2.23. The CF_3-phenyl group is deeply embedded in the hydrophobic pocket and significantly contributes to the interaction between compound **81** and AF-6 PDZ.

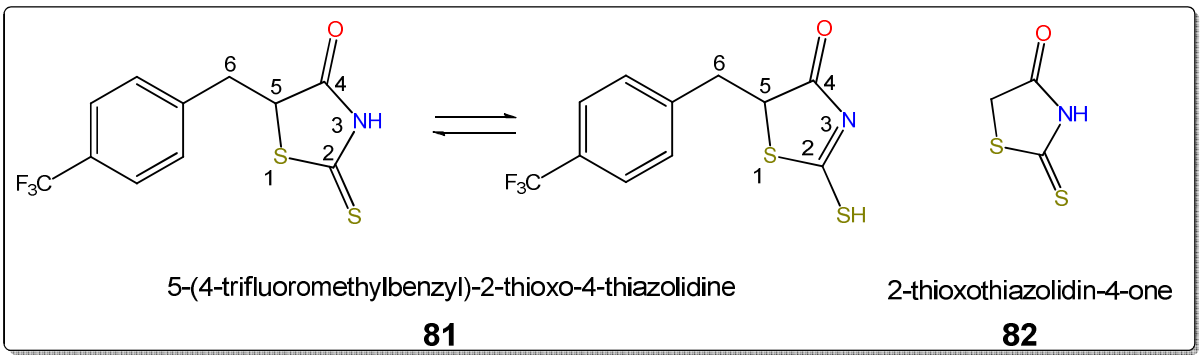

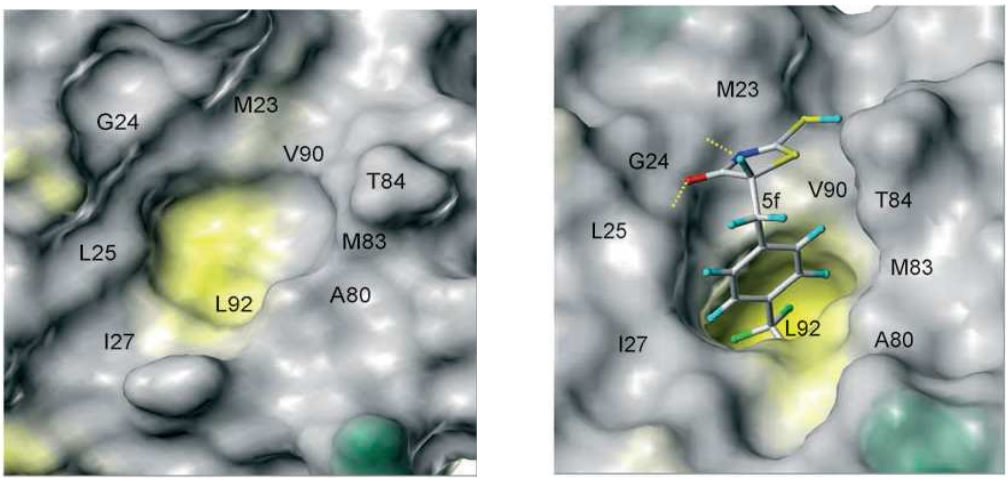

A B

Figure 2.23: A) Surface representation of the AF-6 PDZ domain without ligand, 1XZ9, B) Solution structure of AF-6 PDZ in complex with **81**: hydrophobic areas (yellow); hydrophilic areas (green); hydrogen bonding interaction (yellow-dote line).

The N3 and the O4 of ligand **81**, form hydrogen bond with the backbone HN´s of residues Gly24 and Leu25. Compound **81** contains the 2-thioxothiazolidin-4-one **82** heterocycle also known as rhodanines, which is well known as a privileged scaffold in drug discovery. As an example, 5-arylidenerhodanine-3-carboxylic acids

83 are known as inhibitors of antiapoptotic protein-protein interaction between Bcl-2 and the Bax receptor.[148]

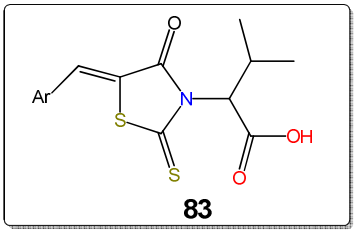

Figure 2.24: Inhibitors of interaction of Bcl-Xl and BH3 protein

In this part of the work, our attention will be focused on three points:

i) - The substitution of the rhodanine heterocyclic ring **82** by other heterocyclic rings and to investigate their role in the interaction. These heterocyclic rings include 2-iminothiazolidin **84**, pyrrolidine **85** and diyhdrofuran-2,5-dione **86**.

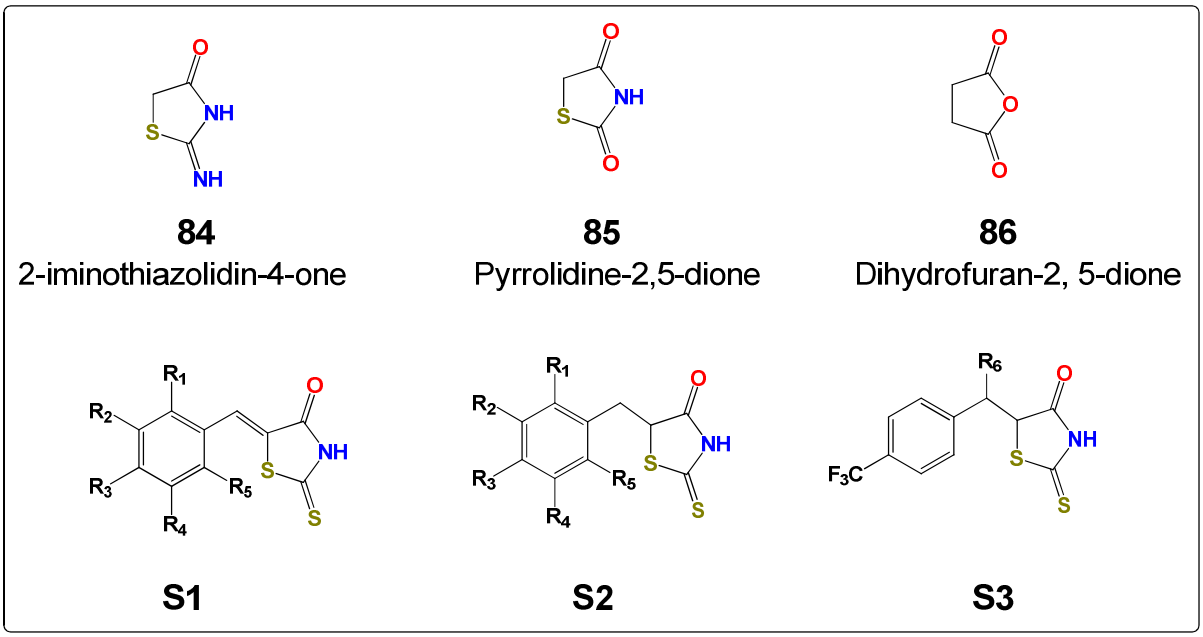

Figure 2.25: new hetorocyclic ring (84, 85, 86) and derivatives (S1, S2, S3) to be explored

ii) -The CF_3- group in compound **81** which is deeply embedded in the hydrophobic pocket in AF-6 PDZ will be replaced by other substituents on the benzene ring (**S1** and **S2**).

iii) Substitution at the 6-position of the linker (**S3**).

2.2.1 Effect of compounds containing 2-iminothiazolidin-4-one, pyrrolidine-2,5-one and dihydrofuran-2,5-dione on AF-6 PDZ

The activities of compounds **91a**, **91b**, **95** and **100** containing different heterocyclic rings were evaluated against AF-6 PDZ. The ΔCSP yielded are reported in table Table 2.14. Five amino acid residues including Leu25, Ser26, Ile27, Met83, Thr84 that surround the binding pocket as indicated in figure 2.23 were selected for the evaluation of chemical shift perturbations.

Compound **91a** (ΔCSP< 0.01) and **91b** (ΔCSP< 0.01) were completely inactive as compared to compound **81**; The SH group of the lead scaffold **81** is replaced by the NH group in compound **91a** and **91b**. NH and SH are all hydrogen bonding donors, however, they do not have the same side. Therefore, the NH group is not fitting into the hydrophobic pocket in which the SH group of the lead scaffold **81** was fitting. This could be the reason for the drastically loss of the activities of **91a** and **91b**.

Compound Nr	Compound structure	ΔCSP (ppm)
91a	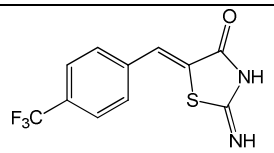	< 0.01
91b	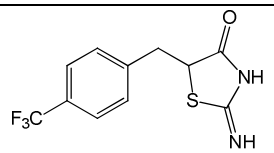	< 0.01
95	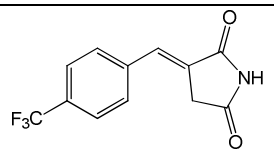	< 0.01
100	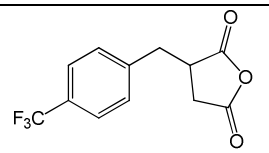	0.03

Table 2.14: Relative activity of compounds 91a, 91b, 95, 100 against AF-6 PDZ.

ΔCSPs values for 5 selected amino-acid residues of AF-6 PDZ (Leu25, Ser26, Ile27, Met83, Thr84).

The same argument could be used to justify the non-activity of compound **95** in which the **SH** group of the lead scaffold **81** was replaced by the oxygen atom. Compound **95** is also lacking the sulfur atom at the 1-position. This could be the main reason, because in the work of Vargas,[149] a ΔCSP value of of 0.11 ppm was observed for compound **81c** in which the sulfur atom was kept at the 1-position. Therefore, the replacement of the sulfur atom at the 1-position by a carbon atom renders the compound inactive. Despite the fact that compound **100** is already a reduced form, it exhibited a ΔCSP value of 0.03 ppm indicating very weak activity. The results obtained are a clear indication that the 2-thioxothiazolidin-4-one scaffold plays a very important role in the interaction between AF-6 PDZ and the ligand. The lead scaffold compound **81** undergoes thione-thiol tautomerism in solution.[150]

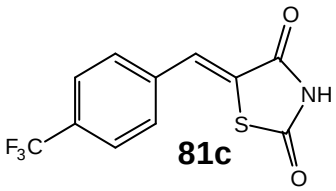

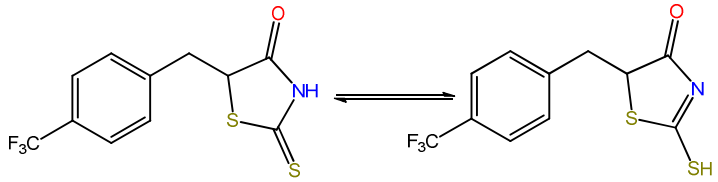

Figure 2.15: Tautomerism equilibrium of thiol/thione

This feature enables the SH group at the 2-position to be oriented towards a small hydrophobic cleft as observed in the complex structure shown in Figure 2.14. Therefore, replacement of the 2-thioxothiazolidin-4-one moiety **82** with other heterocycles such as 2-iminothiazolidin-4-one, Pyrrolidine-2,5-dione and dihydrofuran-2,5-dione resulted in a loss of activity.

2.2.2 Structure-Activity Relationships of 4-Thiazolidinone compounds series S1 and S2

Beside the synthesis, some compounds of **S1** were obtained from Kristian Strømgaard, our cooperation partner of the Department of Medicinal Chemistry at the University of Copenhagen.

The activities of compounds series **S1 (101a-101t)** and **S2 (101a-101i)** for the AF-6 PDZ are reported in (Table 2.15).

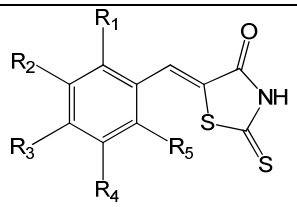

S1 = 101a-101t

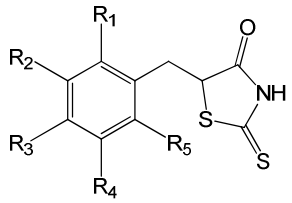

S2 = 102a-102j

S1	**S2**	R_1	R_2	R_3	R_4	R_5	ΔCSP(ppm)	
							S1	**S2**
101a	**102a**	OCH_3	H	OCH_3	H	H	0.05	0.1
101b	**102b**	OCH_3	H	H	OCH_3	H	0.05	0.1
101c	**102c**	F	F	F	F	F	0.08	0.17
101d	**102d**	OEt	H	H	OEt	H	0.05	0.10
101e	**102e**	F	H	F	H	H	0.07	0.15
101f	**102f**	OCH_3	H	OCH_3	H	OCH_3	0	-
101g	**102g**	OCH_3	H	OCH_3	OCH_3	H	0	-
101h	**102h**	OH	H	H	NO_2	H	0.05	0.08
101i	**102i**	OH	H	OH	H	OH	0	-
101j	-	OH	OCH_3	H	NO_2	H	0	-
101k	-	F	H	NO_2	H	H	0.01	-
101l	-	OH	OH	H	OH	H	0	-
101m	-	OH	H	OH	H	H	0	-
101n	-	OH	OH	OH	H	H	0	-
101o	-	OH	H	OH	H	H	0	-
101p	-	H	H	OH	OH	H	0	-
101q	-	OH	H	H	OH	H	0	-
101r	-	OH	H	H	H	H	0	-
101s	-	H	OH	H	H	H	0	-
101t	-	H	H	H	NO_2	H	0	-

Table 2.15: Relative activity of compounds S1 and S2 for AF-6 PDZ. CSPs values for 5 selected residues of AF-6 PDZ (Leu25, Ser26, Ile27, Met83, Thr84). i) 0 indicates no residue showing chemical shift changes; ii) – indicate not measured

The SAR investigation focused first on substitutions on the benzylidene ring with electron – donating groups such as methoxy **101a, 101b, 101f and 101g**.

Compounds **101a** and **101b** that contain two methoxy groups respectively at the (1,3) and the (1,4) position exhibited weak activity with the same value of ΔCSP = 0.05 ppm. On the contrary, compound **101f** and **101g** that contain three methoxy groups respectively at the (1,3,5) and the (1,3,4) positions were inactive. The replacement of methoxy groups at position (1,4) with ethoxy groups did not enhance the activity as observed for compound **101d** (ΔCSP = 0.05 ppm). We explored the 4-position with the electron-withdrawing group NO_2 (**101t**). No activity was observed. However, the addition of an OH group at the 1-position (**101h**) led to an active compound with a ΔCSP value of 0.05 ppm. The addition of a methoxy group at the 2-position led again to an inactive compound, **101j**. No activity was observed if the benzylidene ring was substituted by one or more hydroxyl groups. The substitution of two fluorines at 1-position and 3-position resulted in an increase of activity **101e** (ΔCSP = 0.07 ppm). Additional fluorine further improved the activity (**101c**, ΔCSP = 0.08ppm). Not surprisingly, the reduced forms of **101c** and **101e** exhibited the highest ΔCSP value **102c** (ΔCSP = 0.17) ppm and **102e** (ΔCSP = 0.15ppm). (Table 2.15).These are in agreement with the previous work[102] and a clear confirmation that the flexibility of the C-C bond linking the phenyl moiety and the heteroatom ring system is very important for the interactions. Compounds indication groups and position in favour or in disfavour of interactions with AF-6 PDZ are summarised in Table 2.16.

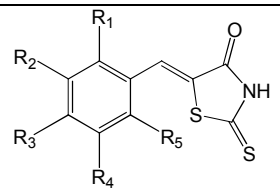

101a-101t

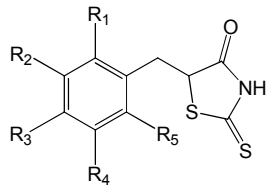

102a-102j

R_1	R_2	R_3	R_4	R_5	Observation
OCH_3	H	OCH_3	H	H	Favour
OCH_3	H	H	OCH_3	H	Favour
OCH_2CH_3	H	H	OCH_2CH_3	H	Favour
OCH_3	H	OCH_3	H	OCH_3	Disfavoured
OCH_3	H	OCH_3	OCH_3	H	Disfavoured
F	H	F	H	H	Favour
F	F	F	F	F	Favour
OH	H	H	NO_2	H	Favour
H	H	H	NO_2	H	Disfavoured
OH	OCH_3	H	NO_2	H	Disfavoured

Table 2.16: Summary of compounds indicating groups and position in favour or in disfavour of activity against AF-6 PDZ.

The binding constants of two compounds **102c** and **102e** that exhibited the highest values of ΔCSP were determined. The cross peak of Thr84 was one of those that was followed upon NMR titrations. The observed gradual change of chemical shifts indicates fast exchange between compound **102c** and the AF-6 PDZ. (Figure 2.17 B). A K_D value of (88.2 ± 6.3) µM was found for compound **102c** while a value of (150.4 ± 16.6 µM) was obtained for **102e.** These values are in the same order of magnitude as the value obtained for the lead scaffold **81** which was 100 µM. However, these results demonstrated that the hydrophobic pocket of the AF-6 PDZ prefers electronegative substituents on the benzene ring. The fluorine is the most electronegative compound while the electronegativity of CF_3 is intermediate between fluorine and chlorine. This can explain the fact that compound **102c** (K_D = 88 µM) binds a bit tighter than scaffold compound **81** (K_D = 100 µM).

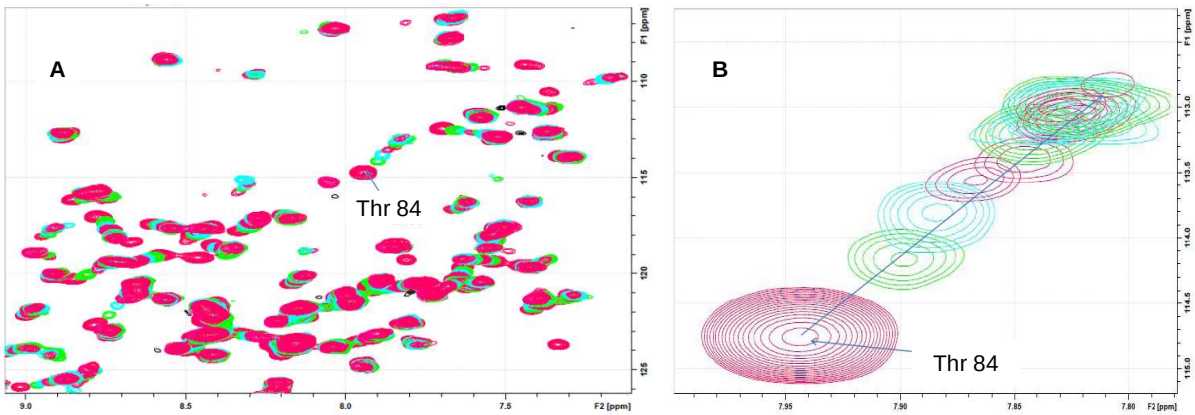

Figure 2.17: A) Overlay of ^{1}H-^{15}N-HSQC spectra showing the chemical shift changes upon titration of AF-6 PDZ with compound **102c**.The spectra shown are for 50 µM protein concentration and compound concentrations of 25, 50, 75, 100, 125, 150, 200, 250, 300, and 400 µM. B) Evolution of Thr 84 chemical shifts.

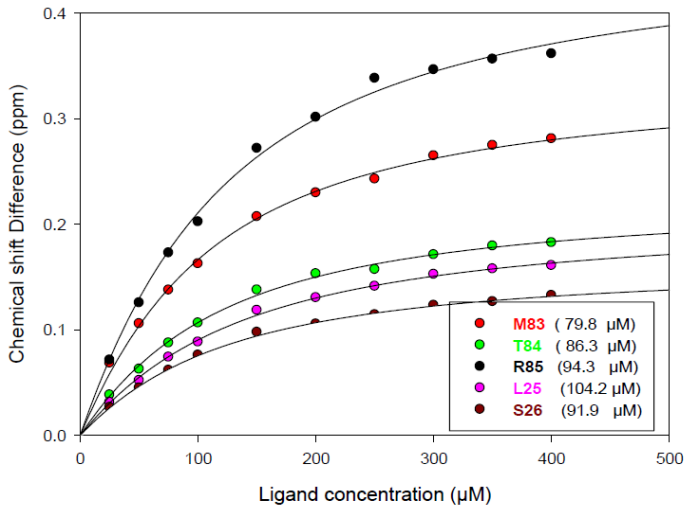

Figure 2.18: Determination of bindind affinities of AF-6 PDZ-102c interactions by NMR. 50 µM of AF-6 PDZ was titrated with increasing amounts of **102c**, and changes in the perturbed amide resonances (ΔCSP) were determined. Plots of (ΔCSP) as a function of ligand concentration are shown for 5 residues.

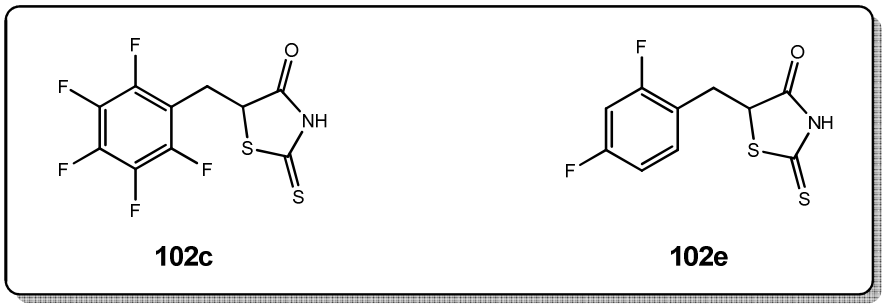

2.2.3: Structure-Activity Relationships study of 5-(4-Trifluoromethylbenzyl)-2-thioxo-4-thiazolidi-none: Compounds S3 (107a-107i)

Guided by the three dimensional solution structure of compound **81** in complex with AF-6 PDZ, some synthetically feasible molecules with substitutions at the 6-position of the linker were designed. Christian Schillinger, (Bioinformatics group of the FMP) performed the molecular modelling prior to the synthesis.

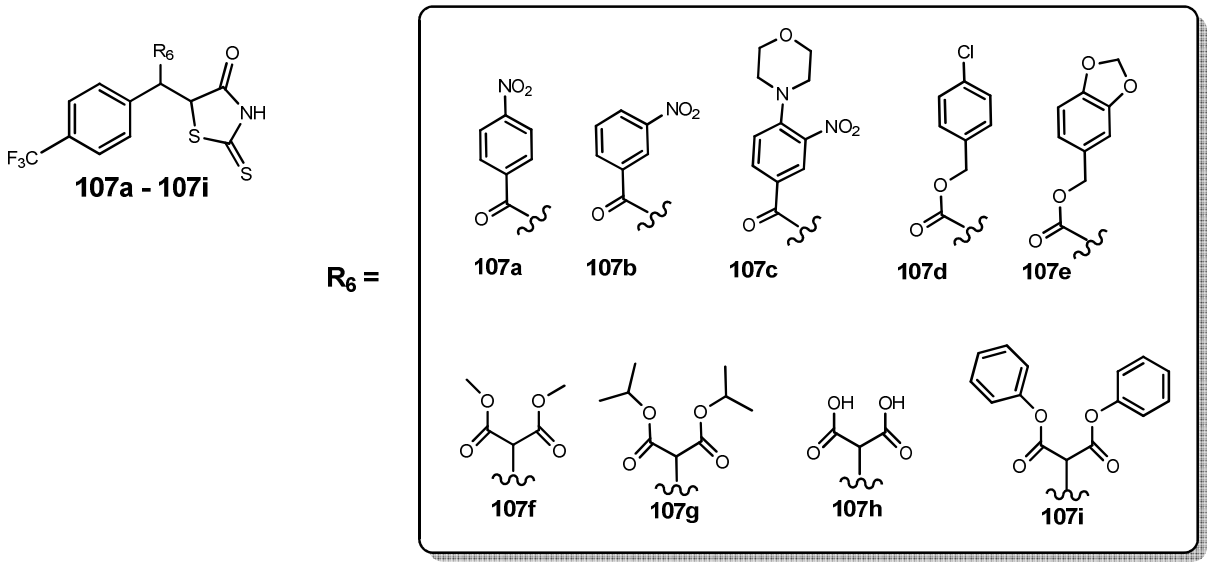

Figure: 2.19: structures of compounds series 107a-107i

The modification at the 6-position of scaffold **81** yielded the largest ΔCSP in the range of 0.04 - 0.31 ppm.The highest ΔCSP value was observed for compound **107b** (ΔCSP = 0.31 ppm) that contains a nitro group. However, the addition of the morpholino ring lowers the activity as observed for compound **107c** (ΔCSP = 0.12 ppm). This observation could be explained by the fact that there is no space in AF-6 PDZ that could facilitate the interaction with both groups and therefore a clash is observed, reducing activity. The same explanation could be given concerning compound **107i** (ΔCSP = 0.04) which contains two phenyl moieties. Compounds **107a** and **107b** contain both a nitro group at *meta* and *para* with respect to the ester group. Substitutions in the *meta*-position (**107b**) are preferred to the *para*-position (**107a)**. The binding constant obtained for the *meta*-position (**107b**) was 62.2 ± 3.2 µM while for the *para*-position (**107a**) it was 95.8 ± 6.3 µM. With the elongation of

substituent **107d** (ΔCSP = 0.1 ppm) and **107e** (ΔCSP = 0.16ppm) better ΔCSP values could not be obtained. Compound **107g** (K_D = 88.4 ± 4.3 µM) with isopropyl group was better compare to compound **107f** (K_D = 192.3 ± 11.1µM) which contain methoxy groups. Compound **107h** (K_D = 221.5 ± 13.2 µM) which contains hydroxyl groups was the least binder.

Compound Nr	ΔCSP (ppm)	K_D (µM)
107a	0.25	95.8 ± 6.3
107b	0.31	62.2 ± 3.2
107c	0.12	-
107d	0.1	-
107e	0.16	-
107f	0.2	192.3 ± 11.1
107g	0.26	88.4 ± 4.3
107h	0.2	221.5 ± 13.2
107i	0.04	-

Table 2.17: Chemical shift perturbation values of AF-6 PDZ resonances for compounds (107a-107i). Dissociation constant derived from NMR methods for compounds (107a, 107b, 107f, 107g, and 107h) derived from NMR methods

2.2.3 Testing compounds series S1 (101a - 101t) and S2 (102a - 102h) as ligand for other PDZ domains

Some compounds from the series **S1** and **S2** were evaluated against five other PDZ domains. Shank-3 PDZ, Dvl-1 PDZ, Dvl-3 PDZ, PSD95-1 PDZ and PSD95-2 PDZ The ΔCSP resulted are reported in Table 2.18.

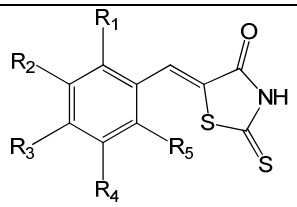

S1 = 101a-101t

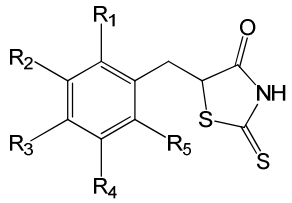

S2 = 102a-102j

S1	S2	Shank-3 PDZ		Dvl-1 PDZ		Dvl-3 PDZ		PSD95-1 PDZ		PSD95-2 PDZ	
		ΔCSP(ppm)		ΔCSP(ppm)		ΔCSP(ppm)		ΔCSP(ppm)		ΔCSP(ppm)	
		S1	**S2**	**S1**	**S2**	**S1**	**S2**	**S1**	**S2**	**S1**	**S2**
101a	**102a**	-	0.01	-	-	-	-	-	-	-	-
101b	**102b**	-	-	-	-	-	0	0	-	-	0.06
101c	**102c**	0.02	0.01	-	-	-	0	-	-	-	0.06
101d	**102d**	0.01	0.03		-	-	-	-	-	-	-
101e	**102e**	0	0	-	-	-	0.01	0	-	0	-
101h	**102h**	0.20	0.02	-	0	-	-	-	-	0	0
101i	**102i**	0	0.02	-	-	0.01	-	0	-	0	-
101j	**102j**	0	-	-	-	0	-	0	-	0.2	-
101l	-	0.05		-	-	0	-	0		0.07	-
101n	-	0.05	-	-	0	-	0	-	0.09	-	-
101q	-	0.05	0.01	-	-	-	-	-	-	-	-
101r	-	-	-	-	-	0.09	-	0	-	0	-
101s	0.05	0.01	-	-	0.04	-	0	-	0	-	-

Table 2.18: Relative activities of compounds **S1** and **S2** against Shank-3 PDZ, Dvl-1 PDZ, Dvl-3 PDZ, PS95-1 PDZ, PSD95-2 PDZ. i) 0 indicate no residue showing chemical shift changes; ii) – indicate not measured.

We observed that some compounds that have shown a ΔCSP greater than 0.05 ppm for the AF-6 PDZ domain were inactive against these other PDZ domains.

In the contrary, some compounds that were not interacting with the AF-6 PDZ domain revealed to be active against two other PDZ domains, Shank-3 PDZ and PSD95-2 PDZ. Compound **101h** has caused a ΔCSP of 0.2 ppm for shank-3 PDZ while compound **101j** has caused a ΔCSP of 0.2 ppm for PSD95-1 PDZ. Interestingly, compound **101h** was inactive against PSD95-2 PDZ while compound **101j** was

inactive against shank-3 PDZ. **101h** binds to shank-3 PDZ with K_D of 340.5 ± 71.1 µM and **101j** binds PSD95-2 PDZ with K_D of 199.1 ± 49.5 µM. These two compounds could be considered as new starting point for designing inhibitors of Shank-3 PDZ and PSD95-2 PDZ, respectively.

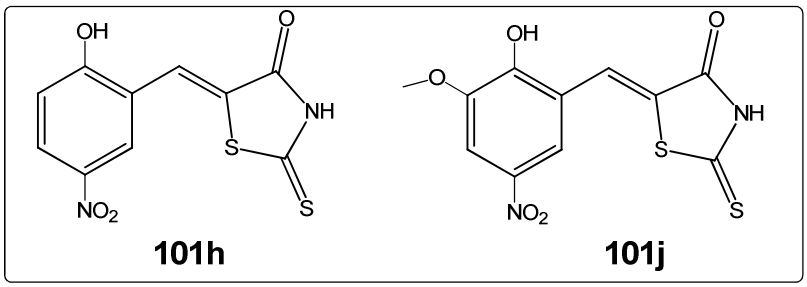

Figure 2.20: Hits compounds for Shank-3 PDZ (101h) and PSD95-PDZ (101j)

In the present work, small molecules that selectively bind to Dvl PDZ in the lower micromolar range have been identified. X-ray crystal structures of Dvl-3 PDZ complexed with three different compounds gave insight into the protein-ligand interactions. The structures show that these compounds form hydrogen bonds with the amide groups of residues L262, G263 and I264 in the PDZ-domain loop and the side chains of residues H326 and R322. The x-ray crystal structures supports HSQC results where the residues that show larger CSPs are those surrounding the conserved loop.

The activity is explained by the role that residue R322 plays in the interactions between the compounds and Dvl PDZ. R322, which occurs only in Dvl PDZ, was needed for the interaction of our compounds with the domain. A second reason might be the larger hydrophobic cavitiy for the side chain of the C-terminal residue of the interacting peptide.

The binding affinity of compound **61** (K_D = 2.4 ± 0.2) µM was better than the Frizzled peptide (K_D ~ 10 µM) which is a native Dvl PDZ domain binding partner in the Wnt signaling pathway. The key interaction in the Wnt signaling pathway is the direct recognition between Dvl PDZ and the conserved sequence (KTXXXW) in Frizzled-7. The small molecules developed in this study are shown to inhibit the Wnt pathway through Dvl binding.

The creation of more efficient compounds is under way. The structure of the Dvl-3 PDZ in complex with compound **36** serves as a basis for further developments. Small molecules targeting the R322 side chain will be developed to further improve selectivity.

Other PDZ domain targets that were investigated originally for reasons of specificity testing, or in context of an initial PDZ-inhibitor development (by C. Vargas, AF-6 PDZ)[149] are being pursued. In this context, all molecules previously identified as AF-6 PDZ binders were modified for improved binding affinity. Additionally “hits” were found for Shank-3 and PSD95-2 PDZ domains.

This work has confirmed NMR as valuable tool for drug development. Results obtained confirm the hypothesis that small molecules antagonists of Dvl PDZ can inhibit the Wnt signaling pathway.

4.1 NMR screening methodology of small molecules for Dvl PDZ

Two-dimensional ^{1}H-^{15}N HSQC (Heteronuclear Single Quantum Correlation) spectra were used to screen a library of 212 compounds designed by the company Enamine for PDZ domains. 50 µM of ^{15}N-labelled protein samples were prepared in a 20 mM sodium phosphate buffer, containing 50 mM sodium chloride, 0.02 % (w/v) NaN_3, at pH 7.4. Stock solutions of small molecules were prepared in DMSO-*d6* at a concentration of 160 mM. A ^{1}H-^{15}N HSQC spectrum of Dvl PDZ was acquired at 300k with 5% DMSO-*d6* in the absence of ligand as reference spectrum. Mixtures of 16 compounds were added to ^{15}N-labelled Dvl PDZ at 8-fold molar excess each. The final concentration of DMSO-*d6* in the protein-ligand solutions was 5 %.

Spectra were acquired with 8 scans and 256 points in the indirect dimension.

Binding was deduced if the resonance position of a cross-peak was significantly shifted compared to the reference spectrum. The active compound was obtained through successive deconvolution. Experiments were recorded on a Bruker DRX600 spectrometer equipped with a triple-resonance cryoprobe. The preparation of samples was done automatically by a Tecan Genesis RSP 150 pipetting robot. Spectra were analysed using the program TOPSPIN and SPARKY.[151]

4.2 Determination of chemical shift perturbation

Chemical shift perturbations were obtained by comparing the ^{1}HN-^{15}N backbone resonances of protein alone to those of protein-ligand complex. The mean shift difference (Δδ in ppm) was calculated using the equation 1.

$$\Delta\delta = \sqrt{\left[\frac{1}{2}(\Delta\delta H)^2 + \frac{1}{25}(\Delta\delta N)^2\right]} \quad \text{(Eq.1)}$$

Here Δδ*N* and Δδ*H* are the amide nitrogen and amide proton chemical shift difference between the free and the bound states of the protein.

4.3 Determination of binding constant by NMR

In order to estimate binding constants, titration experiments monitored by NMR were done. A series of ^{1}H-^{15}N HSQC were recorded as a function of ligand concentration. Residues showing a continuous chemical shift change and for which the intensity remained strong were classified as being in fast exchange. Chemical shift

perturbations for the abovementioned residues were then quantified as described in equation 1.

In a fast exchange regime, one-to-one binding of protein (P) and a ligand (L) to form a protein-ligand complex (PL) can be described according to equilibrium:

$$P + L \Leftrightarrow PL \quad \text{(Eq.2).}$$

$$K_D = \frac{[L].[P]}{[PL]} \quad \text{(Eq.3).}$$

The concentration of the protein and the ligand can be expressed by the law of mass action as P_T = [P] + [PL] and L_T = [L] + [PL], therefore

$$K_D = (P_T - [PL])\frac{(L_T - [PL])}{PL} \quad \text{(Eq.4).}$$

The amount of protein-ligand complex can be estimated using equation 5

$$[PL] = \frac{[L_T] + [P_T] + K_D - \sqrt{([L_T] + [P_T] + K_D)^2 - 4[L_T][P_T]}}{2} \quad \text{(Eq.5).}$$

The observed change in chemical shift during the titration of protein with the ligand is given by

$$\Delta\delta = \frac{[PL]}{P_T}(\delta_b - \delta_f) = \frac{[PL]}{P_T}\delta_{\max}$$

Where δ_f is the chemical shift of the protein domain in the absence of ligand and δ_b is the chemical shift of the protein domain bound to ligand. Finally, the dissociation binding constant was estimated by fitting the observed chemical shift to equation 6

$$\Delta\delta = \frac{\Delta\delta_{\max}\left([L_T] + [P_T] + K_D - \sqrt{([L_T] + [P_T] + K_D)^2 - 4[L_T][P_T]}\right)}{2[P_T]} \quad \text{(Eq.6).}$$

4.4 Determination of binding constant by Isothermal Titration Calorimetry (ITC)

Isothermal Titration Calorimetry (ITC) experiments were performed using a VP-ITC system (MicroCal). In (20 mM Hepes buffer, 50 mM NaCl, pH 7.4), protein was centrifuged and degassed before the experiment. A 200 µM ligand solution

containing 2% DMSO was injected 30 times in 10 µL aliquots at 120 s intervals with a stirring speed of 1000 rpm into a 1.4 mL sample cell containing the Dvl PDZ domain at a concentration of 20 µM and at 25℃. Control experiment was initially determined by titrating ligand into buffer at same conditions. Titration of ligand into buffer yielded negligible heats. Thermodynamic properties and binding constants were determined by fitting the data with a nonlinear least-squares routine using a single-site binding model with Origin for ITC v.7.2 (Microcal).

4.5 Chemical synthesis of small molecules

4.5.1 Materials and Instrumentation

All reagents and starting materials were purchased from Sigma-Aldrich Chemie GmbH, ABCR GmBH & Co.KG, alfa Aesar GmbH & Co.KG, Acros Organics and used without further purification. All air or moisture-sensitive reactions were carried out under dry nitrogen using standard Schlenk techniques. Solvents were removed by evaporation on Heidolph laborota 4000 with vacuum provided by a PC 3001 vaccubrand pump. Thin-layer chromatography (TLC) was performed on plastic-backed plates pre-coated with silica gel 60 F_{254} (0.2 mm). Visualization was achieved by an ultraviolet (UV) lamp (254 and 366 nm). Flash chromatography was performed using J.T Baker silica gel 60 (30-63 µm). Analytical high-performance liquid chromatography (HPLC) as performed on a Shimadzu LC-20 (degasser DGU-20A3, controller CBM-20A, autosampler SIL-20A) with a DAD-UV detector (SPD-M20A), using a reverse-phase C18 column (Nucleodur 100-5, 5µM, 250 mm x 4mm, Macherey-Nagel, Düren, Germany). Separation of compounds by preparative HPLC was performed on a Shimadzu LC-8A system equipped with a UV detector (SPD-M20A), using a semi-preparative C18 column (Nucleodur 100-5, 5µM, 250 mm x 10 mm, Macherey-Nagel) or preparative C18 column (Nucleodur 100-5, 5 µM, 250 mm x 21 mm, Macherey-Nagel). The detection wavelength was 254 nm. Gradients of acetonitrile-water with 0.1 TFA were used for elution at flow rates of 1mL /min, 8mL/min, and 14mL/min on the analytical, semi-preparative and preparative columns respectively. Melting points (mp) were determined with Stuart Melting Point

Apparatus SMP3 and are not corrected. Mass spectra were recorded on a 4000Q TRAP LC/MS/MS/ System for AB Applied Biosystems MDS SCIEX. NMR spectra were recorded on Bruker AV300 spectrometer instrument operating at 300 MHz for proton frequency using DMSO-d6 solutions. Chemical shifts were quoted relative to the residual DMSO peak (^{1}H: δ = 2.50 ppm, ^{13}C: δ = 39.52 ppm). Coupling constants (J) are given in Hertz (Hz). Splitting patterns are indicated as follows: singlet(s), doublet (d), triplet (t), quartet (q), multiple (m), broad (b).

4.5.2 Synthesis of substrates

4.5.2.1 Synthesis of 2-(5,6,7,8-tetrahydronaphthalene-2-sulfoamido)-5-(trifluoromethyl) benzoic acid (50) and derivatives.[152] Compounds 48 - 55

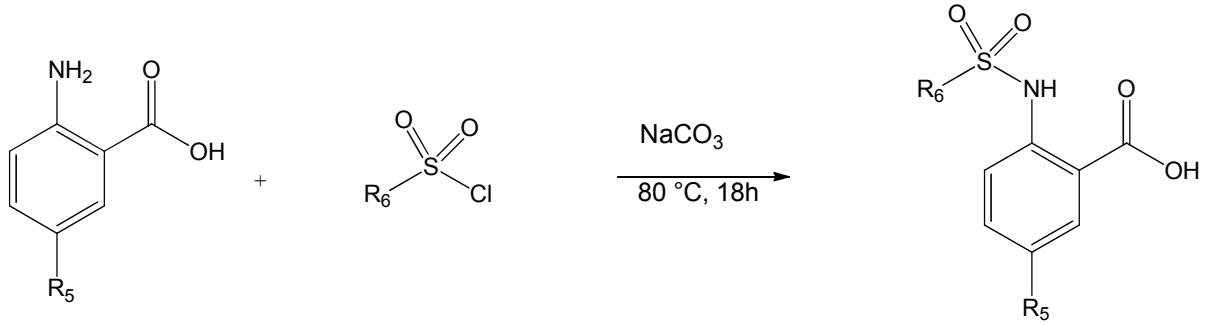

48-55

Scheme 1: Synthesis of compounds 48 – 55

2-(5,6,7,8-tetrahydronaphthalene-2-sulfoamido)-5-(trifluoromethyl)benzoic acid

To a solution of 2-amino-5-(trifluoromethyl) benzoic acid (0.27g, 1.32 mmol) sodium carbonate (0.36g, 3.17 mmol) in water (2mL) at 80℃ . 5,6,7,8-tetrahydronaphthalene-2-sulfonyl chloride (0.36g, 1.58 mmol) was added over a period of 5 min, and then stirred for 18 hours at 80℃. The reaction mixture was cooled to room temperature and acidified with 6N HCl and the resulting solid precipitate was filtered, washed with water and dried to give crude product. Crystallization from EtOH gave pure compound **50**. (0.52 g, 74%). Compounds **48**, **49**, **51**, **52**, **53**, **54** and **55** were synthesized with the same procedure.

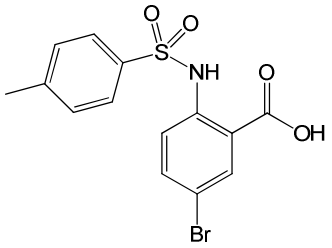

48

5-bromo-2-(4-trimethylphenylsulfoamido)benzoic acid

(0.4 g, 57% yield) **^{1}H-NMR** (300 MHz, DMSO-d6): δ = 11.5 (s, 1H, OH), 9.7 (s, 1H, NH), 7.88 (d, J = 1.3 Hz, 1H, Ar), 7.59 (d, J = 4.1Hz, 1H, Ar), 7.35 (d, J = 1.2 Hz, 1H, Ar), 7.32 (d, J = 1.3 Hz, 2H, Ar), 7.22 – 7.30 (m, 2H, Ar) 2.29 (s, 3H, CH_3)
^{13}C-NMR (300 MHz, DMSO-d6): δ = 168.1, 142.6, 138.5, 137.2, 133.8, 133.4, 129.7, 126.1, 118.5, 113.2, 112.5, 21.17; mp: 184; MS (ESI): *m*/z 369 $[M+H]^+$.

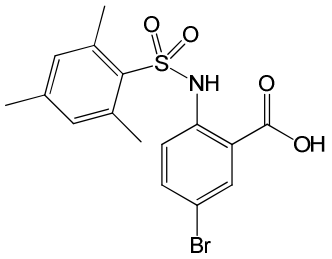

49

5-bromo-2-(2,4,6-trimethylphenylsulfoamido)benzoic acid

(0.6 g, 78% yield) **^{1}H-NMR** (300 MHz, DMSO-d6): δ = 11.77 (s,1H, OH), 9.98 (s, 1H, NH), 7.68 (d , J = 4.4 Hz, 1H, Ar) , 7.17 (s, 1H, Ar), 7.14 (s, 1H, Ar), 7.04 (s, 2H, Ar), 2.56 (s, 6H, CH_3), 2.21 (s, 3H, CH_3);-**^{13}C-NMR** (300 MHz, DMSO-d6): δ = 168.8, 143.3, 139.5, 139.0, 137.3, 134.0, 133.0, 132.5, 119.1, 117.9, 114.3, 22.5, 20.7; mp: 185; MS (ESI): *m/z* 399 $[M+H]^+$

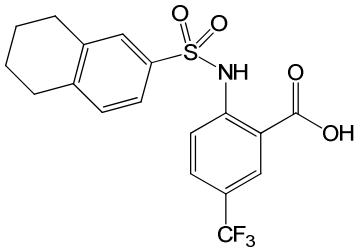

50

2-(5,6,7,8-tetrahydronaphthalene-2-sulfoamido)-5-(trifluoromethyl)benzoic acid

(0.52 g, 74% yield) **^{1}H-NMR** (300 MHz, DMSO-d6): δ = 11.77 (s, 1H, OH), 8.13 (s, 1H, NH), 7.85 (dd, J = 4.4 Hz, 1H, Ar) 7.53 - 7.68 (m, 4H, Ar), 7.24 (d, J= 4.2 Hz, 1H, Ar) 2.73 (s, 4H, CH_2); 1.6 (s, 4H, CH_2);-**^{13}C-NMR** (300 MHz, DMSO-d6): δ = 169.1, 152.7, 143.8, 138.7, 135.9, 130.4, 128.7, 127.5, 124.0, 121.6, 118.2, 116.9, 29.0, 28.8, 22.3, 22.2; mp: 177; MS (ESI): *m*/z 400 $[M+H]^+$.

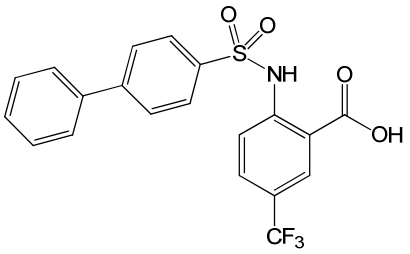

51

2-(biphenyl-4-ylsulfonamido)-5-(trifluoromethyl)benzoic acid

(0.48 g, 80% yield) **^{1}H-NMR** (300 MHz, DMSO-d6): δ = 12.27 (s, 1H, OH); 11.39 (s, 1H, NH), 8.13 (s, 1H, Ar), 7.77 – 8.02 (m, 3H, Ar), 7.81 (dd, J = 4.4 Hz, 2H, Ar), 7.29 – 7.74 (m, 4H, Ar), 6.88 (d, J = 5 Hz, 2H, Ar);- **^{13}C-NMR** (300 MHz, DMSO-d6): δ = 168.8, 154.2, 147.1, 140.6, 139.9, 129.5, 129.3, 127.9, 127.4, 127.0, 126.1, 177.2,109.0, 145.6, 138.1, 137.2, 130.2, 128.9; mp:173; MS (ESI): *m*/z 422 $[M+H]^+$.

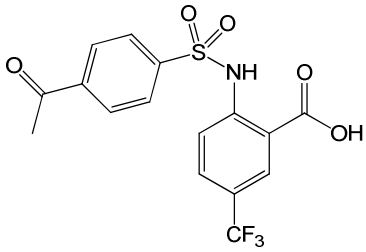

52

2-(4-acetylphenylsulfoamido)-5-(trifluoromethyl)benzoic acid

(0.4 g, 63% yield) **^{1}H-NMR** (300 MHz, DMSO-d6): δ = 12.28 (s, 1H, OH); 12.10 (s, 1H, NH), 8.11 (d, J= 2.5 Hz, 2H, Ar), 8.08 (s, 1H, Ar), 7.86 (dd, J = 4.5 Hz, 2H, Ar), 7.64 (d, J = 4.3 Hz, 2H) , 2.50 (s, 3H, CH_3);-**^{13}C-NMR** (300 MHz, DMSO-d6): δ = 197.9, 169.1, 151.8 143.5, 142.5, 140.6, 131.4, 129.6, 128.6, 127.6, 126.4, 125.7, 123.0, 118.7, 117.7, 27.3; mp: 170; MS (ESI): *m*/z 388 $[M+H]^+$.

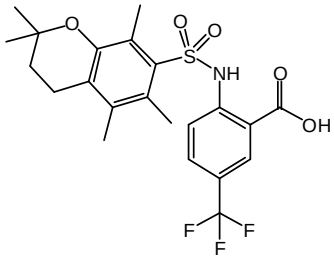

53

2-(2,2,5,7,8-pentamethylchroman-6-sulfoamido)-5-(trifluoromethyl)benzoic acid

(0.3 g, 53% yield) **^{1}H-NMR** (300 MHz, DMSO-d6): δ = 12.33 (s,1H), 11.70 (s, 1H); 8.14 (s, 1H), 7.80 (dd, J = 4.7 Hz, 1H, Ar), 7.21 (d, J = 4.5 Hz, 1H, Ar), 2.55 – 2.65 (m, 2H), 2.07 (s, 3H), 2.02 (s, 6H, CH_3), 1.23 (s, 6H, CH_3); -**^{13}C-NMR** (300 MHz, DMSO-d6): δ = 170.2, 153.5, 151.5, 146.4, 135.5, 132.7, 129.1, 124.4, 121.1, 119.3, 117.8, 116.1, 87.1, 31.9, 27.9, 23.1, 22.1, 18.2, 16.4, 12.8; mp:160; MS (ESI): *m*/z 472 $[M+H]^+$.

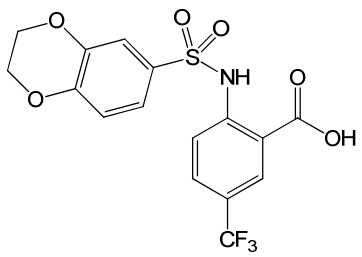

54

2-(2,3-dihydrobenzo[*b*][1,4]dioxine-6-sulfonamido)-5-(trifluoromethyl)benzoic acid

(0.4 g, 65% yield) **^{1}H-NMR** (300 MHz, DMSO-d6): δ = 11.48 (s, 1H, OH), 8.13(s, 1H, NH) , 7.89 (dd, J = 4.3 Hz, 1H, Ar), 7.66 (d, J = 3.9 Hz, 1H, Ar), 7.33 – 7.40 (m, 3H, Ar), 7.02 (d, J = 4.1, Hz, 1H, Ar), 4.23 – 4.31 (m, 5H);-**^{13}C-NMR** (300 MHz, DMSO-d6): δ = 168.9, 148.3, 143.8, 143.5, 131.3, 130.8, 128.6, 125.7, 122.1, 120.9, 118.3, 118.1, 116.8, 64.7, 64.3; mp: 178; MS (ESI): *m*/z 404 $[M+H]^{+}$.

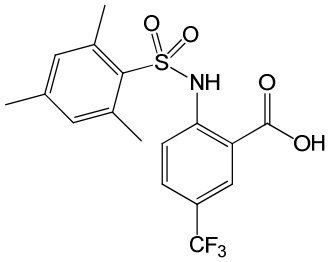

55

5-(trifluoromethyl)-2-(2,4,6-trimethylphenylsulfoamido)benzoic acid

(0.38 g, 62% yield) ^{1}H-NMR (300 MHz, DMSO-d6): δ = 12.28 (s, 1H, OH), 11.60 (s, 1H, NH), 8.15(d, J = 0.8 Hz, 1H, Ar) 7.92 (s, 7.9 Hz, 1H, Ar) 7.87 (dd, J = 4.3 Hz, 1H, Ar), 7.48 (dd, J = 4.3 Hz, 1H, Ar) 7.07 (s, 1H, Ar) 2.60 (s, 6H, CH_3), 2.23 (s, 3H, CH_3);-**^{13}C-NMR** (300 MHz, DMSO-d6): δ = 169.3, 154.2, 143.6, 139.1, 132.9, 132.5, 131.5, 130.1, 128.7, 122.5, 117.0, 115.7,109.0,22.4, 20.8; mp:184; MS (ESI): *m*/z 388 $[M+H]^{+}$.

4.5.2.2 Synthesis of (Z)- 2-Imino-5-[4-(trifluoromethyl)phenethyl]1,3-thiazolidin- 4-one (91a) and 2-imino-5-(4-(trifluoromethyl)benzyl)thiazolidin-4-one (91b) [153, 154]

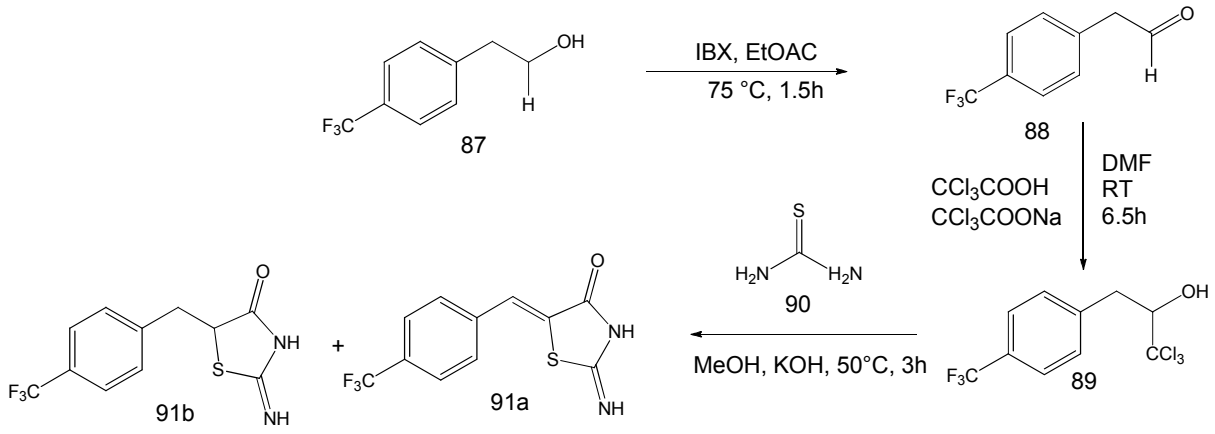

Scheme 2: Synthesis of compounds **91a** and **91b**

To a solution of 547 mg (1.78 mmol) of phenethyl(trichloromethyl)carbinol and 270 mg (3.56 mmol) of thiourea in 1.80 mL of methanol at 50℃, was added dropwise over a period of 2 hours a methanolic potassium hydroxide solution prepared by dissolving 700 mg (12.47 mmol) of KOH pellets in 1.76 mL of methanol. The temperature was maintained at 50 - 55℃ during the addition. After all the base was added, the mixture was stirred an additional hour at 50℃, then allowed to cool to room temperature. The potassium chloride was filtered off and washed with methanol. The combined filtrates were diluted with an equal volume of water, the base-insoluble materials extracted with several large portions of ether, and the aqueous layer was slowly acidified to pH 6.9 with HCl (4N). An immediate precipitate of 2-Imino-5- [phenyl-4-thiazolidinone was formed and was filtered off after cooling the solution to give 300 mg of crude product. The flash chromatography in a mixture of ethyl acetate/ethanol (19:1) gave a mixture of **91a** (30 %) and **91b** (70%)

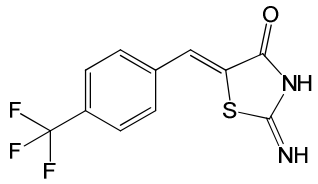

91a

(Z)-2-imino-5-(4-(trifluoromethyl)benzylidene)thiazolidin-4-one

^{1}H-NMR (300 MHz, DMSO-d6): δ = 9.54 (s, 1H, NH), 9.27 (s, 1H, NH), 7.86 (d, J = 4.26 Hz, 2H, Ar), 7.77 (d, J = 4.06 Hz, 2H, Ar), 7.02 (s, 1H, CH);- **^{13}C-NMR** (300 MHz, DMSO-d6): δ = 189.5, 181.6, 143.7, 138.3, 132.5, 130.6, 127.2, 125.6, 125.0, 124.1 , 117.2; MS (ESI): m/z 273 $[M+H]^{+}$.

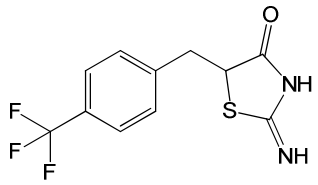

91b

2-imino-5-(4-(trifluoromethyl)benzyl)thiazolidin-4-one

^{1}H-NMR (300 Mhz, DMSO-d6): δ = 8.92 (s, 1H, NH), 8.69 (s, 1H, NH), 7.64 (d, J = 3.9 Hz, 2H), 7.45 (d, J = 4.09 Hz, 2H), 4.61 – 4.67 (m, 1H), 3.42 (dd, J = 7 Hz, 1H), 3.05 (dd, J = 7Hz, 1H);- **^{13}C-NMR** (300 MHz, DMSO-d6): δ = 188.9, 181.0, 143.2, 129.9, 129.8, 127.1 126.0, 125.9, 125.0.,57.2, 38.0; MS (ESI): m/z 275 $[M+H]^{+}$.

4.5.2.3 Synthesis of 4-trifluoromethyl benzylidenesuccinimide [155]

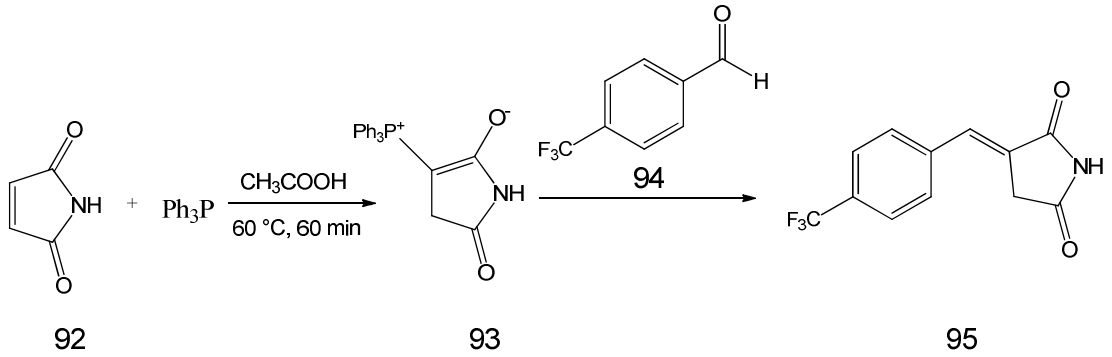

Scheme 3: Synthesis of compound 95

Maleimide **92** (1 g) and 2.6 g of triphenylphosphine were stirred in 20 mL of glacial acetic acid for 60 min at 60 ℃. Ether (200 mL) was added and left at 4℃. The crystalline precipitated was recrystallized from acetone giving triphenylphosphoanylidenesuccinimide (**93**) as intermediate product. 1 g of **93** and 2 mL of 4-(trifluoromethyl)benzaldehyde **94** were mixed at room temperature. An exothermic reaction occurred. After the initial reaction, the mixture was warmed at 60 ℃ for 30 min and left standing at room temperature for 2 hours. Ether was added and crude product was filtered off. Recrystallization from methanol gave compound **95** as white product (2.1g, 56% yield)

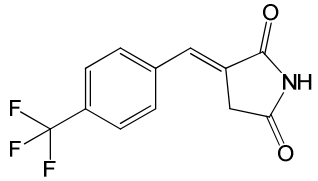

95

(E)-3-(4-(trifluoromethyl) benzylidene)pyrrolidine-2,5-dione

(2.1 g, 56 % yield) **^{1}H-NMR** (300 MHz, DMSO-d6): δ = 11.54 (s,1H), 7.73 - 7.87 (m, 4H), 7.44 (s, 1H);-**^{13}C-NMR** (300 MHz, DMSO-d6): δ = 175.6, 171.7, 139.1, 138.2, 130.6, 129.2,128.5, 126.6, 125.6, 125.4, 124.5, 44.2; MS (ESI): m/z 256 $[M+H]^{+}$.

4.5.2.4 Synthesis of 3-(4-(trifluoromethyl) benzyl dihydrofuran-2,5-dione [156, 157]

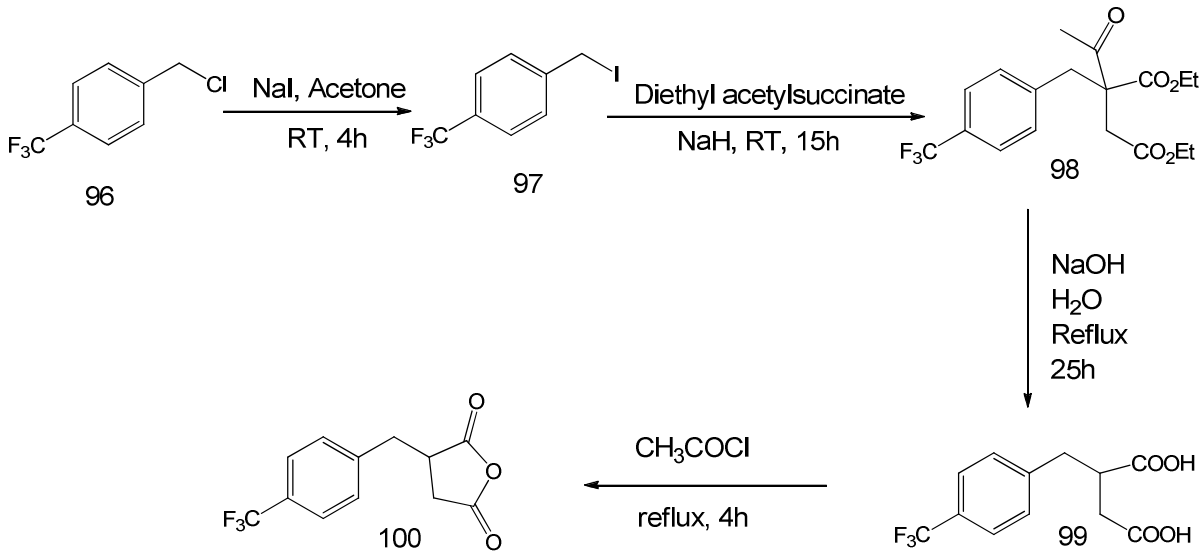

Scheme 4: Synthesis of compound 100

4.5.2.4.1 Synthesis of 4-(trifluoromethyl)benzyl iodine

To a solution of 4-(trifluoromethyl)benzylchloride (4g, 20.56 mmol) in acetone (28.89 ml) was added sodium iodide (3.40g, 22.63 mmol). The mixture was stirred at room temperature for 3h30. Sodium iodide (80.25 g, 1.67 mmol) was added, the mixture was stirred for an additional 60 min. The reaction mixture was then dilute with water (10 mL) and extracted with hexane. The extract was washed with water, dried over $MgSO_4$ and evaporated in vacuo to give 4.81 g (81%) of compound **97** as purple oil that crystallised immediately at RT.

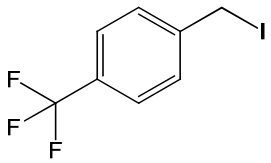

97

4-(trifluoromethyl)benzyl iodine

^{1}**H-NMR** (300 MHz, DMSO-d6): δ = 7.58 – 7.78 (m, 4H, Ar), 4.68 (s, 2H)
^{13}**C-NMR** (300 MHz, DMSO-d6): δ = 144.8, 132.7, 131.1, 129.7, 125.5, 5.4

3.5.2.4.2 Synthesis of diethyl-2-acetyl-2-(4-(trifluoromethyl)benzyl succinate

To a solution of diethylacethylsuccinate (2.51 mL, 12.56 mmol) in toluene (33.61 mL) was added 0.296 g (12.37 mmol) of sodium hydride oil suspension. (4g, 13.98 mmol) of compound **97** was added. The reaction mixture was stirred at room temperature overnight, then acidified by aqueous hydrochloric acid and extracted with toluene. The extract was washed with water, dried over $MgSO_4$ and evaporated in vacuo to give (3.95 g, 75% yield) of compound **98**.

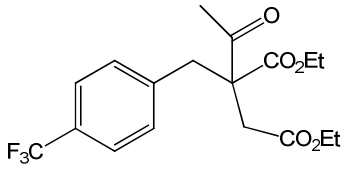

98

diethyl-2-acetyl-2-(4-(trifluoromethyl)benzyl succinate

^{1}**H-NMR** (300 MHz, DMSO-d6): δ = 7.58-7.67 (m, 2H), 7.29 (d, J = 4.4 Hz, 2H, Ar), 3.94 – 4.20 (m, 4H), 3.16 – 3.41 (m, 2H), 2.67 – 2.89 (m, 2H), 2.27 (s, 3H), 1.1 – 1.21 (m, 6H);-^{13}**C-NMR** (300 MHz, DMSO-d6): δ = 203.1, 170.1, 169.8, 140.7, 130.9, 125.5, 124.9, 61.7, 61.2, 60.5, 37.8, 31.9, 29.5, 13.4

4.5.2.4.3 Synthesis of 2-(4-(trifluoromethyl)benzyl succinic acid

To compound **98** (3. 95g, 10.55 mmol) was added a solution of sodium hydroxyde (1.265 g, 31.64 mmol) in water (14.54 mL), and the mixture was refluxed for 19 h. Sodium hydroxide (0.218 g, 5.44 mmol) in water (1.45 mL) was added and the mixture was refluxed for additional 5 hours. The reaction mixture was cooled, acidified with aqueous hydrochloric acid and extracted with ether. The extract was washed with water, dried over $MgSO_4$, and evaporated in vacuo to afford yellow oil. The residue was recrystallized from ethyl-hexane to give (50 mg, 1.7% yield) of compound **99**.

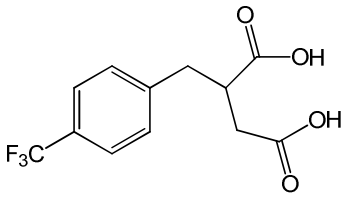

99

2-(4-(trifluoromethyl)benzyl succinic acid

^{1}**H-NMR** (300 MHz, DMSO-d6): δ = 12.1 (b, 2H, OH), 7.67 (d, J = 4.25 Hz, 2H, Ar), 7.48 (d, J = 4.25 Hz, 2H, Ar), 3.15 – 3.27 (m, 2H), 2.72 – 2.82 (m, 1H), 2.91 – 3.0 (m, 2H);-^{13}**C-NMR** (300 MHz, DMSO-d6): δ = 174.4, 171.7, 143.3, 129.6, 127.4, 125.4, 125.141.4, 34.6, 33.7

4.5.2.4.4 Synthesis of 3-(4-(trifluoromethyl)benzyl dihydrofuran-2,5-dione (100)

A mixture of compound **99** (29 mg) and acetyl chloride (0.15 mL) was refluxed for 4 h. The solution was then concentrated to give compound **100** as pure product (20 mg, 74 % yield).

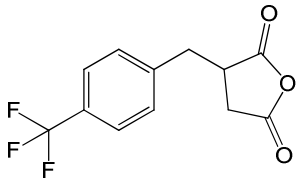

100

3-(4-(trifluoromethyl)benzyl)dihydrofuran-2,5-dione

(0.02 g, 74 % yield) ^{1}**H-NMR** (300 MHz, DMSO-d6): δ = 7.66 (d, J = 4.15, 2H), 7.48 (d, J = 3.98, 2H) 3.54 – 3.67 (m, 1H), 3.22 (dd, J = 6.90, 1H), 2.77 (dd, J = 9.35, 1H), 2.98 – 3.09 (m, 1H), 2.85 – 2.96 (m, 1H);-^{13}**C-NMR** (300 MHz, DMSO-d6): δ = 174.3, 171.2, 143.2, 129.7, 129.5, 125.4,125.3, 41.4, 34.6, 33.6. MS (ESI) m/z 259 $[M+H]^{+}$.

4.5.2.5 Synthesis of 5-Methylene-2-thioxo-4-thiazolidinones[158] Compounds (101a-101j)

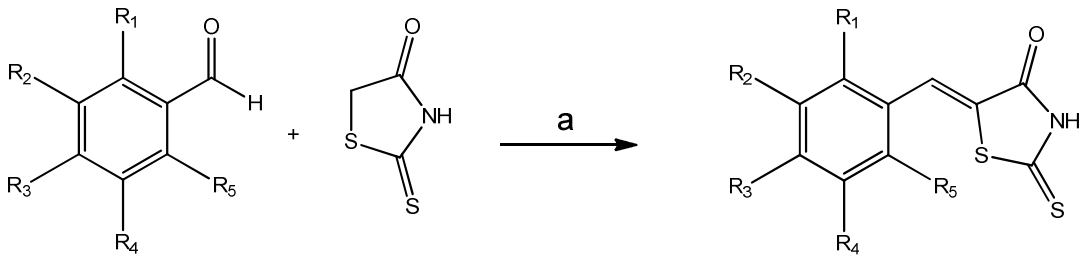

S1= 101a-101j

Scheme 4: synthesis of compounds series

(a): HOAc, NaOAc

R_1 = F, OCH_3, OH, H R_3 = F, OH, OCH_3, H

R_2 = F, OCH_3, OH, R_4 = F, OH, OCH_3, NO_2 R_5 = F, H

Into a 100 mL three-neck flask equipped with a magnetic stirrer, thermometer, reflux

condenser, was charged 40 mL of glacial acetic acid which was then heated to 80℃. Corresponding benzyl aldehyde (40 mmol) and 2,4-thiazolidinone (40 mmol) were added to the hot glacial acid, and the mixture was stirred until a solution had formed. Anhydrous NaOAc (140 mmol) was added in one portion followed by heating the reaction to reflux for 60 min. The reaction mixture was cooled to room temperature and poured into 124 mL of water upon which the product precipitated out as bright yellow crystalline solid. This was collected on a suction filter and washed with water, cold 1:1 H_2O/EtOH, and Et_2O. Vacuum drying at 40℃ gave products **(101a-101j)**.

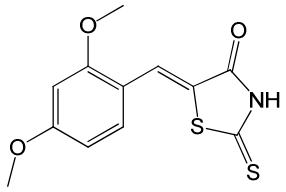

101a

(Z)-5-(2,4-dimethoxybenzylidene)-2-thioxothiazolidin-4-one

(5.1 g, 65% yield) **^{1}H-NMR** (300 MHz, DMSO-d6): δ = 13.6 (s, 1H), 7.74 (s, 1H), 7.33 (d, 1H, Ar, J = 4.31 Hz) 6.70 (d, 2H, Ar, J = 5.58Hz), 3.86 (d, 6H, J = 8.16Hz); **^{13}C-NMR** (300 MHz, DMSO-d6): δ = 195.9, 169.3, 163.6, 160.1, 131.7, 126.9, 121.5, 114.4, 107.2, 98.8, 55.9, 55.7; MS (ESI m/z 282 $[M+H]^+$.

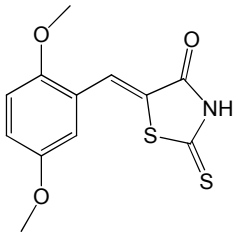

101b

(Z)-5-(2,4-dimethoxybenzylidene)-2-thioxothiazolidin-4-one

(4.2 g, 54% yield) **^{1}H-NMR** (300 MHz, DMSO-d6): δ = 13.76 (s, 1H, NH), 7.74 (s, 1H), 7.09 (s, 2H), 6.88(s, 1H) 3.79 (d, 6H, 12.5Hz);-**^{13}C-NMR** (300 MHz, DMSO-d6): δ = 196.1, 169.6, 153.2, 152.5, 126.7,125.9, 121.8, 118.6, 113.9, 113.2, 56.1, 55.6. MS (ESI) m/z 282 $[M+H]^+$.

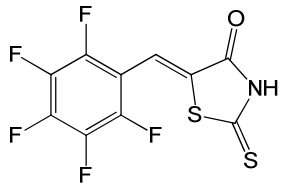

101c

(Z)-5-(perfluorobenzylidene)-2-thioxothiazolidin-4-one

(3.5 g, 44% yield) **^{1}H-NMR** (300 MHz, DMSO-d6): δ = 13.96 (b, 1H), 7.37(s, 1H); **^{13}C-NMR** (300 MHz, DMSO-d6): δ = 195.5, 168.8, 145.3, 142.1, 139.1, 138.9, 134.8, 115.1, 110.3, 108.8; MS (ESI): m/z 311.9 $[M+H]^{+}$.

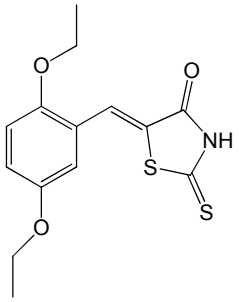

101d

(Z)-5-(2,5-diethoxybenzylidene)-2-thioxothiazolidin-4-one

(4.1 g, 51% yield) **^{1}H-NMR** (300 MHz, DMSO-d6): δ = 13.80 (s, 1H), 7.77 (s, 1H), 7.06 (s, 1H, Ar), 6.95 (s, 1H, Ar), 6.82 (s, 1H, Ar), 3.91 – 4.15 (m, 6H, OCH3), 1.26 – 1.39 (m, 6H, CH_3);-**^{13}C-NMR** (300 MHz, DMSO-d6): δ = 195.6, 169.5, 152.4, 131.7, 126.1, 122.4, 119.4, 116.7, 114.1, 64.8, 63.9, 14.9; MS (ESI): m/z 310 $[M+H]^{+}$.

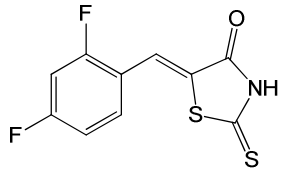

101e

(Z)-5-(2,4-difluorobenzylidene)-2-thioxothiazolidin-4-one

(5.1 g, 56% yield) **^{1}H-NMR** (300 MHz, DMSO-d6): δ = 13.95 (s, 1H), 7.42 – 7.64 (m, 3H), 7.28 (t, 1H, J = 4.1Hz);-**^{13}C-NMR** (300 MHz, DMSO-d6): δ = 195.6, 169.6, 162.1, 159.4, 131.1, 127.8, 121.5, 117.6, 113.5, 105.1. MS (ESI): m/z 258 $[M+H]^{+}$.

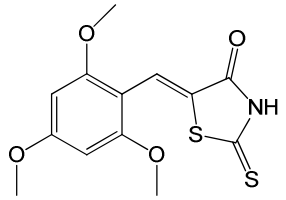

101f

(Z)-2-thioxo-5-(2,4,6-trimethoxybenzylidene)thiazolidin-4-one

(5.3 g, 56% yield) ^{1}**H-NMR** (300 MHz, DMSO-d6): δ = 13.45 (s, 1H), 7.91 (s, 1H), 6.39 (s, 2H, Ar) 3.95 (d, 9H, CH_3, J = 2.6 Hz);-^{13}**C-NMR** (300 MHz, DMSO-d6): δ = 193.5, 168.7, 164.8, 160.1, 133.5, 126.1, 103.6, 91.2, 90.5, 55.8, 55.6, 55.5. MS (ESI): m/z 312 $[M+H]^+$.

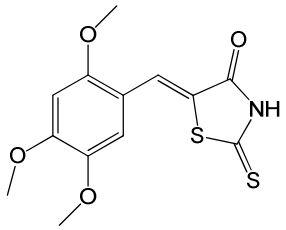

101g

(Z)-2-thioxo-5-(2,4,5-trimethoxybenzylidene)thiazolidin-4-one

(4.7g, 48% yield) ^{1}**H-NMR** (300 MHz, DMSO-d6): 13.66 (s, 1H), 7.79 (s, 1H), 6.91 (s, 1H, Ar), 6.79 (s, 1H), 3.89 (d, 6H, CH_3, J = 3.2 Hz), 3.76 (s, 3H, CH_3);^{13}**C-NMR** (300 MHz, DMSO-d6): δ 193.5, 168.8, 164.6, 159.8, 133.3, 125.9, 112.1, 97.9, 56.4, 56.0, 55.8; MS (ESI): m/z 312 $[M+H]^+$.

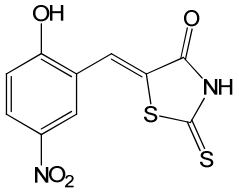

101h

(Z)-5-(2-hydroxy-5-nitrobenzylidene)-2-thioxothiazolidin-4-one

(3.7 g, 56% yield) ^{1}**H-NMR** (300 MHz, DMSO-d6): δ = 13.16 (s, 1H), 8.13 – 8.24 (m, 2H, Ar), 7.72 (s, 1H), 7.11 (d, J = 4.7Hz, 1H, Ar) 5.02 (s, 1H, OH);-^{13}**C-NMR** (300 MHz, DMSO-d6): δ = 195.4, 169.3, 163.1, 139.9, 127.7, 127.2, 125.1, 124.6, 120.4, 116.6; MS (ESI): m/z 283 $[M+H]^+$.

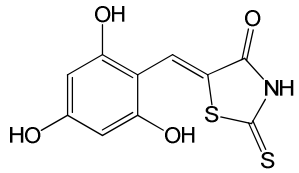

101i

(Z)-2-thioxo-5-(2,3,5-trihydroxybenzylidene)thiazolidin-4-one

(6.1 g, 69% yield) **^{1}H-NMR** (300 MHz, DMSO-d6): δ =13.54 (s, 1H) , 10.15 (s, 1H), 9.54(S, 1H), 8.75(s, 1H), 7.80(s, 1H), 6.69 (d, J = 4.2 Hz, 1H), 6.48 (d, J = 4.3 Hz, 1H);-**^{13}C-NMR** (300 MHz, DMSO-d6): δ = 196.4, 170.6, 150.3, 148.3, 133.4, 128.6, 120.8, 118.4, 113.3, 108.7. MS (ESI): m/z 270 $[M+H]^{+}$.

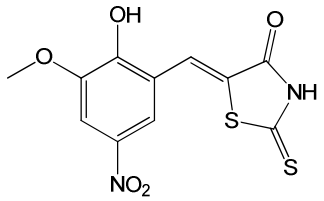

101j

(Z)-5-(2-hydrxy-3-methoxy-5-nitrobenzylidene)-2-thioxothiazolidin-4-one

(4.6 g, 58% yield) **^{1}H-NMR** (300 MHz, DMSO-d6): δ = 13.53 (s, H), 10.34 (s, H), 7.74(s, 1H), 7.80 – 7.85 (m, 2H), 3.96 (s, 3H);-**^{13}C-NMR** (300 MHz, DMSO-d6): δ = 195.7, 169.7, 153.3, 148.3, 139.9, 127.5, 125.3, 120.0, 117.2, 108.6, 56.9. MS (ESI): m/z 313 $[M+H]^{+}$.

4.5.2.6 Reduction of 5-Methylene-2-thioxo-4-thiazolidinones to 5-Methyl-2-thioxo-4-thiazolidinones.[159] Compounds (102a-102h)

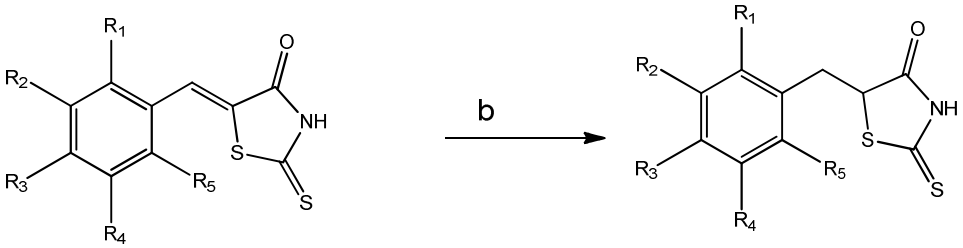

Scheme 4: synthesis of compounds series

(b): LiBH4, THF, Pyridine R_1 = F, OCH_3, OH, H R_2 = F, OCH_3, OH R_3 = F,OH, OCH_3, H R_4 = F, OH, OCH_3, NO_2 R_5 = F, H

A 2.0 molar solution of lithium borohydride in tetrahydrofuran (THF) (2.2 equiv) was added dropwise to a stirred solution of the corresponding compound from series **(101a-101h)** (5.8 mmol) in pyridine (7.3 mL) and THF (6 mL) at 25℃ under nitrogen to give an orange solution. Effervescence was control by the addition rate. The mixture was heated to reflux and stirred for 5h. The cooled mixture was carefully added to a stirred solution of hydrochloric acid (4.3 mL) and 28 mL of distilled water at 5℃, and extracted into ethyl acetate (3 x 30 mL). The combined organic extracts were washed with water (2 x 60 ml), dried over Na_2SO_4 and the solvent removed in vacuo to afford crude product. The final products were obtained after flash chromatography using mixtures of ethyl acetate-hexane as eluants to afford compounds series **(102a – 102h).**

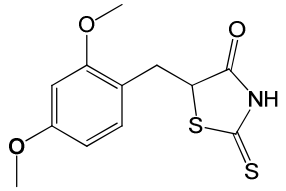

102a

5-(2,4-dimethoxybenzyl)-2-thioxothiazolidin-4-one

(0.7 g, 46 %) **^{1}H-NMR** (300 MHz, DMSO-*d6*): δ = 13.14 (s, 1H) 7.03 (dd, J = 4.13, 1H), 6.53 – 6.55 (m 2H, Ar), 4.88 (dd , J = 5.01 Hz, 1H) 3.35 (dd, J = 6.8 Hz, 1H), 2.97 (dd, J = 6.7 Hz, 1H);- **^{13}C-NMR** (300 MHz, DMSO-d6): δ = 203.7, 178.1, 160.0, 157.8, 130.8, 116.7, 104.6, 98.4, 55.3, 55.1, 54.7, 31.6; MS (ESI): m/z 284 $[M+H]^+$.

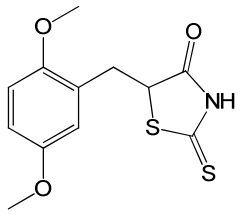

102b

5-(2, 5-dimethoxybenzyl)-2-thioxothiazolidin-4-one

(0.75 g, 49% yield) **^{1}H-NMR** (300 MHz, DMSO-*d6*): δ = 13.17(s, 1H), 6.67 – 6.90 (m, 3H, Ar), 4.96 (dd, J = 4.6 Hz, 1H), 3.66 – 4.01 (m, 6H), 3.39 (dd, J = 6.9 Hz, 1H) , 2.97 (dd, J = 6.89, 1H);-**^{13}C-NMR** (300 MHz, DMSO-d6): δ = 203.7, 178.1, 152.0, 150.5, 126.0, 117.2, 113.4, 112.7, 63.6, 63.2, 54.5, 32.0. MS (ESI): m/z 284 $[M+H]^+$.

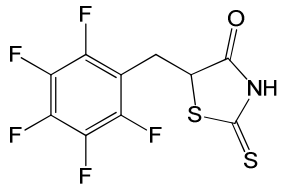

102c

5-(perfluorobenzyl)-2-thioxothiazolidin-4-one

(0.65 g, 43 % yield) **^{1}H-NMR** (300 MHz, DMSO-*d6*): δ = 13.30 (s, 1H), 4.85 (dd, J = 7.8, 1H), 4.01 (dd, J = 7.2 Hz, 2H), 3.42 (t, J = 4.8 Hz, 2H);-**^{13}C-NMR** (300 MHz, DMSO-d6): δ = 203.2, 177.2, 146.5, 143.4, 138.6, 135.3, 116.1, 141.7, 59.8, 24.7. MS (ESI): *m/z* 314 $[M+H]^+$.

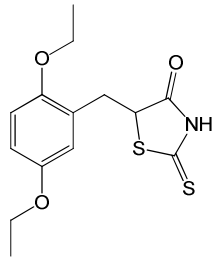

102d

5-(2,5-diethoxybenzyl)-2-thioxothiazolidin-4-one

(0. 81 g, 53% yield) **^{1}H-NMR** (300 MHz, DMSO-*d6*): δ 13.16 (s, 1H), 6.87 (d, 1H, Ar, J = 4.4 Hz), 6.70 – 6.79 (m, 2H, Ar), 4.93 – 5.1 (m, 1H), 3.87 – 4.1 (m, 4H, CH_2), 3.29 (s, 1H), 3.89 (dd, 1H, J = 7.05, CH), 2.98 (dd, 1H, J = 7.05, CH), 1.12 – 1.34 (m, 6H);-**^{13}C-NMR** (300 MHz, DMSO-d6): δ 203.6, 178.2, 152.3, 150.2, 126.1, 117.1, 113.5, 112.7, 63.7, 63.4, 54.4, 32.1, 14.7; MS (ESI): *m/z* 312 $[M+H]^+$.

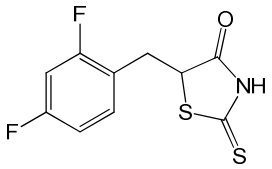

102e

5-(2,4-difluorobenzyl)-2-thioxothiazolidin-4-one

(0.9 g, 59% yield) **^{1}H-NMR** (300 MHz, DMSO-*d6*): δ 13.21 (s, 1H), 7.01 – 7.40 (m , 3H), 4.95 (dd, J = 4.0 , 1H), 4.01 (dd, J = 7.39, 1H), 3.37 (dd, J = 7.2 Hz 1H), 3.20 (dd, J = 7.2Hz, 1H);- **^{13}C-NMR** (300 MHz, DMSO-d6): δ = 203.4, 177.6, 162.2, 160.0 132.6, 120.8, 111.4, 104.2, 59.8, 29.6; MS (ESI): *m/z* 260 $[M+H]^+$.

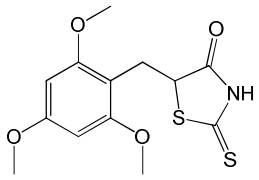

102f

2-thioxo-5-(2,4,6-trimethoxybenzyl)thiazolidin-4-one

(1.1 g, 73% yield) **^{1}H-NMR** (300 MHz, DMSO-*d6*): δ =13.14 (s, 1H), 6.21 (s, 2H, Ar), 4.75 – 4.82 (m, 1H), 3.75 (d, J = 2.5 Hz, 9H, CH_3,), 3.16 – 3.24 (m, 1H), 3.0 – 3.1 (m, 1H);**^{13}C-NMR** (300 MHz, DMSO-d6): δ = 201.8, 170.7, 160.3, 158.8, 104.8, 90.8, 90.9, 55.7, 55.2, 54.2, 25.1. MS (ESI): *m/z* 314 $[M+H]^+$.

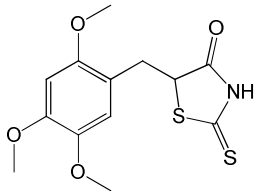

102g

2-thioxo-5-(2,4,5-trimethoxybenzyl)thiazolidin-4-one

(0.5 g, 33% yield) **^{1}H-NMR** (300 MHz, DMSO-*d6*): δ = 13.20(s, 1H), 6.8 (s, 1H), 6.7 (s, 1H), 4.88 – 4.94 (m, 1H), 3.77 (s, 6H, CH_3), 3.66 (s, 3H, CH_3), 3.34 – 3.42 (m, 1H), 2.82 – 3 (m, 1H);-**^{13}C-NMR** (300 MHz, DMSO-d6): δ = 203.9, 178.5, 151.7, 148.7, 142.7, 115.6, 115.0, 98.2, 56.1, 55.9, 55.8, 54.9, 31.6; MS (ESI): m/z 314 $[M+H]^+$.

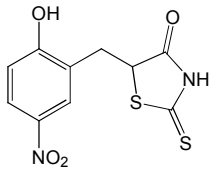

102h

5-(2-hydroxy-5-nitrobenzyl)-2-thioxothiazolidin-4-one

(0.43 g, 39% yield) **^{1}H-NMR** (300 MHz, DMSO-*d6*): δ =12.33 (s, 1H), 8.56 (s, 1H, Ar), 7.97 – 8.18 (m, 1H, Ar), 7.67 (s, 1H, Ar), 6.1 (s, 1H, OH), 3.46 (m, 1H), 3.2 (m, 1H);-**^{13}C-NMR** (300 MHz, DMSO-d6): δ = 203.3, 177.6, 161.5, 147.2, 140.3, 126.3, 115.2, 53.4, 31.9. MS (ESI): m/z 285 $[M+H]^+$.

4.5.2.7 Synthesis of 5 - (4-trifluoromethylbenzyl)-2-thioxo- 4-thiazolidinone and derivatives.[160] Compounds (107a - 107i)

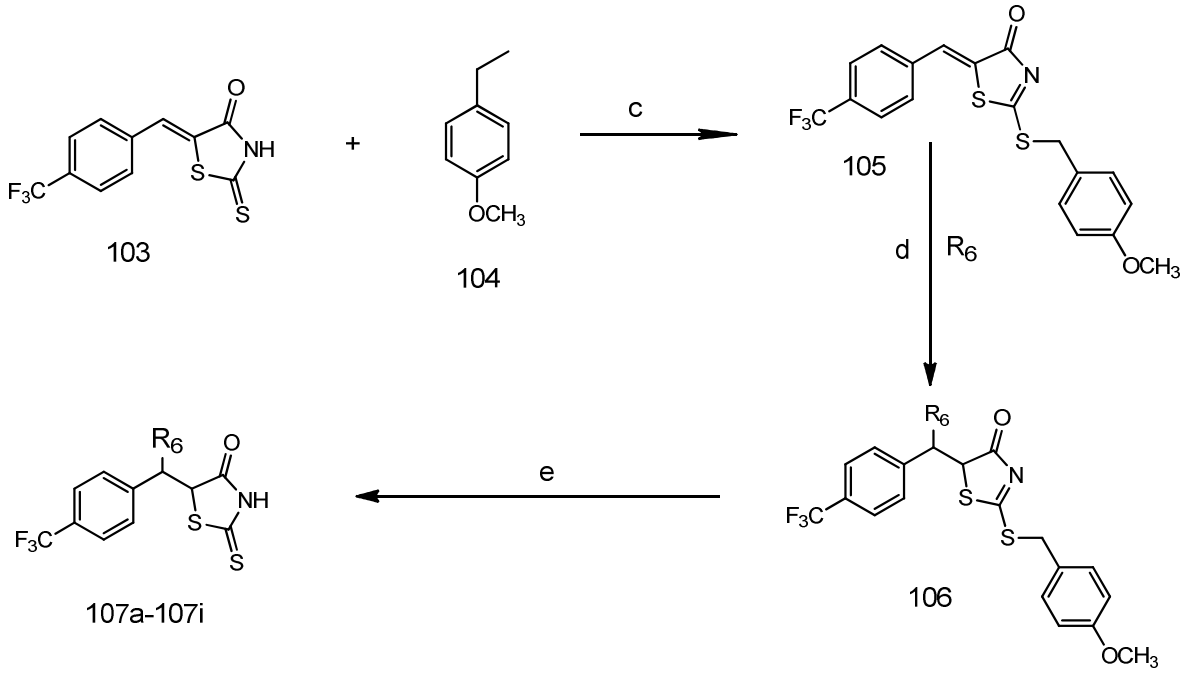

Scheme 5: Synthesis of compounds series (107a – 107i)

c) NaH, THF, Reflux; d) LDA, THF, -78℃; e) T FA, Reflux

4.5.2.7.1 Synthesis of (Z)-2-thioxo-5-(4-(trifluoromethyl) benzylidene)-thiazolidine-4-one (103)

Compound **103** was prepared according to the method described in section 4.5.2.5

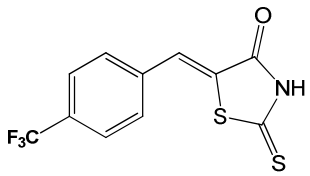

103

(4g, 48% yield) **^{1}H-NMR** (300 MHz, DMSO-*d6*): δ = (s,13.9, NH), 7.88 (d, J = 4.44 Hz, 2H, Ar), 7.80 (d, J = 4.21 Hz, 2H, Ar), 7.70 (s, 1H);- **^{13}C-NMR** (300 MHz, DMSO-d6): δ = 195.8, 169.7, 137.1, 131.7, 129.7, 128.9, 126.4, 125.9, 122.1; MS (ESI): m/z 290 $[M+H]^{+}$.

4.5.2.7.2 Synthesis of (Z)- 5 - (4 - trifuluoromethylbenezylidene)-2-(4-methoxybenzylthio)-4-thiazoilinone (105)

A 60 % dispersion of NaH in mineral oil (0.456, 11.4mmol) was washed with hexane 82 x 10 mL) under nitrogen, and the supernatant was removed with a syringe. NaH was suspended in 40 mL THF and stirred. A solution of **103** (3g, 10.38 mmol) in THF (15mL) was slowly added to it. After stirring for 30 min, 4-methoxybenzyl chloride (1.38mL, 10.38 mmol) was added dropwise, and the mixture was stirred for 30 min and heated to reflux for 2h. The reaction was monitored by TLC. The residue was then washed with water and extracted with dichloromethane (2 x 75mL). The organic extracts were combined, dried over $MgSO_4$, filtered and concentrate in vacuo to afford crude product. The purification by flash chromatography in a mixture of ethyl acetate-hexane gave (3.1 g, 73%) of compound **105**

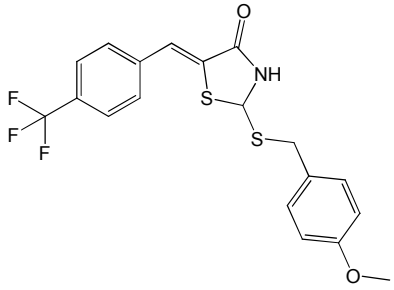

105

(Z)-5-(4-trifluoromethylbenzylidene)-2-(4-methoxybenzylthio)-4-thiazolidinone

(3.1 g, 73% yield) ^{1}**H-NMR** (300 MHz, DMSO-*d6*): δ 7.91 (s, 1H); 7.87(d, J = 8.6 Hz, 2H); 7.82 (d, J = 8.6 Hz, 2H), 7.31 (d, J = 8.2 Hz, 2H), 6.97 (d, J = 8.2 Hz, 2H), 5.01 (s, 2H), 3.81 (s, 3H);-^{13}**C-NMR** (300 MHz, DMSO-d6):
δ = 196.1,177.2,154.1,141.3,131.2,129.6,129.3,129.1, 128.9, 125.8, 125.1, 124.2, 116.2, 58.1, 37.1 MS (ESI): m/z 412 $[M+H]^+$.

4.5.2.7.3 Synthesis of 5-(3-(4-nitrophenyl)-3-oxo-1-(4-(trifluoromethyl)phenyl)propyl)-2-thioxothiazolidin-4-one (107a) and analogues

A solution of 1.6 M n-Buli in hexane (2 equi) was added to 0.35 M diisopropylamine

(2 equiv) in THF at 0℃ under Nitrogen atmosphere. The mixture was stirred for 30 min and cooled to -78 ℃ in dry-ice-acetone bath. T o this solution was added 4-nitrophenyl acetophenone (2 equiv). After stirring for 60 min, compound **105** (1 equiv) was added dropwise to the reaction mixture, and stirring was continued for 60 minutes. The reaction was warmed to room temperature, quenched with saturated ammonium chloride (10 mL), and diluted with water (10 mL). The aqueous layer was extracted with dichloromethane (2 x 50 mL), washed with water (2 x 40 ml) and brine (15 mL), dried over $MgSO_4$, filtered and concentrated in *vacuo*.

The crude material was purified by flash chromatography in a mixture of hexane-ethyl acetate to give intermediate compound.The intermediate compound was then dissolved in trifluoroacetic acid and heated to refflux for 60 min. The solvent was evaporated in *vacuo*, and the crude material was purified by preparative HPLC to yield compound **107a** as diastereomers (1 and 2). Compounds (**107b** to **107i)** were synthesized by following the same procedure.

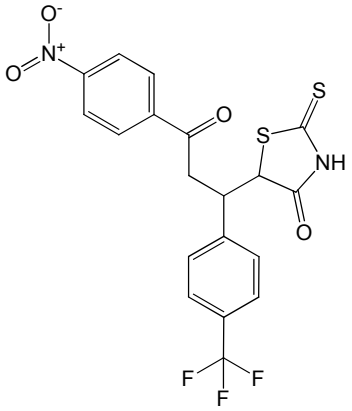

107a

5-(3-(4-nitrophenyl)-3-oxo-1-(4-(trifluoromethyl)phenyl)propyl)-2-thioxothiazolidin-4-one

(30 mg, 27% yield) Diastereomer 1: **^{1}H-NMR** (300 MHz, DMSO-*d6*): δ 13.20 (s, 1H), 8.28 – 8.45 (m, 4H, Ar), 7.94 (d, J = 1.6 Hz, 2H, Ar), 7.62 – 7.81 (m, 2H, Ar), 5.16 (d, J = 2.8 Hz, 1H, CH), 5.05 (d, J = 5.6 Hz, 1H, CH), 4.074 – 4.30 (m, 1H) 3.80 – 3.91 (m, 1H);-**^{13}C-NMR** (300 MHz, DMSO-d6): δ = 202.6, 197.6, 177.2, 155.3, 152.3, 143.4, 139.6, 137.9, 129.6, 129.3, 128.8, 126.1, 125.2, 123.76 (J_{CF} = 35.28 Hz) MS (ESI): *m/z* 455 $[M+H]^+$.

Diastereomer 2: **^{1}H-NMR** (300 MHz, DMSO-*d6*): δ 13.04 (s, 1H), 8.09 – 8.25 (m, 4H, Ar), 7.62 (d, J = 1.1 Hz, 2H, Ar), 7.42 – 7.81 (m, 2H, Ar), 5.12 (d, J = 1.9 Hz , 1H), 4.77 (d, J = 5.6 Hz, 1H), 3.91 – 4.07 (m, 2H), 3.50 – 3.78 (m ,2H);-**^{13}C-NMR** (300 MHz, DMSO-d6): δ = 199.5, 196.7, 177.0,154.7,150.0,143.3, 139.3, 137.7, 129.4, 129.01, 128.5, 125.9, 125.9, 122.8; (J_{CF} = 35.1) MS (ESI): *m/z* 455 $[M+H]^{+}$.

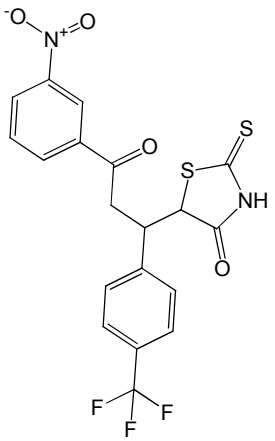

107b

5-(3-(3-nitrophenyl)-3-oxo-1-(4-(trifluoromethyl)phenyl)propyl)-2-thioxothiazolidin-4-one

(27 mg, 24% yield) Diastereomer 1: **^{1}H-NMR** (300 MHz, DMSO-*d6*): δ = 13.16(s,1H), 8.65(s, 1H, Ar), 8.46(d, J = 4.36Hz, 1H, Ar), 8.38 (d, J = 3.95Hz, 1H, Ar), 7.84 (t, J = 6.03, 1H, Ar), 7.67 (d, J = 3.9 Hz, 2H, Ar), 7.58 (J = 4.1 Hz, Ar), 5.16 (d, J = 2.8 Hz, 1H) , 4.21 – 4.30 (m, 1H), 3.96 - 4.09 (m , 1H), 3.72 – 3.83 (m, 1H);-**^{13}C-NMR** (300 MHz, DMSO-d6): δ = 203.1, 196.0, 177.2, 148.0, 144.4, 137.4, 134.2, 130.5, 129.7, 129.0, 128.2, 127.7, 127.6, 125.2, 122.4, 59.6, 41.6, 38.1; MS (ESI): *m/z* 455 $[M+H]^{+}$. Diastereomer 2: **^{1}H-NMR** (300 MHz, DMSO-*d6*): δ 13.04(s, 1H), 8.63(s, 1H, Ar), 8.46 (d , J = 4.36 Hz, 1H, Ar), 8.30 (d, J = 3.9 Hz, 1H, Ar), 7.84 (t, J = 6.0Hz, 1H, Ar), 7.67(d, J = 3.9 Hz, 2H, Ar), 7.58(d, J = 4.1 Hz, 2H, Ar), 5.12 (d, J = 1.9 Hz, 1H, CH), 4.11 – 4.2 (m, 1H), 3.84 – 3.94 (m, 1H), 3.60 – 3.72 (m, 1H);-**^{13}C-NMR** (300 MHz, DMSO-d6): δ = 202.6, 195.6, 177.0, 148.0, 143.4, 137.3, 134.2, 130.5, 129.5, 128.6, 128.1, 127.7, 127.5, 124.9, 122.4, 58.9, 41.4, 38.1 MS (ESI): *m/z* 455 $[M+H]^{+}$.

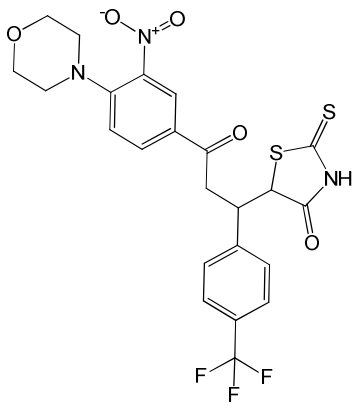

107c

5-(3-(4-morpholino-3-nitrophenyl)-3-oxo-1-(4-(trifluoromethyl)phenyl)propyl)-2-thioxothiazolidin-4-one

((20 mg, 18% yield) Diastereomer 1: **^{1}H-NMR** (300 MHz, DMSO-*d6*): δ 13.15 (s,1H), 8.38 (d, J = 1.18Hz, 1H, Ar), 8.35 (d, J = 1.1 Hz, 1H, Ar), 8.31 (d, J = 1.1 Hz, 1H, Ar), 7.65 (d, J = 4.0 Hz, 2H, Ar), 7.28 – 7.35 (m, 2H, Ar), 5.14 (d, J = 2.7 Hz, 1H, CH), 3.96 – 4.06 (m, 1H), 3.65 – 3.74 (m, 4H), 3.09 – 3.19 (m, 4H);-**^{13}C-NMR** (300 MHz, DMSO-d6): δ = 203, 195.3, 177.6, 148.1, 144.9, 139.5, 133.4, 130.0, 129.3, 128.3, 127.5, 127.2, 126.2, 125.5, 120.2, 66.0, 60.0, 50.7, 42.0, 26.7 MS (ESI): *m/z* 540 $[M+H]^{+}$.

Diastereomer 2: **^{1}H-NMR** (300 MHz, DMSO-*d6*): δ 13.01(s, 1H), 8.07 (d, J = 1.15 Hz, 1H, Ar), 8.04 (d, J = 1.15Hz, 1H, Ar), 8.01 (d, J = 1.2 Hz, 1H, Ar), 3.65 – 3.74 (m, 4H), 3.095 – 3.19 (m, 4H);-**^{13}C-NMR** (300 MHz, DMSO-d6): δ = 201.0, 194.7, 177.4, 148.0, 143.7, 139.4, 133.4, 133.1, 130.016, 129.3, 128.3, 127.4, 127.1, 126.2, 125.2, 120.1, 66.0, 60.0, 50.6, 41.0, 26.7 MS (ESI): *m/z* 540 $[M+H]^{+}$.

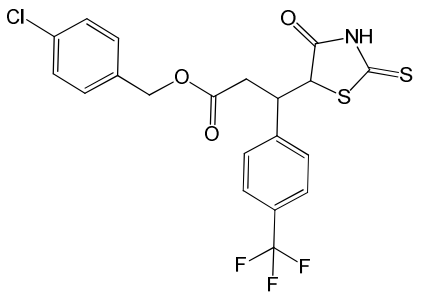

107d

4-chlorobenzyl 3-(4-oxo-2-thioxothiazolidin-5-yl)-3-(4-(trifluoromethyl)phenyl)propanoate

(26 mg, 24% yield) Diastereomer 1: **^{1}H-NMR** (300 MHz, DMSO-*d6*): δ 13.09 (s, 1H), 7.64 (d, J = 4.4Hz, 2H, Ar), 7.43 – 7.51 (m, 2H, Ar), 7.25 – 7.3 (m, 2H, Ar), 7.10 – 7.18 (m, 2H, Ar), 5.40 (s, 1H, CH), 5.10 – 5.17 (m, 1H, CH), 4.95 (d, J = 2.0 Hz, 1H), 3.96 – 4.06 (m, 1H);**^{13}C-NMR** (300 MHz, DMSO-d6): δ = 203.2, 177.7, 170.7, 158.8, 149.6, 135.4, 133.2, 129.5,129.2, 128.2, 125.3, 65.1, 60.1, 37.2, 31.2 MS (ESI): m/z 475 $[M+H]^{+}$.

Diastereomer 2: **^{1}H-NMR** (300 MHz, DMSO-*d6*): δ 13.09 (s, 1H), 7.64 (d, J = 4.36Hz, 2H, Ar), 7.43 – 7.51 (m, 2H, Ar), 7.256 – 7.34 (m, 2H, Ar), 7.10 – 7.18 (m, 2H, Ar), 5.40 (s, 1H, CH), 5.0 – 5.08 (m, 1H, CH), 4.95 8d, J = 2.03 Hz, 1H), 3.96 – 4.06 (m, 1H);-**^{13}C-NMR** (300 MHz, DMSO-d6): δ = 203.2, 177.7, 170.7, 158.8, 149.6, 135.3, 133.2, 129.5, 129.2, 128.2, 125.3, 62.4, 59.6, 37.2, 31.2; MS (ESI): m/z 475 $[M+H]^{+}$.

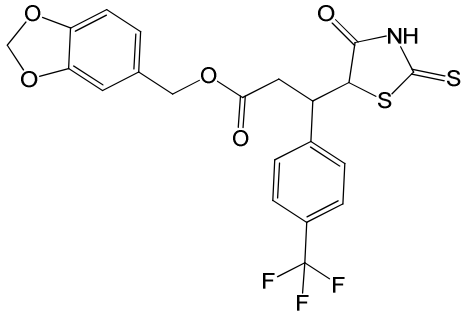

107e

benzo[d][1,3]dioxol-5-ylmethyl 3-(4-oxo-2-thioxothiazolidin-5-yl)-3-(4-(trifluoromethyl)phenyl)propanoate

(33 mg, 30% yield) Diastereomer 1: **^{1}H-NMR** (300 MHz, DMSO-*d6*): δ = 13.20 (s,1H), 7.88 (d, J = 4.04 Hz, 2H, Ar), 7.62 – 7.73 (m, 2H, Ar), 7.05 (d, J = 5.67Hz, 1H, Ar), 6.72 – 6.86 (m, 1H, Ar), 6.33 (d, J = 5.1 Hz, 1H, Ar), 5.84 – 6.02 (m, 1H, CH),

5.14 (d, J = 3.2 Hz, 1H, CH), 3.96 – 4.02 (m, 1H), 3.66 – 3.73 (m, 1H);-^{13}**C-NMR** (300 MHz, DMSO-d6): δ = 203, 177.3, 172.1, 144.2, 153.4, 129.8, 129.3, 125.6, 125.2, 101,2, 60.0, 59.15, 37.4, 35.7; MS (ESI): *m/z* 484 $[M+H]^+$.

Diastereomer 2: ^{1}**H-NMR** (300 MHz, DMSO-*d6*): δ = 13.20 (s, 1H), 7.80 (d, J = 4.35 Hz, 2H, Ar), 7.44 -7.59 (m, 2H, Ar), 7.05 (d, J = 5.67 Hz, 1H, Ar), 6.57 – 6.72 (m, 1H, Ar), 6.33 (d, J = 5.1 Hz, 1H, Ar), 5.82 – 5.98 (m, 1H, CH), 5.03 (d, J = 3.1 Hz, 1H, CH) 3.66 – 3.73 (m, 1H, CH), 2.70 – 2.84 (m, 1H);-^{13}**C-NMR** (300 MHz, DMSO-d6): δ = 203, 177.3, 172.1, 144.2, 143.4, 129.8, 129.3, 125.6, 125.2, 101.1, 60.0, 58.9, 37.4, 35.7; MS (ESI): *m/z* 484 $[M+H]^+$.

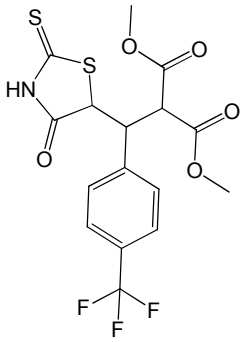

107f

Dimethyl 2-((4-oxo-2-thioxothiazolidin-5-yl)(4-(trifluoromethyl)phenyl)methyl)malonate

(52 mg, 47 % yield) Diastereomer 1: ^{1}**H-NMR** (300 MHz, DMSO-*d6*): δ = 13.16 (s,1H), 7.70 (d, J = 3.7 Hz, 2H, Ar), 7.52 (d , J = 4.0 Hz, 2H, Ar), 5.08 – 5.12 (m, 1H, CH), 4.12 – 4.32 (m, 1H, CH), 4.58 (s, 1H, CH), 4.05 (s, 6H), 3.78 – 3.91 (m, 1H CH);-^{13}**C-NMR** (300 MHz, DMSO-d6): δ = 203.1, 177.4, 166.8, 158.8, 141.5, 130.6, 129.1, 128.8, 125.5, 125.2, 62.3, 61.5, 57.4, 54.0, 54.0, 45.7, 14.3; MS (ESI): m/z 422 $[M+H]^+$

Diastereomer 2: ^{1}**H-NMR** (300 MHz, DMSO-*d6*): δ = 13.00 (s, 1H), 7.67(d, J = 3.8 Hz, 2H, Ar), 7.46 (d, J = 4.0 Hz, 2H, Ar), 5.08 – 5.12 (m, 1H, CH), 3.98 – 4.11 (m, 1H, CH), 4.54 (s, 2H), 4.21 (s, 6H), 3.65 – 3. 73 (m, 1H);-^{13}**C-NMR** (300 MHz, DMSO-d6): δ = 202.8, 177.1, 167.3, 166.6, 158.3, 140.0, 130.0, 130.0, 129.0, 128.7, 125.1,125.5, 62.2, 61.0, 56.3, 53.3, 45.0,14.2 MS (ESI): *m/z* 422 $[M+H]^+$

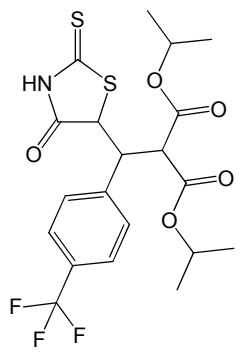

107g

Diisopropyl 2-((4-oxo-2-thioxothiazolidin-5-yl)(4-(trifluoromethyl) phenyl)methyl) malonate

(62 mg, 56% yield) Diastereomer 1: **^{1}H-NMR** (300 MHz, DMSO-*d6*): δ 13.1 (s, 1H), 7.68 (t, J = 5.1 Hz, 2H, Ar), 7.52 (t, J = 5.0 Hz, 2H, Ar), 5.15 (d, J = 2.0 Hz, 1H, CH), 4.94 – 5.01 (m, 1H, CH), 4.53 – 4.66 (m, 1H, CH), 4.25 - 4.33 (m, 2H), 1.12 – 1.27 8 (m, CH_3);-**^{13}C-NMR** (300 MHz, DMSO-d6): δ = 202.8, 177.4, 166.5, 166.6, 141.8 , 141.8, 139.6, 130.3, 129.8, 129.8, 129.7, 128.8, 128.4, 126.2, 125.1, 69.6, 68.8, 59.7, 57.2, 54.0, 21.1; MS (ESI): *m/z* 478 $[M+H]^+$

Diastereomer 2: **^{1}H-NMR** (300 MHz, DMSO-*d6*): δ 12.99 (s, 1H), 7.68 (t, J = 5.1 Hz, 2H, Ar), 7.44 (t, J = 5.1 Hz, 2H, Ar), 5.08 (d, J = 2.0 Hz, 1H, CH), 4.69 – 4.82 (m, 1H, CH), 4.45 – 453 (m, 1H, CH), 4.15 – 4.24 (m, 2H), 0.77 – 0.94 (m, CH_3);-**^{13}C-NMR** (300 MHz, DMSO-d6): δ = 202.4,176.7, 165.9, 165.6, 141.8, 138.8, 130.3, 129.8, 129.4, 128.7, 128.3, 125.8, 124.8, 69.5, 68.8, 59.7, 55.9, 53.3; MS (ESI): m/z 412 $[M+H]^+$.

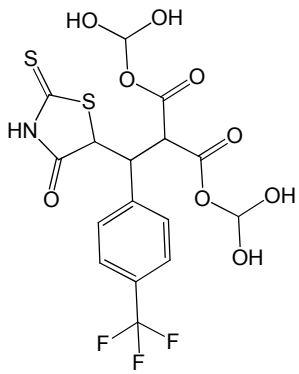

107h

Bis(dihydroxymethyl)2-((4-oxo-2-thioxothiazolidin-5-yl)(4-(trifluoromethyl)phenyl)methyl)malonate

(47 mg, 42% yield) Diastereomer 1: **^{1}H-NMR** (300 MHz, DMSO-*d6*): δ = 13.09 (s,1H, OH), 12.04 (s, 1H, NH), 7.65 – 7.73 (m, 2H, Ar), 7.52 (d, J = 4.2 Hz, 2H, Ar), 5.07 - 5.13 (m, 2H), 4.59 (d, J = 1.8 Hz, 1H, CH), 4.13 – 4.26 (m, 2H):-**^{13}C-NMR** (300 MHz, DMSO-d6): δ = 202.8, 177.7, 175.3, 157.2, 135.1, 130.7, 129.7, 129.2, 125.5, 125.5, 124.6, 141.5, 62.3, 61.5, 31.0 MS (ESI): *m/z* 486 $[M+H]^{+}$.

Diastereomer 2: **^{1}H-NMR** (300 MHz, DMSO-*d6*): δ = 13.04 (s,1H, OH), 11.93 (s, 1H, NH), 7.65 – 7.73 (m, 2H, Ar), 7.45 (d, J = 4.1 Hz, 2H, Ar), 4.96 – 5.00 (m, 2H), 4.55 (d, J = 1.7 Hz, 1H, CH), 3.97 – 4.06 (m, 2H);-**^{13}C-NMR** (300 MHz, DMSO-d6):
δ = 202.6, 177.0, 175.5, 156.8, 135.0, 130.6, 129.1, 125.2, 125.1, 124.3, 141.2, 62.2, 62.0, 31.0; MS (ESI): *m/z* 486 $[M+H]^{+}$.

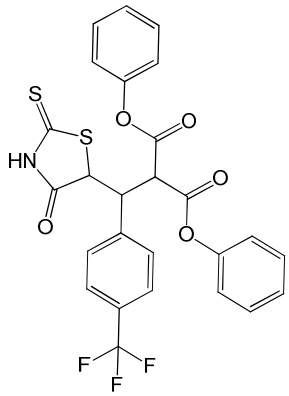

107i

Diphenyl 2-((4-oxo-2-thioxothiazolidin-5-yl)(4-(trifluoromethyl)phenyl)methyl)malonate

(15 mg, 13% yield) Diastereomer 1: **^{1}H-NMR** (300 MHz, DMSO-*d6*): δ 13.1(s, 1H), 7.88 (d, J = 7.14Hz, 4H, Ar) 7.67 – 7.78 (m, 6H, Ar), 7.36 (d, J = 6. 4 Hz, 2H, Ar), 6.97 – 7.11 (m, 2H, Ar), 5.14 – 5.28 (m, 1H, CH), 4.37 – 4.54 (m, 1H, CH), 3.95 – 4.11 (m, 1H, CH);- **^{13}C-NMR** (300 MHz, DMSO-d6): δ = 195.9, 177.9, 170.8, 158.8, 135.4, 131.1, 130.7, 130.4, 130.0, 129.79, 129.2, 129.0, 128.8, 128.5, 126.4, 125.2, 67.1, 60.0, 55.5, 31.0; MS (ESI): m/z 546 $[M+H]^{+}$.

Diastereomer 2: **^{1}H-NMR** (300 MHz, DMSO-*d6*): δ 13.03 (s, 1H), 7.88 (d, J = 7.14Hz, 4H, Ar), 7.54 – 7.67 (m, 6H, Ar), 7.25 (d, J = 6.4 Hz, 2H, Ar), 6.68 – 6.90 (m, 2H, Ar), 4.79 – 4.97 (m, 1H, CH), 4.22 – 4.36 (m, 1H, CH), 3.95 – 4.11 (m 1H, CH);-**^{13}C-NMR** (300 MHz, DMSO-d6): δ = 195.9, 177.9, 170.8, 158.2, 131.1, 130.7, 130.4, 129.97, 129.7, 129.2, 129.0, 128.6, 128.4, 126.4, 125.2, 67.1, 60.0, 55.5, 31.0; MS (ESI): m/z 546 $[M+H]^{+}$

[1] James, A.; Christopher, L.M. Reaching for high-hanging fruit in drug discovery at protein-protein interfaces. *Nature*. **2007**, 450, 1001 -1009.

[2] Eric, M.P.; Stanley, F. Protein-protein Interactions: Methods for Detection and Analysis. *Microbiological Reviews*. **1995**, 59(1), 94 -123.

[3] Monod, J.; Wyman, J.; Changeux, J.P. On the nature of allosteric transitions: a plausible model. *J. Mol. Biol*. **1965**, 12**,** 88 -118.

[4] Porpaczy, Z.; Sumegi, B.; Alkonyi, I. Association between the a-ketoglutarate dehydrogenase complex and succinate thiokinase. *Biochim. Biophys. Acta*, **1983**, 749**,** 172 -179.

[5] Yanofsky, C.; Rochmeler, M. The exclusion of free indole as an intermediate in the biosynthesis of tryptophan in Neurospora crassa*. Biochim. Biophys. Acta*. **1958**, 28, 640 - 645

[6] Weber, J.; R. Lee, S.F.; Wilke-Mounts, S.; Grell, E.; Senior, A. E. Combined application of site-directed mutagenesis, 2-azido-ATP labeling, and *lin*-benzo-ATP binding to study the noncatalytic sites of *Escherichia coli* F1-ATPase. *J. Biol. Chem.***1993**, 268, 6241 - 6247.

[7] Hill, R. L.; Brew, K.; Lactose synthetase. *Adv. Enzymol*. **1975,** 43, 411 - 490.

[8] Susskind, M. M.; Youderian, P. Bacteriophage P22 antirepressor and its control. *In* R. W. Hendrix, J. W. Roberts, F. W. Stahl, and R. A. Weisberg (ed.), Lambda II. Cold Spring Harbor Laboratory Press, Cold Spring Harbor, N.Y. **1983**, 347 - 363.

[9] Ingham, R.J.; Colwill, K.; Howard. C.; Dettwiler, S.; Lim, C.S.; Yu, J.; Hersi, K.; Raaijmakers, J.; Gish, G.; Mbamalu, G.; Taylor, L.; Yeung, B.; Vassilovski, G.; Amin, M.; Chen, F; Matskova, L.; Winberg, G.; Ernberg, I.; Linding, R.;O´donnel, P.; Starostine, A.; Keller, W.; Metalnikov, P.; Stark, C.; Pawson, T. WW domains provide a platform for the assembly of multiprotein networks, *Moll cell Biol*. **2005**, 25 (16) 7092 - 7106.

[10] Pawson, T. Protein modules and signaling networks**.** *Nature.***1995**, 373**,** 573 - 580.

[11] Simon, J.A.; Schreiber, S.L. Grb2 SH3 binding to peptides from Sos evaluation of a general model for SH3 – ligand interactions. *Chem& Biol*. **1995,** 2**,** 53 - 60.

[12] Pawson, T. Dynamic control of signalling by modulator adaptor proteins*, Curr Opin Cell Biol*. **2007**, 19, 112 -116.

[13] Sheng, M; Sala, C. PDZ domains and the organization of supramolecular complexes. *Annu Rev Neurosci*. **2001**, 24, 1 - 29.

[14] Zhang, M; Wang, W. Organization of signalling complexes by PDZ-domain scaffold proteins. *Acc Chem Res*. **2003**, 36, 530 - 538.

[15] David C. Fry. Protein-Protein Interactions as Targets for Small Molecule Drug Discovery. *Biopolymers (Peptide Science)*. **2006**, 84, 535 - 552.

[16] Jones, S.; Thornton, J. Principles of protein-protein interactions*. Proc Natl Acad Sci*. USA. **1996**, 93, 13 -20.

[17] Hopkins, A.L.; Groom, C.R. The druggable genome. *Nature rev. Drug Discov*. **2002**, 1, 727-730.

[18] Alan, C. C.; Ryan, G. C.; Kathleen, T. S.; Qing, C.; Patricia, S,; Daniel, R. C.; Anna, C. S.; Enoch, S. H. Structure-based maximal affinity model predicts small-molecule druggability. *Nature Biotechnol.* **2007**, 25, 71 - 75.

[19] Smith, R. D. Hu, L; Falkner, J.A; Benson, M.L.; Nerothin, J.P.; Carlson, H.A. Exploring protein - ligand recognition with Binding MOAD *J. Mol. Graph. Model*.

2006, 24, 414 - 425.

[20] Conte, L. L.; Chothia, C.; Janin, J. The atomic structure of protein–protein recognition sites. *J. Mol. Biol.* **1999**, 285, 2177 - 2198.

[21] Graham, T.A.; Weaver, C.; Mao, F.; Kimelman, D.; Xu, W. Crystal structure of a ß-catenin/Tcf complex. *Cell*. **2000**, 103, 885 - 896.

[22] Poy, F.; Lepourcelet, M.; Shivdasani, R.A.; Eck, M.J. Structure of a human Tcf4-ß-catenin complex. *Nat Struct Biol*. **2001**, 12, 1053 -1057

[23] Bogan, A.A.; Thorn, K.S.; Anatomy of hot spots in protein interfaces, *J. Mol. Biol*. **1998**, 280, 1 - 9.

[24] Clackson,T.; Wells, J.A.; A hot spot of binding energy in a hormone-receptor interface, *Science*. **1995**, 267, 383 - 386.

[25] Michelle, R.A.; James, A.W. Small-Molecule Inhibitors of protein-protein interactions: Progressing towards the dream, *Nature Reviews Drug Discovery*.**2004**, 3, 301 - 317.

[26] Peczuh, M.W; Hamilton, A.D. Peptide and protein recognition by designed molecules. *Chem Rev*. **2000**, 100, 2479 - 2494.

[27] Kallen, J; Welzenbach, K; Ramage, P; Geyl, D; Kriwacki, K; Legge, G; Cottens,S; Weitz-Schmidt, G; Hommel, U. Structural basis for LFA-1 inhibition upon lovastatin binding to the CD11a I-domain. *J Mol Biol*. **1999**, 292, 1- 9.

[28] Emerson, S.D; Palermo, R; Liu, C.M.; Tilley, J.W.; Chen, L.; Danho, W.; Madison, V.S.; Greeley, D.N.; Ju, G.; Fry, D.C. NMR characterization of interleukin-2 in complexes with the IL-2Rα receptor component and with low molecular weight compounds that inhibit the IL-2/IL-Rα interaction, *Protein Sci* . **2003**, 12, 811- 822.

[29] Vassilev, L.T.; Vu, B.T.; Graves, B.; Carvajal, D.; Podlaski, F.; Filipovic, Z.;Kong, N.; Kammlott, U.; Lukacs , C.; Klein , C.; Fotouhi, N.; Liu , E.A. In vivo activation of the p53 pathway by small-molecule antagonists of MDM2. *Science*. **2004**, 303, 844 - 848.

[30] Lipinski, C.A.; Drug-like properties and the causes of poor solubility and poor permeability, *J. Pharmacol. Toxicol. Methods*. **2001**, 44, 235 - 249.

[31] Lipinski, C.A.; Lombardo, F.; Dominy, B.W.; Feeney, P.J. Experimental and computational approaches to estimate solubility and permeability in drug discovery and development settings, *Adv.Drug Deliv.Rev*. **1997**, 23, 3 - 25.

[32] Cho, K.O.; Hunt, C.A.; kennedy, M.B.; The rat brain postsynaptic density fraction contains a homolog of the *Drosophila* discs-large tumor suppressor protein, *Neutron*. **1992**, 9, 929 - 942.

[33] Woods, D.F.; Bryant, P.J. Zo-1, DlgA and PSD-95/SAP90: homologous protein in tight, septate and synaptic cell junctions. *Mech.Dev*, **1993**, 44(2-3), 85 - 89.

[34] Schultz, J.; Milpetz, F.; Bork, P.; Ponting, C.P.; SMART, a simple modular architecture research tool: identification of signaling domains. *Proc Natl Acad Sci USA*, **1998,** 95(11), 5857- 5864.

[35] Kennedy, M.B. Origin of PDZ (DHR, GLGF) domains. *Trends Biochem.Sci*. **1995**. 20(9), 350.

[36] Ponting, C.P.; Phillips, C.; Davies, K.E., Blake, D.J. PDZ domains: targetin signalling molecules to submembranous sites. *Bioassays*. **1997**, 19, 469 - 479.

[37] Zhang, M; Wang, W. Organization of signalling complexes by PDZ-domain scaffold proteins. *Acc Chem Res*. **2003**, 36(7), 530 - 538.

[38] Fanning, A.S; Anderson, J.M., Protein-protein interactions: PDZ domain networks. *Curr Biol*. **1996**, 6(11), 1385 - 1388.

[39] Kurakin, A; Swistowski, A.; Wu, S.C.; Bredesen, D.E. The PDZ domain as a complex adaptive system. *PLoS ONE*, **2007**, 2(9), e953.

[40] Wen, W.; Wang, W.; Zhang, M. Targeting PDZ domain proteins for treatingNMDA receptor-mediated excitotoxicity. *Curr Top Med Chem*. **2006**, 6(7), 711 – 721.

[41] Day, P.; Kobilka, B. PDZ-domains arrays for identifying components of GPCR signaling complexes. *Trends Pharmacol Sci*. **2006**, 27(10), 509 - 511.

[42] Schulte, G; Bryja, V. The Frizzled family of unconventional G-protein-coupledreceptors. *Trends Pharmacol Sci*. **2007**, 28(10), 518 - 525.

[43] Morais, C.J.H.; Petosa, C.; Sutcliffe,M.J. Crystal structure of a PDZ domain. *Nature*. **1996**, 382 (6592), 649 - 652.

[44] Harrison, S.C. Peptide-surface association. The case of PDZ and PTB domains. *Cell*. **1996**, 86, 341-343.

[45] Baruch, Z.H.; Wendell, A.L. Mechanism and role of PDZ domains in signalling complex assembly. *Journal of Cell Science*. **2001**, 114, 3219 - 3231.

[46] Albert Y.H.; Morgan, S. PDZ domains: Structural Modules for Protein Complex Assembly. The Journal of Biological Chemistry. **2002**, 227(8), 5699 - 5702.

[47] Doyle, D.A.; Lee, A.; Lewis, J.; Kim, E.; Sheng, M.; Mackinnon, R. Crystal structures of a complexed and peptide-free membrane protein-binding domain: molecular basis of peptide recognition by PDZ. *Cell*. **1996**, 85, 1067-1076.

[48] Subramanian, K; Teli, L; John, A. Structural Basis of the Na1/H1 ExchangerRegulatory Factor PDZ1 Interaction with the Carboxyl-terminal Region of the Cystic Fibrosis Transmembrane Conductance Regulator, *J.Biol.Chem*. **2001**, 23(8), 19683-19686.

[49] Laskowski, R.A.; Chistyakov, V.V.; Thornton, J.M.; PDBsum more: new summaries and analyses of the known 3D strutures of proteins and nucleic acids. *Nucleic Acids Res*, **2005**, 33, D266 - D268.

[50] Songyang, Z.; Fanning, A.S.; Fu,C.; Xu,J.; Marfatia, S.M.; Chisti, A.H.; Crompton, A.; Chan, A.C.; Anderson, J.M.; Cantley, L.C. Recognition of unique carboxyl-terminals motifs by distinct PDZ domains. *Science*. **1997**, 275, 73 -77.

[51] Schultz, J; Hoffmüller, U.; Krause, G.; Ashurts, J.; Macias, M.J.; Schmieder, P.; Schneider-Mergener, J.; Oschkinat, H. Specific interactions between the syntrophin PDZ domain and voltage-gated sodium channels, *Nat.Struct.Biol*. **1998**, 5, 19 - 24.

[52] Tochio, H.; Hung, F.; Li, M.; Zhang, M. Solution structure and backbone dynamics of the second PDZ domains. *Science.* **1997**, 275, 73 -77.

[53] Stephen, H.G.; Stéphane, Q.; Christian, R.L.; Josée, C.; Single-Amino Acid Substitutions Alter the Specificity and Affinity of PDZ domains for Their Ligands. *Biochemistry* . **2000**, 39, 14638 -14646.

[54] Lee, H,J.; Zhang, J.J.; PDZ domains and their binding partners: structure, specifity, and modification. *Cell communication and Signaling* **2010**, 8:8 Http://www.biosignaling.com/content/8/1/8.

[55] Im, Y.J.; Lee, J.H.; Park, S.H.; Rho, S.H.; Kang, G.B.; Kim, E.; Eom, S.H.; Crystal structure of the Shank PDZ-ligand complex reveals a class I PDZ interaction and a novel PDZ-PDZ dimerization. *J Biol Chem*, **2003,** 278, 48099 – 48104.

[56] Im, Y.J.; Park, S.H.; Rho, S.H.; Lee, J.H.; Kang, G.B.; Sheng, M.; Kim, E.; Eom, S.H.; Crystal structure of GRIP1 PDZ6-peptide complex reveals the structural basis of class II PDZ target recognition and PDZ domain-mediated multimerization. *J Biol Chem*, **2003,** 278, 8501 - 8507.

[57] Utepbergenov DI, Fanning AS, Anderson JM. Dimerization of the scaffolding protein ZO-1 through the second PDZ domain. *J Biol Chem* **2006**, 281, 24671 – 24677.

[58] Wu J, Yang Y, Zhang J, Ji P, Du W, Jiang P, Xie D, Huang H, Wu M, Zhang G, Wu J, Shi Y. Domain-swapped dimerization of the second PDZ domain of ZO2 may provide a structural basis for the polymerization of claudins**.** *J Biol Chem* **2007**, 282, 49, 35988 – 35999.

[59] Chen J, Pan L, Wei Z, and Zhao Y, Zhang M. Domain-swapped dimerization of ZO-1 PDZ2 generates specific and regulatory connexin43-binding sites**.** *EMBO J* **2008**, 27, 2113 - 2123.

[60] Brian, J. H. ; Karen, S. C.; Kenneth, E. P. ; David, S. B.; Wendell, A. L. Unexpected Modes of PDZ Domain Scaffolding Revealed by Structure of nNOS-Syntrophin Complex, *Science*. **1999**, 284, 808 - 812.

[61] Hartmut, O.; A new type of PDZ domain recognition, *Nat. Struct.Biol*. **1999**, 5, 408 - 410.

[62] Subbaiah, V.K.; Kranjec, C.; Thomas, M.; Banks, L. PDZ domains: the building blocks regulating tumorgenesis. *Biochem J*. **2011** , 439(2),195 - 205.

[63] Salmena, L.; Carracedo, A.; Pandolfi, P.P. Tenets of PTEN tumor suppression. *Cell*. **2008**, 133, 403 - 414.

[64] Chen, X.; Macara, I.G. Par-3 controls tight junction assembly through the Rac Exchange factor Tiam1. *Nat. Cell Biol*. **2005**, 7, 262 - 269.

[65] Wheeler, D.S.; Barrick, S.R.; Grubisha, M.J.; Brufsky, A.M.; Friedman, P.A.; Romeo, G. Direct interaction between NHERF1 and Frizzled regulates β-catenin signalling. *Oncogene*. **2011**, 30, 32 - 42.

[66] Fahmy, O. G.; Fahmy, M. New mutants report. *Dros. Inf. Serv.* **1959**, 33, 82 - 94.

[67] Perrimon, N.; Mahowald, A. P. Multiple functions of segment polarity genes in Drosophila. *Dev. Biol.* **1987**, 119, 587- 600.

[68] Krasnow, R. E.; Wong, L. L.; Adler, P. N. Dishevelled is a component of the frizzled signaling pathway in Drosophila. *Development.* **1995**, 121, 4095 - 4102.

[69] Theisen, H.; Purcell, J.; Bennett, M.; Kansagara, D.; Syed, A.; Marsh, J. L. dishevelled is required during wingless signaling to establish both cell polarity and cell identity. *Development.* **1994**, 120, 347 - 360.

[70] Axelrod, J. D.; Miller, J. R.; Shulman, J. M.; Moon, R. T.; Perrimon, N. Differential recruitment of Dishevelled provides signalling specificity in the planar cell polarity and Wingless signaling pathways. *Genes Dev.* **1998**, 12, 2610 – 2622.

[71] Boutros, M., Paricio, N., Strutt, D. I. and Mlodzik, M. Dishevelled activates JNK and discriminates between JNK pathways in planar polarity and wingless signaling. *Cell*. **1998,** 94, 109 -118.

[72] Shosei, K.; Hideki, Y.; Akira, K.; Wnt-3a and Dvl Induce Neurite Retraction by Activating Rho-Associated Kinase. *Molecular and Cellular Biology*. **2004**, 24(10), 4487- 4501.

[73] Wallingford, B.J.; Raymond H.; The developmental biology of Dishevelled: an enigmatic protein governing cell fate and cell polarity. *Development*. **2005**, 132, 4421- 4436.

[74] Uematsu, K.; He, B.; You, L.; Xu, Z.; McCormick, F.; Jablons, D. M. Activation of the Wnt pathway in non small cell lung cancer: evidence of dishevelled overexpression. *Oncogene*. **2003,** 22, 7218 -7221.

[75] Uematsu, K.; Kanazawa, S.; You, L.; He, B.; Xu, Z.; Li, K.; Peterlin, B. M. McCormick, F.; Jablons, D. M. Wnt pathway activation in mesothelioma: evidence of dishevelled overexpression and transcriptional activity of β-catenin *Cancer Res.* **2003**,63, 4547 - 4551.

[76] Bui, T. D.; Beier, D. R.; Jonssen, M.; Smith, K.; Dorrington, S. M.; Kaklamanis, L.; Kearney, L.; Regan, R.; Sussman, D. J.; Harris, A. L. cDNA cloning of a human dishevelled DVL-3 gene, mapping to 3q27, and expression in humanbreast and colon carcinomas *Biochem. Biophys. Res. Commun.* **1997**, 239, 510 - 516.

[77] Mizutani, K.; Miyamoto, S.; Nagahata, T.; Konishi, N.; Emi, M.; Onda, M. Upregulation *and* Overexpression of DVL1, the Human. Counterpart of the Drosophila Dishelved Gene, in Prostate Cancer *Tumori.* **2005**, 91, 546 - 551.

[78] Wong, H.; Mao,J.; Nguyen, J.T.; Srinivas, S.; Zhang, W.; Liu, B.; Li, L.; Wu, D.; Zheng,J. Structural basis of the recognition of the dishevelled DEP domain in the Wnt signaling pathway. *Nat. Struct. Biol*. **2000**, 7, 1178 -1184.

[79] Capelluto, D. G.; Kutateladze, T. G.; Habas, R.; Finkielstein, C. V.; He, X.; Overduin, M. The DIX domain targets dishevelled to actin stress fibres and vesicular membranes. *Nature*. **2002**, 419, 726 -729.

[80] Penton, A.; Wodarz, A.; Nusse, R.; A mutational analysis of dishevelled in Drosophila defines novel domains in the dishevelled protein as well as novel surprising alleles of axin. *Genetics*, **2002**, 161, 747 - 762.

[81] Rothbächer, U.; Laurent, M. N.; Deardorff, M. A.; Klein, P. S.; Cho, K. W. Y.; Fraser, S. E. Dishevelled phosphorylation, subcellular localization and homomerization regulate its role in early embryogenesis EMBO *J.* **2000***,* 19,1010-1022.

[82] Malbon, C. C.; Wang, H. Y. Dishevelled: a mobile scaffold catalyzing development. *Curr. Top Dev. Biol.* **2006***,* 72, 153 - 166.

[83] Uthoff,S.M.; Eichenberger, M.R.; McAuliffe, T.L.; Galandiuk, S.; Wingless-type frizzled protein receptor signaling and its putative role in human colon cancer. *Mol Carcing.* **2001** 31(1), 56-62.

[84] Keith.A; Wharton.Jr. Runnin with the Dvl: Proteins That Associate with Dsh/Dvl and Their Significance to Wnt Signal Transduction, *Developemental Biology*, **2003**, 253, 1 - 17.

[85] Weeraratna, A.T.; Jiang, Y.; Hostetter, g,; Rosenblatt, k.; Duray, P.; Bittner, M.; Trent. J.M.; wnt5a signalling directly affects cell motility and invasion of metastic melanoma, *Cancer Cell*, **2002**, 1, 279 - 288.

[86] Yuzugullu, H.; benhaj, K.; Ozturk, N.; Senturk, S., celik, E.; toylu, A., Tasdemir, N.; Yilmaz, M.; Erdal, E.; Akcali, K.C.; Cananical Wnt signaling is antagonized by non-canonical wnt5a in heptacellular carcinoma cells. *Mol.Cancer*, **2009**, 8, 90

[87] Wong, H.C.; Bourdelas, A.; Krauss, A.; Lee, H.J.; Shao, Y.; Wu, D.; Mlodzik, M.; Shi, D.L.; Zheng, Direct binding of the PDZ domain of Dishevelled to a conserved internal sequence in the C-terminal region of Frizzled *J. Mol. Cell*, **2003**, 12(5), 1251 - 1260.

[88] Yingnan, Z.; Brent, A.A.; Christian, W.; ted, Lau.; Mike, Costa.; Rami, N.H.;Sachdev, S.S.; Inhibtion of Wnt signaling by Dishevelled PDZ peptides, *natur chemical biology*, **2009**, 5 (4); 217 -219.

[89] Chandanamali, P.; Antonio, M.F.; Robert, C.; Patrick, R.; Naoaki, F.; Sequence requirement and subtype specificity in the high-affinity interaction between human frizzled and dishevelled proteins, *Protein Science*, **2009**, 18, 994 - 1002.

[90] Cheyette, B.N.; Waxman, J.S.; Miller, J.R.; Takemaru, K.; Sheldahl, L.C.; khlebtsova, N.; Fox, E.P.; Earnest, T.; Moon, J.R. Dapper, a Dishevelled-associated antagonist of β-catenin and JNK signalling is required for notochord formation *Dev.cell*, **2002**, 2, 449 - 461.

[91] Lee, H.J.; Wang, X.N.; Shao, Y.; Zhenz, J.J.; Identification of tripeptides recognized by the PDZ domain of Dishevelled, Bioorganic &Medicinal Chemistry, **2009**, 17(4) , 1701 - 1708.

[92] Su, L.; Hattori, Moriyama, M.; Murata, N.; Harazaki, M.; Kaibuchi, K.; Minato, N.; AF-6 controls integrin-mediated cell adhesion by regulating Rap1 activation through the specific recruitment of Rap1GTP and SPA-1. *J.Biol.Chem*. **2003**, 278, 15232 - 15238.

[93] Ponting C.P.; Benjamin, D.R.; A novel family of Ras-binding domains. **1996**,*Trends Biochem Sci*. 21(11), 422 - 425.

[94] Hofmann, K.; Bucher, P.; The FHA domain: a putative nuclear signalling domain found in protein kinases and transcription factors. *Trends Biochem Sci*. **1995**, 20(9), 347 - 349.

[95] Ponting, C.P.; AF-6/cno: neither a kinesin nor a myosin, but a bit of both.*Trends Biochem Sci*. **1995** 20(7), 265 - 266.

[96] Zhou, H.; Xu, Y.; Yang, Y.; Huang, A.; Wu, J.; Shi, Y. ; Solution structure of AF-6 PDZ domain and its interaction with the C-terminal peptides from Neurexin and Bcr, *J Biol Chem*. **2005**, 280(14), 13841 - 13847.

[97] Radziwill, G., Erdmann, R.A.; Margelisch, U.;Moelling, K.; The Bcr kinase downregulates Ras signaling by phosphorylating AF-6 and binding to its PDZ domain. *Mol.Cell.Biol*. **2003**, 23, 4663 - 4672.

[98] Ebnet, K.; Schulz, C.U.; Meyer Zu Brickwedde, M.K.;Pendl, G.G.; Vestweber, D.; Junctional adhesion molecule interacts with the PDZ domain-containing proteins AF-6 and ZO-1. *J Biol Chem*. **2000**, 275(36), 27979 - 27988.

[99] Takahashi, K.; Nakanishi, H.; Miyahara, M.; Mandai, K.; Satoh, K:; Satoh, A.; Nishioka, H.; Aoki, J.; Nomoto, A.; Mizoguchi, A.; Takai, Y.; Nectin/PRR: an

immunoglobulin-like cell adhesion molecule recruited to cadherin-based adherens junctions through interaction with Afadin, a PDZ domain-containing protein. *J Cell Biol*.**1999** , 145(3), 539 - 549.

[100] Hock, B.; Böhme, B.; Karn, T.; Yamamoto, T.; Kaibuchi, K.; Holtrich, U.; Holland, S.; Pawson,T.; Rübsamen-Waigmann, H.; Strebhardt, K.; PDZ-domain-mediated interaction of the Eph-related receptor tyrosine kinase EphB3 and the ras-binding protein AF6 depends on the kinase activity of the receptor. *Proc Natl Acad Sci U S A*. **1998**, 95(17), 9779 - 9784.

[101] Wiedemann, U., Boisguerin, P., Leben, R., Leitner, D., Krause, G., Moelling, K., Volkmer-Engert, R. Oschkinat, H. Quantification of PDZ Domain Specificity, Prediction of Ligand Affinity and Rational Design of Super-binder Peptides.
2004, *J. Mol. Biol.* 343, 703 -718.

[102] Joshi,M.; Vargas, C.; Boisguerin, P.; Diehl, A.; Krause, G.; Schmieder, P.; Moelling, K.; Hagen, V.; Oschkinat, H. Discovery of low-molecular weight ligands for the AF6 PDZ domain. *Angew.Chem.Int.Ed*. **2006**, 45, 3790 - 3795.

[103] Oertner, T.G.; Matus, A.; Calcium regulation of actin dynamics in dendritic spines. *Cell Calcium*. **2005**, 37, 477- 482.

[104] Jao, H.M.; Carlo. P.; Michael, J.S.; Sami, R.; Olwyn, B.; Florence, P.; Shirin, M.M.; Athar, H.C.; Robert, C.L.; Crystal structure of a PDZ domain,**1996**, *Nature*, 382, 649 - 652.

[105] Piserchio, A.; Pellegrini,M.; Mehta, S.; Blackman, S.M.; Garcia, E.P.; Marshall, J.; Mierke, D.F.; The PDZ1 domain of Sap90. Characterization of structure and binding. **2002**, *J.Biol.Chem*. 277, 6967 - 6973.

[106] Kornau, H.C.; Schenker, L.T.; Kennedy, M.B.; Seeburg, P.H.; Domain interaction between NMDA receptor subunits and the postsynaptic density protein PSD-95.*Science*. **1995**, 22, 269(5231), 1737 - 1740.

[107] Brenman, J.E.; Chao, D.S.; Gee, S.H.; McGee, A.W.; Craven, S.E.; Santillano,D.R.; Wu, Z.; Huang, F.; Xia, H.; Peters, M.F.; Froehner, S.C.; Bredt, D.S.; Interaction of nitric oxide synthase with the postsynaptic density PSD-95 and alpha1-syntrophin mediated by PDZ domains*Cell*, 1996, 84(5), 757 - 767.

[108] Bach, A.; Chi, C.N.; Pang, G.F.; Olsen, L.; Kristensen, A.S.; Jemth, P.; StrΦmgaard, K.; Design and synthesis of high potent and plasma-stable dimeric inhibitors of the PSD-95/NMDA receptor interaction. Angew *Chem Int Ed.* **2009**, 48(51), 9685 - 9689.

[109] Andrea, P.; Gregory, D.S.; Tao, L.; John, M.; Mark, R.S.; Dale, F.M.; Targeting Specific PDZ Domains of PSD-95: Structural Basis for Enhanced Affinity and Enzymatic Stability of a Cyclic Peptide. *Chemistry & Biology*. **2004**, 11, 469 -473.

[110] Sheng, M.; Kim, E.; The Shank family of scaffold proteins. *J Cell Sci*. **2000**, 113, 1851 - 1856.

[111] Tu, J.C.; Xiao, B.; Naisbitt, S.; Yuan, J.P.; Petralia, R.S.; Brakeman, P.; Doan, A.; Aakalu, V.K.; Lanahan, A.A.; Sheng, M.; Worley, P.F.; Coupling of mGluR/Homer and PSD-95 complexes by the Shank family of postsynaptic density proteins. **1999,** *Neuron*. 23(3),583 - 592.

[112] Böckers, T.M.; Mameza, M.G.; Kreutz, M.R.; Bockmann, J.; Weise, C.; Buck, F.; Richter, D.; Gundelfinger, E.D.; Kreienkamp, H.J.; Synaptic scaffolding proteins in rat brain. Ankyrin repeats of the multidomain Shank protein family interact with the cytoskeletal protein alpha-fodrin. **2001**, *J Biol Chem*. 276(43):40104 - 40212.

[113] Gunnar, S.; Marta, R.; Jan, G.; Tobias, M.B.; Eckart, D.G.; Walter, B.; The neuronal scaffold protein Shank3 mediates signaling and biological function of the receptor tyrosine kinase re in epithelial cells. *J.Cell.Biol*. **2004**, 167(5), 945 - 952.

[114] Naisbitt, S.; Kim, E.; Tu, J.C.; Xiao, B.; Sala, C.; Valtschanoff, J.; Weinberg, R.J.; Woley, P.F.; Sheng, M.; Shank, a novel family of postsynaptic density proteins that binds to the NMDA receptor/PSD-95/GKAP complex and cortactin. *Neuron*. **1999**, 23, 569 - 582.

[115] Saupe,J.; Roske,Y.; Schillinger,C.; Kamdem,N.; Radetzki,S.; Diehl, A.; Oschkinat,H.; Krause,G.; Heinemann, U.; Rademann, J. Discovery, Structure – Activity relationship Studies , and Crystal Structure of Nonpetide Inhibitors bound to the Shank3PDZ Domain. *ChemMedChem*. **2011**, 6(8), 1411 -1422.

[116] Adams, M.E.; Butler, M.H.; Dwyer, T.M.; Peters, M.F.; Murnane, A.A.; Froehner, S.C.; Two forms of mouse syntrophin, a 58 kd dystrophin-associated protein, differ in primary structure and tissue distribution. *Neuron*. **1993** 11(3),531 - 540.

[117] Cho, K.O.; Hunt, C.A.; Kennedy, M.B.; The rat brain postsynaptic density fraction contains a homolog of the Drosophila discs-large tumor suppressor protein. *Neuron*. **1992** , 9(5), 929 - 942.

[118] Ponting, C.P.; Phillips, C.; DHR domains in syntrophins, neuronal NO synthases and other intracellular proteins. *Trends Biochem Sci.* **1995**, 20(3), 102 - 103.

[119] Froehner, S.C., Regulation of ion channel distribution at synapses. *Annu Rev Neurosci.* **1993**, 16, 347 - 368.

[120] Brenman, J.E.; Chao, D.S.; Gee, S.H.; McGee, A.W.; Craven, S.E.; Santillano, D.R.; u, Z.; Huang, F.; Xia, H.; Peter, M.F.; Froehner, S.C.; Bredt, D.S.; Interaction of nitric oxide synthase with the postsynaptic density protein PSD-95 and α1-syntrophin mediated by PDZ domains. *Cell*, 1996, 84, 757 - 767.

[121] Schultz, J.; Hoffmüller, U.; Krause, G.; Ashurst, J.; Macis, M.J.; chmieder, P.; Schneider-Mergener, J.; Oschkinat, H.; Specific interactions between the syntrophin PDZ domain and voltage-gated sodium channels. *Nat. Struct. Biol*. **1998**, 5, 19 - 24.

[122] Munehira, Y.; Ohnishi, T.; Kawamoto, S.; Furuya, A.; Shitara, K.; Imamura, M.; Yokota, T.; Takea, S.; Amachi, T.; Kioka, N.; Ueda, K.; α1-syntrophin modulates turnover of ABCA1. *J. Biol.Chem*, **2004**, 279, 15091 -15095.

[123] Chen, Z.; Hague, C.; Hall, R.A.; Minneman, K.P.; Syntrophins regulate alpha 1D-adrenergic receptors through a PDZ domain-mediated ineteraction. *J.Biol.Chem*. **2006**,281(18), 12414 - 12420.

[124] Vandebrouck, A.; Sabourin, J., Rivet, J.; Balghi, H.; Sebille, S.; Kitzis, A.; Raymond, G.; Cognard, C.; Bourmeyster, N.; Constantin, B.; regulation of capacitative calcium entries by alpha1-syntrophin: association of TRPC1 with dystrophin complex and the PDZ domain of alpha1-syntrophin. *The FASEB Journal*. **2007**, 21(2), 608 - 617.

[125] Adams, M.E.; Anderson, K.N.; Froehne, S.C.; The alpha-sytrophin PH and PDZ domains scaffold acetylcholine receptors, utrophin, and neuronal nitric oxide synthase at the neuromuscular junction. *J. neurosci*, **2010**, 30(33), 11004 –11010.

[126] Harris, B.Z.; Hillier, B.J.; Lim, W.A.; Energic determinats of internal motif recognition by PDZ domains. *Biochemistry*. **2001**, 40, 5921 - 5930.

[127] Bernd. M; Thomas. P. NMR Spectroscopy Techniques for Screening and Identifying Ligand Binding to Protein Receptors, *Angew.Chem.Int. Ed*. **2003**, 42(8), 864 - 890.

[128] Zartler. E.R.; Shapiro. M.J. Protein NMR-based screening in drug discovery. *Curr Pharm Des*. **2006**, 12, 3963 - 3972.

[129] Shuker, S.B.; Hajduk, P.J.; Meadows, R.P.; Feisk, S.W.; Discovering high-affinity ligands for proteins: SAR by NMR , *Science*, **1996**, 274(5292), 1531 – 1534.

[130] Zartler, E.R.; Hanson, J.; Jones, B.E.; Kline, A.D.; Martin, G.; Mo, H.; Shapiro, M.J.; Wang, R.; Wu, H.; Yan, J. RAMPED-UP NMR: multiplexed NMR-based screening for drug discovery, *J.Am.Chem.Soc.* **2003**, 125(36), 10941 -10946.

[131] Sem, D.S.; Bertolaet, B.; Baker, B.; Chang, E.; Costache, A.D.; Coutts, S.; Dong, Q.; Hansen, M.; Hong, V.; Huang, X.; Jack, R.M.; Kho, R.; Ma, C.-T.;

Meiniger, D.; Pellechia, M.; Pierre, F.; Villar, H.; Yu, L. Systems-based design of bi-ligand inhibitors of oxidoreductases: filling the chemical proteomic toolbox *Chem.Biol*. **2004**, 11(2), 185 -194.

[132] Mercier, K.A.; Baran, M.; Ramanathan, V.; Revesz, P.; Xiao, R, Montelione, G.T.; Powers, R. FAST-NMR: functional annotation screening technology using NMR spectroscopy *J.Am.Chem.Soc.* **2006**, 128(48), 15292 - 15299.

[133] Stockman, B.J. NMR spectroscopy as a tool for structure- based drug design *Prog. NMR Spectrosc*. **1998**, 33, 109 -151.

[134] Maurizio, P.; Ivano, B.; David, C.; Claudio, D.; Ernest, G.; Wolfgang, J.;Thomas, L. J.; Steve, W. H.; Horst, K.; Claudio, L.; Bernd, M.; Hartmut, O.; Jeff, P.; Harald, S.; Gregg, S.; Perspectives on NMR in drug discovery: a technique comes of age ' *Nature Rev. Drug Discov*. **2007**, (7), 738 - 745.

[135] Philip, J.H.; Jonathan, G.; A decade of fragment-based drug design: strategic advances and lessons learned, *Nature Rev. Drug Discov*. **2007**, (6), 211 - 219.

[136] Selenko, P; Serber, Z; Gadea, B; Ruderman, J; Wagner, G. Quantitative NMR analysis of the protein G. B1 domain in Xenopus laevis egg extracts and intact oocytes. *Proc. Natl Acad. Sci. USA*, **2006**, 103, 11904-11909.

[137] Dalvit, C.; Pevarello, P.; Tato`, M.; Veronesi, M.; Vulpetti, A.; Sundström, M.; Identification of Compounds with binding affinity to proteins via magnetization transfer from bulk water, *J. Biomol. NMR.* **2000**, 18, 65 - 68.

[138] Dalvit, C. Fogliatto, G.P.; Stewart, A.; Veronesi, M.; Stockman, B. WaterLOGSY as a method for primary NMR screening: practical aspects and range of applicability*J. Biomol. NMR*. **2001**, 21, 349 - 359.

[139] Poornima, C.S.; Dean, P.M.; Hydration in drug design. 1. Multiple hydrogen-bonding features of water molecules in mediating protein-ligand interactions *J.Comput. Aided Mol. Des*. 1995, 9, 500 - 512.

[140] Hajduk, P.J; Boyd, S.; Nettesheim, D.; Nienaber, V; severin, J.; Smith, R.; Davidson, D.; Rockway, T.; Fesik, S.W.;, Identification of novel inhibitors of urokinase via NMR-based screening. *J. Med. Chem*. **2000**, 43, 3862 -3866.

[141] Klages, J.; Colesb, M.; Kessler, H.; NMR-based screening: a powerful tool in fragment-based drug discovery *Mol. BioSyst.* **2006**, 2, 318 - 332.

[142] Otting, G.; Wüthrich, K.; Studies of protein hydration in aqueous solution by direct NMR observation of individual protein-bound water molecules *J. Am. Chem . Soc*. **1989**, 111, 1871 - 1875.

[**143]** Otting, G.; Liepinsh, E.; Wüthrich, K.; Protein hydration in aqueous solution *Science*. **1991**, 254, 974 - 980.

[144] Mayer, M.; Meyer, B.; Characterization of Ligand Binding by Saturation Transfer Difference NMR Spectroscopy *Angew.Chem.Int.Ed.* **1999**, 38(12), 1784 - 1788.

[145] W. L. Davies, R. R. Grunnert, R. F. Haff, J. W. McGahen, E. M. Neumeyer, M.Paulshock, J. C. Watts, T. R. Wood, E. C. Hermann, C. E. Hoffmann. Antiviralactivity of 1-adamantamine (amantadine). Science **1964**, 144, 862- 863.

[146] Liu W. J., Bulgaru A., Haigentz M., Stein C. A., Perez-Soler R., Mani S. The BCL2-family of protein ligands as cancer drugs: the next generation of therapeutics. **2003,** *Curr. Med. Chem. Anti Cancer Agents*. **3**, 217–223.

[147] Biifinger, J.C.; kim, H.W.; DiMagno, S.G. The polar hydrophobicity of fluorinated compounds. **2004**, ChemBiochem, 5, 622 - 627.

[148] Degterev A., Lugovskoy A., Cardone M., Mulley B., Wagner G., Mitchison T., Yuan J. Identification of small-molecule inhibitors of interaction between the BH3 domain and Bcl-xl. **2001,** *Nat. Cell Biol*, 3, 173 -182.

[149] Carolyn, V; *Targeting PDZ Domains with Nonpeptidic Small Molecules*. Naturwissenschaftlichen Fakultät I – Biowissenschaften der Martin-Luther-Universität Halle-Wittenberg, **2009**, Dissertation.

[150] Khovratovich N. N. ; Chizhevskaya I. I. The problem of the tautomerism of 2-iminothiazolidin-4-one and some of its derivatives. *Chemistry Heterocyclic Compounds* 3 (2), 2513 - 2515.

[151] Goddard, T.D.; Kneller, D.G. SPARKY 3, University of California, San Francisco, **2003**.

[152] Puranik, P.; Aakanksha, K.; Tadas, S.V.; Robert, D.B.; Lalji, K.G.; Vincent , C.O.N.; Potent anti-prostate cancer agents derived from a novel androgen receptor down-regulating agent. *Bioorganic and Medicinal Chemistry*. **2008**, 16, 3519 - 3529.

[153] Zhe, W.; Silvio, C.; Kaihong, Y.; Guoyou, X.; Michael, E.P.; Joseph, M.F.; Pat, N.C.; A practical Preparation of terminal alkynes from aldehydes. **2000**, *J.Org.Chem*, 65, 1889-1891.

[154] Wikins, R.; Monica, N.; reactions of Aryl (trichloromethyl)carbinols with Sulfur Nucleophiles. Formation and proof of Zwitterionic. Structure of Iminothiazolidones, **1967**, *Journal of the American Chemical Society*. 89(3), 647 – 651.

[155] Hedaya, E.; Theodoropulos, S.; The preparation and reactions of stable phosphorus ylides derived from maleic anhydrides, maleimides or isomaleimides. **1968**, *Tetrahedron*, 24, 2241 -2254.

[156] Toshiya, N.; Akira, O.; Kazuyuki, T.; Sadakazu, Y. A Practical Procedure for the synthesis of Esonarimod, (*R,S*)-2-Acetylthiomethyl-4-(4-methlyphenyl)-4-oxobutanoic Acid, an Antirheumatic Agent. **2002**, *Chem.Pharm.Bull,* 50(10) 1407- 1412.

[157] Balini, R.; Bosica, G.; Fiorini, D.; Righi, P. Nitroalkanes and Dimethyl Maleate as Source of 3-Alkyl Succinic Anhydrides and (E)-3-Alkylidene Succinic Anhydrides. **2002**, *Synthesis*, 5, 681- 685.

[158] Kukolya, S.; Draheim, S.E.; Graves, B.J.; Hunden, D.C.; Pfeil, J.L.; Cooper, R.D.; Ott, J.L.; Counter, F.T.; Orally Absorbable Cephalosporin Antibiotics. 2. Structure-Activity Studies of Bicyclic Glycine Derivatives of 7-Aminodeacetoxycephalosporanic Acid. **1985**, *J.Med.Chem*. 28, 1896 -1903.

[159] Giles, R.G.; Lewis, N.J.; Quick, J.K.; Sasse, M.J.; Urquhart, M.W.J.; Youssef, L.; Regiospecific Reduction of 5-Benzylidene-2,4-Thiazolidinediones and 4-Oxo-thiazolidinethiones using Lithium Borohydride in Pyridine and Tetrahydrofuran. **2002**, *Tetrahedron*. 56, 4531 - 4537.

[160] David , A.O.; Mark, A.H.; Mark, A.S.; Clayton, H.H.; Stereochemistry of the Michael Addition of N,N-Disubstituted Amide and Thioamide Enolates to α,β-unsaturated Ketones, **1990**, *J. Org. Chem*, 55(1), 132 -157.

The appendix is constituted of the list of compounds screened against PDZ domains

			DVL1PDZ			DVL3PDZ			PSD95-1			PSD95-2			PSD95-3			AF6PDZ			Shank3_PDZ			a-SynPDZ		Biological data IC50		Vendor & Ids		
CdId	Structure	Mol Weight	KD_NMR	KD_ITC	CSP	KD_NMR	KD_ITC	CSP	KD_NMR	KD_ITC	CSP	KD_NMR	KD_ITC	CSP	KD_NMR	ITC	CSP	KD_NMR	KD_ITC	CSP	KD_NMR	KI_FP	CSP	KD_NMR	CSP	Wnt3a_inhib	Cyto_tox	Nestor-ID	Vendor_ID	V_name
14	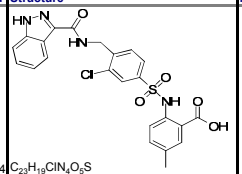 $C_{23}H_{19}ClN_4O_5S$	498.939					9.4	0.3			0.053			0.1			0.05			0.01			0.05		0.08			3E54	Z1098340488	Enanmine
20	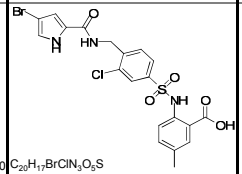 $C_{20}H_{17}BrClN_3O_5S$	526.788		4.7			9.8	0.36			0.06			0.09			0.06			0.01			0.05		0.07			3E56	Z1098340559	Enanmine
4	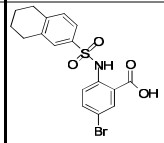 $C_{17}H_{16}BrNO_4S$	410.282	18.2		0.3		11.6				0.01			0.01			0			0.05			0.01		0.01	125	70	2E28	2E28	
26	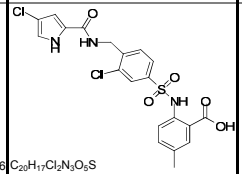 $C_{20}H_{17}Cl_2N_3O_5S$	482.337		4.7			12.5	0.36			0.07			0.09			0.1			0.01			0.05		0.08			3E52	Z1098340560	Enanmine
181	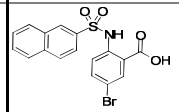 $C_{17}H_{12}BrNO_4S$	406.25					13.8																					JS IV-37		
32	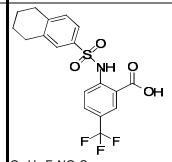 $C_{18}H_{16}F_3NO_4S$	399.384		24.5			17.4	0.38			0.01			0.05			0.02						0.04					N4		
10	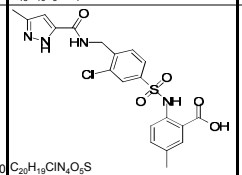 $C_{20}H_{19}ClN_4O_5S$	462.907				163.8	19.5	0.28			0.03			0.08			0.03			0.01			0.05		0.08	140	150	3E63	T6877335	Enanmine
25	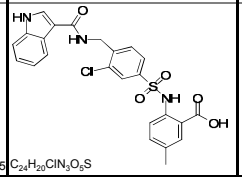 $C_{24}H_{20}ClN_3O_5S$	497.951				30.7	21.8	0.36			0.03			0.02			0.04			0.01			0.05		0.08			3E51	Z1098340555	Enanmine

			DVL1PDZ			DVL3PDZ			PSD95-1			PSD95-2			PSD95-3			AF6PDZ			Shank3_PDZ			a-SynPDZ		Biological data IC50		Vendor & Ids		
CdId	Structure	Mol Weight	KD_NMR	KD_ITC	CSP	KD_NMR	KD_ITC	CSP	KD_NMR	KD_ITC	CSP	KD_NMR	KD_ITC	CSP	KD_NMR	ITC	CSP	KD_NMR	KD_ITC	CSP	KD_NMR	KI_FP	CSP	KD_NMR	CSP	Wnt3a_inhib	Cyto_tox	Nestor-ID	Vendor_ID	V_name
27	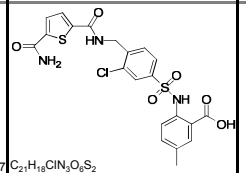 $C_{21}H_{16}ClN_3O_6S_2$	507.967					29.7	0.37			0.04			0.1			0.03			0.01			0.06		0.09			3E62	T6877334	Enanmine
12	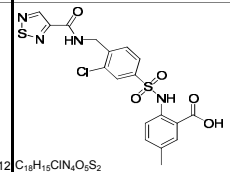 $C_{18}H_{15}ClN_4O_5S_2$	464.942				18.05	32.8	0.35			0.04			0.08			0.05			0.01			0.05		0.08	125	150	3E65	T6877337	Enanmine
45	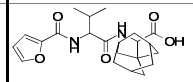 $C_{22}H_{30}N_2O_5$	402.484	288.1		0.23		43.8	0.19			0.01			0.01			0.01			0.01			0.01		0.04			2E20		
22	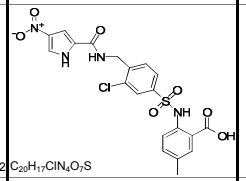 $C_{20}H_{17}ClN_4O_7S$	492.89					43.8	0.37			0.06			0.09			0.05			0.01			0.05		0.08			3E58	Z1098340464	Enanmine
17	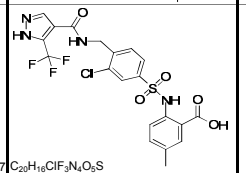 $C_{20}H_{16}ClF_3N_4O_5S$	516.878					47.2	0.36			0.03			0.06			0.04			0.01			0.05		0.06			3E47	Z1098340595	Enanmine
31	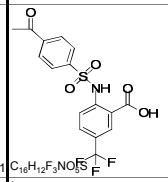 $C_{16}H_{12}F_3NO_5S$	387.33				26.9	52	0.28			0.02			0.04			0.01			0.04			0.05		0.06			N8		
37	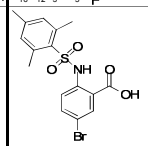 $C_{16}H_{16}BrNO_4S$	398.272					58.1	0.31			0.01			0.05			0.06			0.04			0.05		0.04	50	80	N1		
180	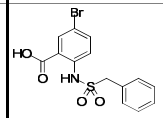 $C_{14}H_{12}BrNO_4S$	370.218					58.5																					JS IV-31		

			DVL1PDZ			DVL3PDZ			PSD95-1			PSD95-2			PSD95-3			AF6PDZ			Shank3_PDZ			a-SynPDZ		Biological data IC50		Vendor & Ids		
CdId	Structure	Mol Weight	KD_NMR	KD_ITC	CSP	KD_NMR	KD_ITC	CSP	KD_NMR	KD_ITC	CSP	KD_NMR	KD_ITC	CSP	KD_NMR	ITC	CSP	KD_NMR	KD_ITC	CSP	KD_NMR	KI_FP	CSP	KD_NMR	CSP	Wnt3a_inhib	Cyto_tox	Nestor-ID	Vendor_ID	V_name
35	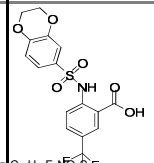 $C_{16}H_{12}F_3NO_6S$	403.33					59.1	0.36			0.02			0.05			0.01			0.04			0.05		0.08	125	148	N11		
13	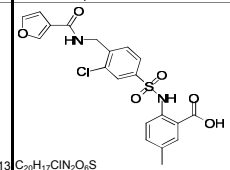 $C_{20}H_{17}ClN_2O_6S$	448.877					59.5	0.36			0.02			0.06			0.01			0.01			0.03		0.07			3E53	Z1098340455	Enanmine
1	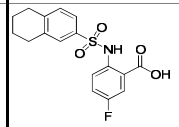 $C_{17}H_{16}FNO_4S$	349.377			0.086	80.6	116	0.27		n.d.	0.091		n.d.	0.055	n.d.	n.d.	0.01		n.d.	0			0		0.05		130	2E11	Kiew	
2	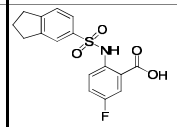 $C_{16}H_{14}FNO_4S$	335.35	114.4		0.3	83.9	139.6	0.26			0.075			0.08			0			0			0		0.07			2E12	2E12	Kiew
3	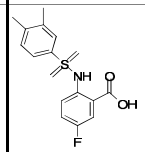 $C_{17}H_{18}FNO_2S$	319.394			0.15	140.6	341.3	0.23			0.05			0			0			0			0.01		0.05			2E10	2E10	kiew
179	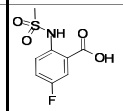 $C_8H_8FNO_4S$	233.217		inactive			1340																					JSII-188		
5	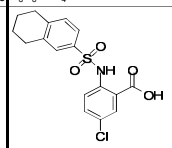 $C_{17}H_{16}ClNO_4S$	365.831	45.6		0.34			0.28			0.01			0			0			0.05			0.01		0.01		80	2E29	2E29	
6	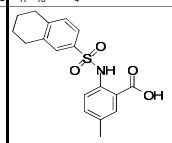 $C_{18}H_{19}NO_4S$	345.413	60.5		0.31			0.26			0.01			0.01			0			0.08			0.01		0.01		130	2E27	2E27	

			DVL1PDZ			DVL3PDZ			PSD95-1			PSD95-2			PSD95-3			AF6PDZ			Shank3_PDZ			a-SynPDZ		Biological data IC50		Vendor & Ids		
CdId	Structure	Mol Weight	KD_NMR	KD_ITC	CSP	KD_NMR	KD_ITC	CSP	KD_NMR	KD_ITC	CSP	KD_NMR	KD_ITC	CSP	KD_NMR	ITC	CSP	KD_NMR	KD_ITC	CSP	KD_NMR	KI_FP	CSP	KD_NMR	CSP	Wnt3a_inhib	Cyto_tox	Nestor-ID	Vendor_ID	V_name
42	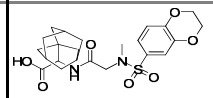 $C_{23}H_{30}N_2O_7S$	478.559	77.8		0.28			0.23			0.01			0.01			0.01			0.01			0.01		0.08			2E22		
38	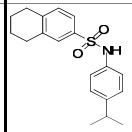 $C_{19}H_{23}NO_2S$	329.456	189.8		0.13			0.09												0.05			0.05					2E26		kiew
7	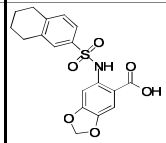 $C_{18}H_{17}NO_6S$	375.396	190		0.2			0.18																				3E45	102193207	Enamine
8	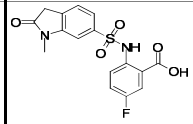 $C_{16}H_{13}FN_2O_5S$	364.348	237		0.2			0.18																				2E81	T5863040	Enamine
40	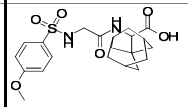 $C_{21}H_{28}N_2O_6S$	436.522	242.6		0.17			0.15												0.06					0.09			2E18		
39	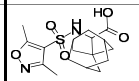 $C_{17}H_{24}N_2O_5S$	368.448	261.4		0.13			0.12																	0.09			2E14	Enamine	
41	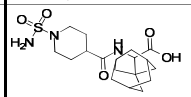 $C_{18}H_{29}N_3O_5S$	399.505	489.3		0.14			0.12			0														0.04			2E21		
34	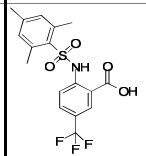 $C_{17}H_{16}F_3NO_4S$	387.373				176.7		0.21																		25	75	N3		

			DVL1PDZ			DVL3PDZ			PSD95-1			PSD95-2			PSD95-3			AF6PDZ			Shank3_PDZ			a-SynPDZ		Biological data IC50		Vendor & Ids		
CdId	Structure	Mol Weight	KD_NMR	KD_ITC	CSP	KD_NMR	KD_ITC	CSP	KD_NMR	KD_ITC	CSP	KD_NMR	KD_ITC	CSP	KD_NMR	ITC	CSP	KD_NMR	KD_ITC	CSP	KD_NMR	KI_FP	CSP	KD_NMR	CSP	Wnt3a_inhib	Cyto_tox	Nestor-ID	Vendor_ID	V_name
52	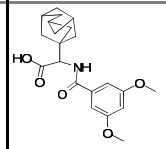 $C_{21}H_{27}NO_5$	373.443			0.1	189.1		0.1																				E051	E051	Enamine
9	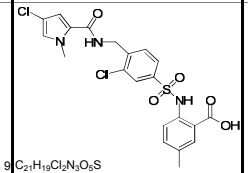 $C_{21}H_{19}Cl_2N_3O_5S$	496.364						0.38			0.04						0.07									125	75	3E61	T6877333	Enanmine
11	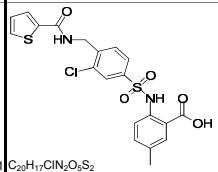 $C_{20}H_{17}ClN_2O_5S_2$	464.942						0.33			0.03						0.06									125	150	3E64	T6877336	Enanmine
15	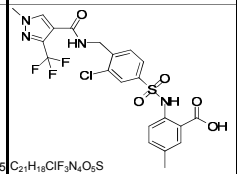 $C_{21}H_{18}ClF_3N_4O_5S$	530.905						0.39			0.03						0.04											3E49	Z1098340573	Enanmine
16	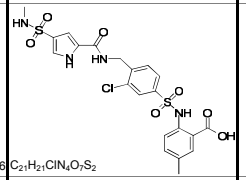 $C_{21}H_{21}ClN_4O_7S_2$	540.997						0.38			0.03						0.03											3E50	Z1098340569	Enanmine
18	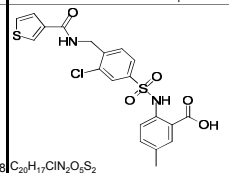 $C_{20}H_{17}ClN_2O_5S_2$	464.942						0.35									0.05											3E48	Z1098340494	Enanmine
19	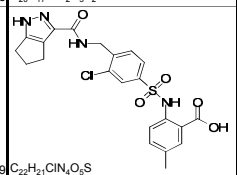 $C_{22}H_{21}ClN_4O_5S$	488.944						0.35									0.04											3E55	Z1098340478	Enanmine
21	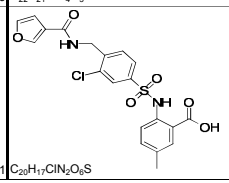 $C_{20}H_{17}ClN_2O_6S$	448.877						0.35									0.02											3E57	Z1098340465	Enanmine

			DVL1PDZ			DVL3PDZ			PSD95-1			PSD95-2			PSD95-3			AF6PDZ			Shank3_PDZ			a-SynPDZ		Biological data IC50		Vendor & Ids		
CdId	Structure	Mol Weight	KD_NMR	KD_ITC	CSP	KD_NMR	KD_ITC	CSP	KD_NMR	KD_ITC	CSP	KD_NMR	KD_ITC	CSP	KD_NMR	ITC	CSP	KD_NMR	KD_ITC	CSP	KD_NMR	KI_FP	CSP	KD_NMR	CSP	Wnt3a_inhib	Cyto_tox	Nestor-ID	Vendor_ID	V_name
23	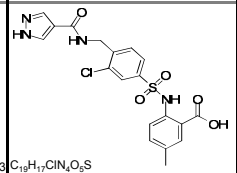 $C_{19}H_{17}ClN_4O_5S$	448.88						0.34									0.02											3E59	T6877331	Enanmine
24	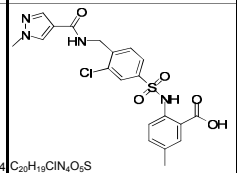 $C_{20}H_{19}ClN_4O_5S$	462.907						0.34									0.02											3E60	T6877332	Enanmine
28	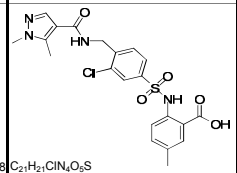 $C_{21}H_{21}ClN_4O_5S$	476.933						0.35									0.01											3E66	T6877338	Enanmine
29	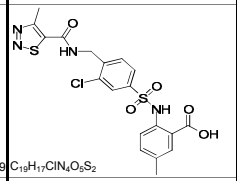 $C_{19}H_{17}ClN_4O_5S_2$	480.945						0.28									0.01											3E67	T6885621	Enanmine
30	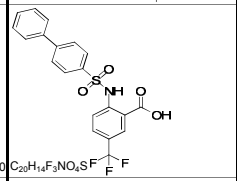 $C_{20}H_{14}F_3NO_4S$	421.39						0.18																				N6		
33	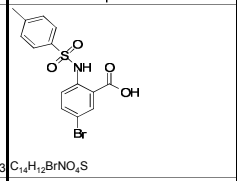 $C_{14}H_{12}BrNO_4S$	370.218						0.35																				N2		
36	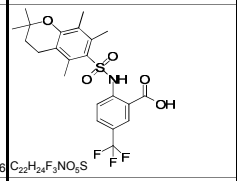 $C_{22}H_{24}F_3NO_5S$	471.49						0.09									0.01									60	80	N9		
43	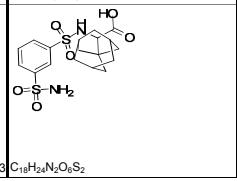 $C_{18}H_{24}N_2O_6S_2$	428.523			0.15			0.15																				2E13		

			DVL1PDZ			DVL3PDZ			PSD95-1			PSD95-2			PSD95-3			AF6PDZ			Shank3_PDZ			a-SynPDZ		Biological data IC50		Vendor & Ids		
CdId	Structure	Mol Weight	KD_NMR	KD_ITC	CSP	KD_NMR	KD_ITC	CSP	KD_NMR	KD_ITC	CSP	KD_NMR	KD_ITC	CSP	KD_NMR	ITC	CSP	KD_NMR	KD_ITC	CSP	KD_NMR	KI_FP	CSP	KD_NMR	CSP	Wnt3a_inhib	Cyto_tox	Nestor-ID	Vendor_ID	V_name
44	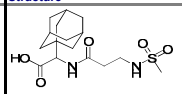 $C_{16}H_{26}N_2O_5S$	358.453			0.1			0.09																				2E17		
46	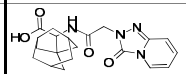 $C_{20}H_{24}N_4O_4$	384.429			0.18			0.1												0.05					0.13			2E23		
47	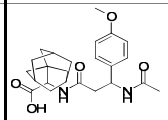 $C_{24}H_{32}N_2O_5$	428.521			0.09			0.08																				2E15		
48	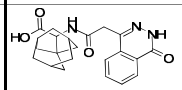 $C_{22}H_{25}N_3O_4$	395.452			0.1			0.06																				2E16		
49	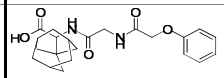 $C_{22}H_{28}N_2O_5$	400.468			0.1			0.09																				2E19		
50	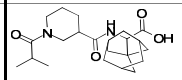 $C_{22}H_{34}N_2O_4$	390.516			0.16			0.08																				2E24		
51	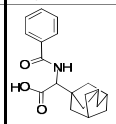 $C_{19}H_{23}NO_3$	313.391			0			0.1																				E024	E024	Enamine
53	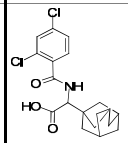 $C_{19}H_{21}Cl_2NO_3$	382.281			0.11			0.1																				E057	E057	Enamine

			DVL1PDZ			DVL3PDZ			PSD95-1			PSD95-2			PSD95-3			AF6PDZ			Shank3_PDZ			a-SynPDZ		Biological data IC50		Vendor & Ids		
CdId	Structure	Mol Weight	KD_NMR	KD_ITC	CSP	KD_NMR	KD_ITC	CSP	KD_NMR	KD_ITC	CSP	KD_NMR	KD_ITC	CSP	KD_NMR	ITC	CSP	KD_NMR	KD_ITC	CSP	KD_NMR	KI_FP	CSP	KD_NMR	CSP	Wnt3a_inhib	Cyto_tox	Nestor-ID	Vendor_ID	V_name
54	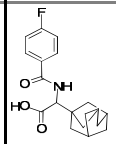 $C_{19}H_{22}FNO_3$	331.381			0			0.03			0			0			0			0			0						E022	E022	Enamine
55	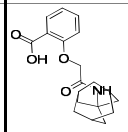 $C_{19}H_{23}NO_4$	329.39			0.01																							2E36		Enamine
56	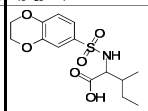 $C_{14}H_{19}NO_6S$	329.369			0			0.12																				E002	E002	Enamine
57	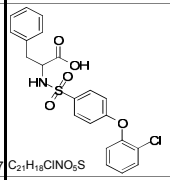 $C_{21}H_{18}ClNO_5S$	431.889			0.12			0.09			0			0			0.02			0			0					E026	E026	Enamine
58	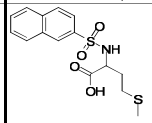 $C_{15}H_{17}NO_4S_2$	339.43			0.05			0.06			0			0			0			0			0					E064	E064	Enamine
59	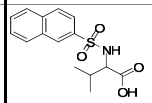 $C_{15}H_{17}NO_4S$	307.365			0			0.06			0			0			0			0			0					E109	E109	Enamine
60	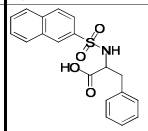 $C_{19}H_{17}NO_4S$	355.408			0.055			0.05			0			0			0.02			0			0					E106	E106	Enamine
61	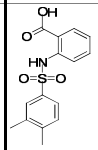 $C_{15}H_{15}NO_4S$	305.349			0.056			0.04			0			0			0	0										E077	E077	Enamine

			DVL1PDZ			DVL3PDZ			PSD95-1			PSD95-2			PSD95-3			AF6PDZ			Shank3_PDZ			a-SynPDZ		Biological data IC50		Vendor & Ids		
CdId	Structure	Mol Weight	KD_NMR	KD_ITC	CSP	KD_NMR	KD_ITC	CSP	KD_NMR	KD_ITC	CSP	KD_NMR	KD_ITC	CSP	KD_NMR	ITC	CSP	KD_NMR	KD_ITC	CSP	KD_NMR	KI_FP	CSP	KD_NMR	CSP	Wnt3a_inhib	Cyto_tox	Nestor-ID	Vendor_ID	V_name
62	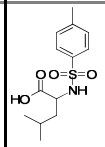 $C_{13}H_{15}NO_4S$	285.359			0			0.07			0			0			0			0			0						E035	E035	Enamine
63	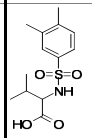 $C_{13}H_{15}NO_4S$	285.359			0.1			0.05			0			0			0			0			0						E108	E108	Enamine
64	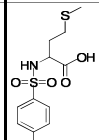 $C_{13}H_{19}NO_5S_2$	333.424			0.05			0.08			0			0			0			0			0						E095	E095	Enamine
65	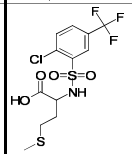 $C_{12}H_{13}ClF_3NO_4S_2$	391.814			0.038			0.05			0			0			0			0			0						E078	E078	Enamine
66	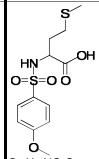 $C_{12}H_{17}NO_5S_2$	319.397			0.04			0.04			0			0			0			0			0						E042	E042	Enamine
67	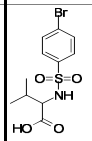 $C_{11}H_{14}BrNO_4S$	336.202			0.06			0.03			0			0			0			0			0						E033	E033	Enamine
68	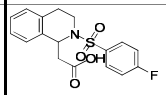 $C_{17}H_{16}FNO_5S$	349.377			0			0.04			0			0			0.02			0			0						E014	E014	Enamine
69	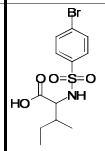 $C_{12}H_{16}BrNO_4S$	350.229			0.06			0.04			0			0			0			0			0						E015	E015	Enamine

			DVL1PDZ			DVL3PDZ			PSD95-1			PSD95-2			PSD95-3			AF6PDZ			Shank3_PDZ			a-SynPDZ		Biological data IC50		Vendor & Ids		
CdId	Structure	Mol Weight	KD_NMR	KD_ITC	CSP	KD_NMR	KD_ITC	CSP	KD_NMR	KD_ITC	CSP	KD_NMR	KD_ITC	CSP	KD_NMR	ITC	CSP	KD_NMR	KD_ITC	CSP	KD_NMR	KI_FP	CSP	KD_NMR	CSP	Wnt3a_inhib	Cyto_tox	Nestor-ID	Vendor_ID	V_name
70	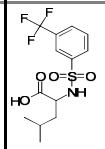 $C_{13}H_{16}F_3NO_4S$	339.331			0.06			0.06			0			0			0.02			0			0					E023	E023	Enamine
71	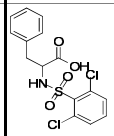 $C_{15}H_{13}Cl_2NO_4S$	374.239			0			0.04			0			0.04			0.02			0			0					E062	E062	Enamine
72	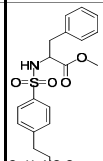 $C_{19}H_{23}NO_4S$	361.455			0			0.03			0			0			0.025			0			0					E117	E117	Enamine
73	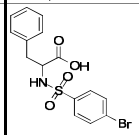 $C_{15}H_{14}BrNO_4S$	384.245			0			0.03			0			0			0			0			0					E019	E019	Enamine
74	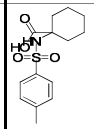 $C_{14}H_{19}NO_4S$	297.37			0.05			0.03			0			0			0			0			0					E025	E025	Enamine
75	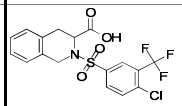 $C_{17}H_{13}ClF_3NO_4S$	419.803			0			0.03			0			0			0.04			0			0					E050	E050	Enamine
76	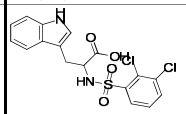 $C_{17}H_{14}Cl_2N_2O_4S$	413.275			0			0.01			0			0			0.01			0			0					E063	E063	Enamine
77	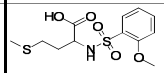 $C_{12}H_{17}NO_5S_2$	319.397			0			0.04			0			0			0			0			0					E107	E107	Enamine

			DVL1PDZ			DVL3PDZ			PSD95-1			PSD95-2			PSD95-3			AF6PDZ			Shank3_PDZ			a-SynPDZ		Biological data IC50		Vendor & Ids		
CdId	Structure	Mol Weight	KD_NMR	KD_ITC	CSP	KD_NMR	KD_ITC	CSP	KD_NMR	KD_ITC	CSP	KD_NMR	KD_ITC	CSP	KD_NMR	ITC	CSP	KD_NMR	KD_ITC	CSP	KD_NMR	KI_FP	CSP	KD_NMR	CSP	Wnt3a_inhib	Cyto_tox	Nestor-ID	Vendor_ID	V_name
78	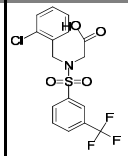 $C_{16}H_{13}ClF_3NO_4S$	407.792			0.055			0.04			0			0			0			0			0						E071	E071	Enamine
79	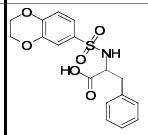 $C_{17}H_{17}NO_6S$	363.385			0.076			0.06									0											2E01	2E01	Enamine
80	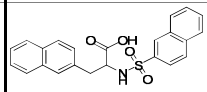 $C_{23}H_{19}NO_4S$	405.466			0.057			0.03									0											2E02	2E02	Enamine
81	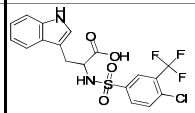 $C_{18}H_{14}ClF_3N_2O_4S$	446.828			0.068			0.03									0											2E04	2E04	Enamine
82	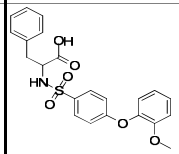 $C_{22}H_{21}NO_6S$	427.47			0.06			0.06									0											2E05	2E05	Enamine
83	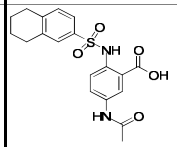 $C_{19}H_{20}N_2O_5S$	388.438			0.037			0									0.02											2E25	2E25	Enamine
84	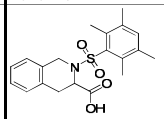 $C_{20}H_{23}NO_4S$	373.466			0.037			0									0.02											E028	E028	Enamine
85	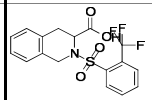 $C_{17}H_{14}F_3NO_4S$	385.358			0.01			0									0.02											E029	E029	Enamine

			DVL1PDZ			DVL3PDZ			PSD95-1			PSD95-2			PSD95-3			AF6PDZ			Shank3_PDZ			a-SynPDZ		Biological data IC50		Vendor & Ids		
CdId	Structure	Mol Weight	KD_NMR	KD_ITC	CSP	KD_NMR	KD_ITC	CSP	KD_NMR	KD_ITC	CSP	KD_NMR	KD_ITC	CSP	KD_NMR	ITC	CSP	KD_NMR	KD_ITC	CSP	KD_NMR	KI_FP	CSP	KD_NMR	CSP	Wnt3a_inhib	Cyto_tox	Nestor-ID	Vendor_ID	V_name
86	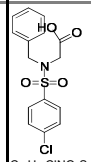 $C_{15}H_{14}ClNO_4S$	339.794			0.024			0									0											E036	E024	Enamine
87	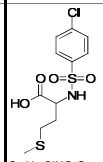 $C_{11}H_{14}ClNO_4S_2$	323.816			0.04			0									0											E044	E044	Enamine
88	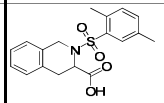 $C_{18}H_{19}NO_4S$	345.413			0.027			0									0											E104	E104	Enamine
89	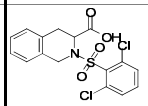 $C_{16}H_{13}Cl_2NO_4S$	386.25			0.01			0									0											E070	E070	Enamine
90	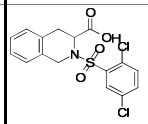 $C_{16}H_{13}Cl_2NO_4S$	386.25			0.05			0									0											E126	E126	Enamine
91	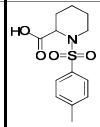 $C_{13}H_{17}NO_4S$	283.343			0.023			0									0											E082	E082	Enamine
92	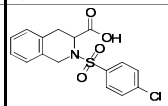 $C_{16}H_{14}ClNO_4S$	351.805			0.01			0.01									0.02											E017	E017	Enamine
93	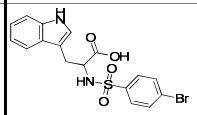 $C_{17}H_{15}BrN_2O_4S$	423.281			0.01			0.01						0.03			0.02											E020	E020	Enamine

			DVL1PDZ			DVL3PDZ			PSD95-1			PSD95-2			PSD95-3			AF6PDZ			Shank3_PDZ			a-SynPDZ		Biological data IC50		Vendor & Ids		
CdId	Structure	Mol Weight	KD_NMR	KD_ITC	CSP	KD_NMR	KD_ITC	CSP	KD_NMR	KD_ITC	CSP	KD_NMR	KD_ITC	CSP	KD_NMR	ITC	CSP	KD_NMR	KD_ITC	CSP	KD_NMR	KI_FP	CSP	KD_NMR	CSP	Wnt3a_inhib	Cyto_tox	Nestor-ID	Vendor_ID	V_name
94	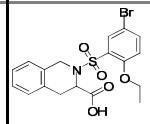 $C_{18}H_{16}BrNO_5S$	440.308			0.01			0.01									0.01											E030	E030	Enamine
95	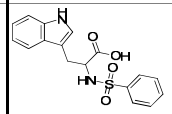 $C_{17}H_{16}N_2O_4S$	344.385			0.01			0.01									0.03											E034	E034	Enamine
96	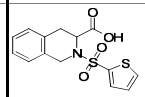 $C_{14}H_{13}NO_4S_2$	323.387			0.01			0.01									0.02											E038	E038	Enamine
97	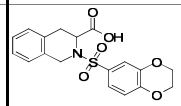 $C_{18}H_{17}NO_6S$	375.396			0.01			0.01									0.03											E039	E039	Enamine
98	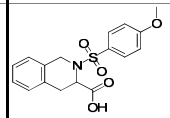 $C_{17}H_{17}NO_5S$	347.386			0.01			0.01									0.01											E040	E040	Enamine
99	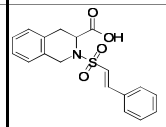 $C_{18}H_{17}NO_4S$	343.397			0.01			0.01									0.01											E041	E041	Enamine
100	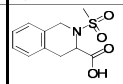 $C_{11}H_{13}NO_4S$	255.29			0.01			0.01									0.01											E067	E067	Enamine
101	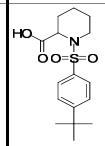 $C_{16}H_{23}NO_4S$	325.423			0.01			0.01									0.01											E072	E072	Enamine

			DVL1PDZ			DVL3PDZ			PSD95-1			PSD95-2			PSD95-3			AF6PDZ			Shank3_PDZ			a-SynPDZ		Biological data IC50		Vendor & Ids		
CdId	Structure	Mol Weight	KD_NMR	KD_ITC	CSP	KD_NMR	KD_ITC	CSP	KD_NMR	KD_ITC	CSP	KD_NMR	KD_ITC	CSP	KD_NMR	ITC	CSP	KD_NMR	KD_ITC	CSP	KD_NMR	KI_FP	CSP	KD_NMR	CSP	Wnt3a_inhib	Cyto_tox	Nestor-ID	Vendor_ID	V_name
102	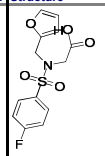 $C_{13}H_{12}FNO_6S$	313.301			0.01			0.01																				E074	E074	Enamine
103	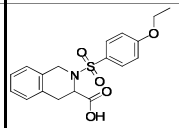 $C_{18}H_{19}NO_5S$	361.412			0			0			0			0			0.03						0					E103	E103	Enamine
104	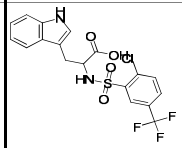 $C_{18}H_{14}ClF_3N_2O_4S$	446.828			0.01			0.01																				2E03	2E03	Enamine
105	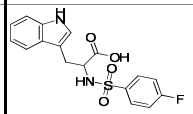 $C_{17}H_{15}FN_2O_4S$	362.375			0			0.01																				2E06	2E06	Enamine
106	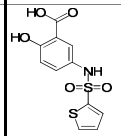 $C_{11}H_9NO_5S_2$	299.323			0.08															0								2E31	T0511-1368	Enamine
107	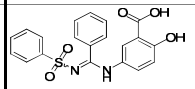 $C_{20}H_{16}N_2O_5S$	396.416			0.01																							2E33	T0504-5654	Enamine
108	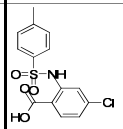 $C_{14}H_{12}ClNO_4S$	325.767			0.13																							2E51	T5270275	Enamine
109	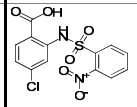 $C_{13}H_9ClN_2O_6S$	356.738			0.13												0.03						0.05					2E69	T5581549	Enamine

			DVL1PDZ			DVL3PDZ			PSD95-1			PSD95-2			PSD95-3			AF6PDZ			Shank3_PDZ			a-SynPDZ		Biological data IC50		Vendor & Ids		
CdId	Structure	Mol Weight	KD_NMR	KD_ITC	CSP	KD_NMR	KD_ITC	CSP	KD_NMR	KD_ITC	CSP	KD_NMR	KD_ITC	CSP	KD_NMR	ITC	CSP	KD_NMR	KD_ITC	CSP	KD_NMR	KI_FP	CSP	KD_NMR	CSP	Wnt3a_inhib	Cyto_tox	Nestor-ID	Vendor_ID	V_name
110	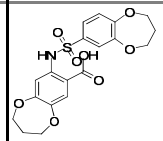 $C_{19}H_{15}NO_8S$	421.421			0.01																							2E71	T5746934	Enamine
111	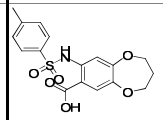 $C_{17}H_{17}NO_6S$	363.385			0.01																							2E73	T5810982	Enamine
112	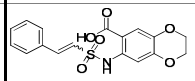 $C_{17}H_{15}NO_6S$	361.369			0.01																							2E77	T5851047	Enamine
113	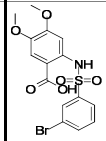 $C_{15}H_{14}BrNO_6S$	416.244			0.01																							2E85	T5879649	Enamine
114	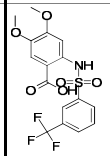 $C_{16}H_{14}F_3NO_6S$	405.346			0.01																							2E87	T5883999	Enamine
115	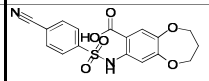 $C_{17}H_{14}N_2O_6S$	374.368			0.01																							2E89	T5885763	Enamine
116	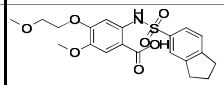 $C_{20}H_{23}NO_7S$	421.464			0.01																							2E91	T5895196	Enamine
117	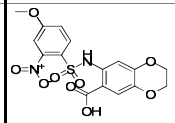 $C_{16}H_{14}N_2O_9S$	410.355			0.03																							2E92	T5907073	Enamine

			DVL1PDZ			DVL3PDZ			PSD95-1			PSD95-2			PSD95-3			AF6PDZ			Shank3_PDZ			a-SynPDZ		Biological data IC50		Vendor & Ids		
CdId	Structure	Mol Weight	KD_NMR	KD_ITC	CSP	KD_NMR	KD_ITC	CSP	KD_NMR	KD_ITC	CSP	KD_NMR	KD_ITC	CSP	KD_NMR	ITC	CSP	KD_NMR	KD_ITC	CSP	KD_NMR	KI_FP	CSP	KD_NMR	CSP	Wnt3a_inhib	Cyto_tox	Nestor-ID	Vendor_ID	V_name
118	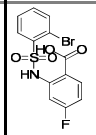 $C_{13}H_9BrFNO_4S$	374.182			0.03																							2E93	T5907084	Enamine
119	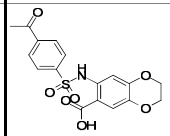 $C_{17}H_{15}NO_7S$	377.369			0.03																							3E10	T6067665	Enamine
120	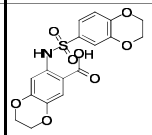 $C_{17}H_{15}NO_8S$	393.368			0.03																							3E12	T6040218	Enamine
121	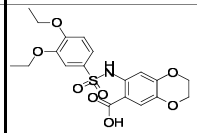 $C_{19}H_{21}NO_8S$	423.437			0.02																							3E13	T6043087	Enamine
122	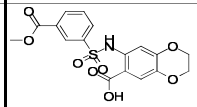 $C_{17}H_{15}NO_8S$	393.368			0.02																							3E15	T6046356	Enamine
123	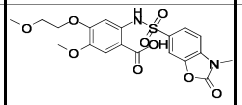 $C_{19}H_{20}N_2O_9S$	452.435			0.01																							3E19	T6115633	Enamine
124	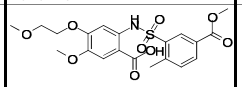 $C_{20}H_{23}NO_9S$	453.463			0.05																							3E20	T6120917	Enamine
125	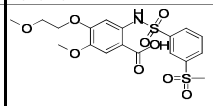 $C_{18}H_{21}NO_9S_2$	459.491			0.01																							3E21	T6132995	Enamine

			DVL1PDZ			DVL3PDZ			PSD95-1			PSD95-2			PSD95-3			AF6PDZ			Shank3_PDZ			a-SynPDZ		Biological data IC50		Vendor & Ids		
CdId	Structure	Mol Weight	KD_NMR	KD_ITC	CSP	KD_NMR	KD_ITC	CSP	KD_NMR	KD_ITC	CSP	KD_NMR	KD_ITC	CSP	KD_NMR	ITC	CSP	KD_NMR	KD_ITC	CSP	KD_NMR	KI_FP	CSP	KD_NMR	CSP	Wnt3a_inhib	Cyto_tox	Nestor-ID	Vendor_ID	V_name
126	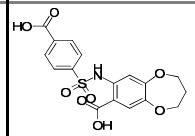 $C_{17}H_{15}NO_8S$	393.368			0.03																							3E22	T6154271	Enamine
127	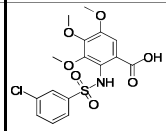 $C_{16}H_{16}ClNO_7S$	401.819			0.02																							3E25	T6224344	Enamine
128	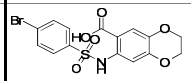 $C_{15}H_{12}BrNO_6S$	414.228			0.05																							3E27	T6231263	Enamine
129	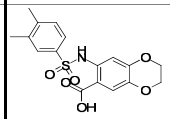 $C_{17}H_{17}NO_6S$	363.385			0.05																							3E28	T6232336	Enamine
130	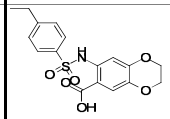 $C_{17}H_{17}NO_6S$	363.385			0.03			0.03																				3E29	T6234034	Enamine
131	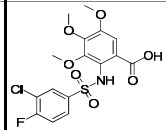 $C_{16}H_{15}ClFNO_7S$	419.809						0.03																				3E3	T5965980	Enamine
132	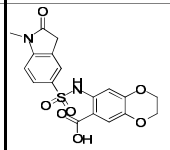 $C_{18}H_{16}N_2O_7S$	404.394			0.03																							3E30	T6268831	Enamine
133	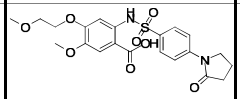 $C_{21}H_{24}N_2O_8S$	464.489			0.01																							3E36	T6298645	Enamine

			DVL1PDZ			DVL3PDZ			PSD95-1			PSD95-2			PSD95-3			AF6PDZ			Shank3_PDZ			a-SynPDZ		Biological data IC50		Vendor & Ids		
CdId	Structure	Mol Weight	KD_NMR	KD_ITC	CSP	KD_NMR	KD_ITC	CSP	KD_NMR	KD_ITC	CSP	KD_NMR	KD_ITC	CSP	KD_NMR	ITC	CSP	KD_NMR	KD_ITC	CSP	KD_NMR	KI_FP	CSP	KD_NMR	CSP	Wnt3a_inhib	Cyto_tox	Nestor-ID	Vendor_ID	V_name
134	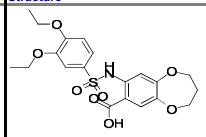 $C_{20}H_{23}NO_8S$	437.464			0.01																							3E39	T6300632	Enamine
135	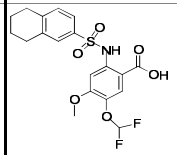 $C_{19}H_{19}F_2NO_6S$	427.419			0.06															0					0.01			3E45	102193207	Enamine
136	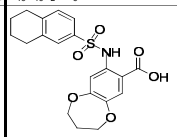 $C_{20}H_{21}NO_6S$	403.449			0.05																							3E46	72421229	Enamine
137	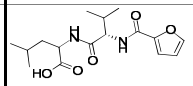 $C_{16}H_{24}N_2O_5$	324.372			0.03			0.04																				E098	E098	Enamine
138	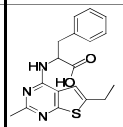 $C_{18}H_{19}N_3O_2S$	341.427			0			0.03			0			0			0			0			0					E110	E110	Enamine
139	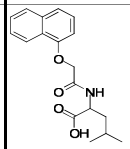 $C_{18}H_{21}NO_4$	315.364			0.04			0.03			0			0			0.02			0			0					E009	E009	Enamine
140	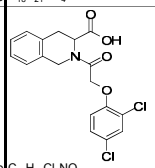 $C_{18}H_{15}Cl_2NO_4$	380.222			0.04			0.04			0			0			0			0			0					E049	E049	Enamine
141	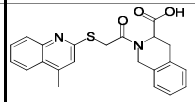 $C_{22}H_{20}N_2O_3S$	392.471			0.03			0									0											E045	E045	Enamine

			DVL1PDZ			DVL3PDZ			PSD95-1			PSD95-2			PSD95-3			AF6PDZ			Shank3_PDZ			a-SynPDZ		Biological data IC50		Vendor & Ids		
CdId	Structure	Mol Weight	KD_NMR	KD_ITC	CSP	KD_NMR	KD_ITC	CSP	KD_NMR	KD_ITC	CSP	KD_NMR	KD_ITC	CSP	KD_NMR	ITC	CSP	KD_NMR	KD_ITC	CSP	KD_NMR	KI_FP	CSP	KD_NMR	CSP	Wnt3a_inhib	Cyto_tox	Nestor-ID	Vendor_ID	V_name
142	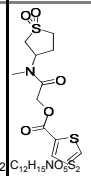 $C_{12}H_{15}NO_5S_2$	317.381			0.01			0									0											E079	E079	Enamine
143	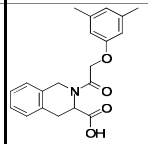 $C_{20}H_{21}NO_4$	339.385			0.02			0.01									0											E075	E075	Enamine
144	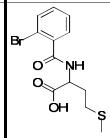 $C_{12}H_{14}BrNO_3S$	332.213			0.01			0.01																				E066	E066	Enamine
145	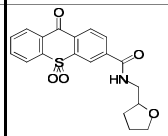 $C_{19}H_{17}NO_5S$	371.407			0.01			0.01									0.01											E005	E005	Enamine
146	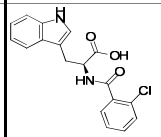 $C_{18}H_{15}ClN_2O_3$	342.776			0.01			0.01									0.02											E016	E016	Enamine
147	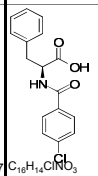 $C_{16}H_{14}ClNO_3$	303.74			0			0			0			0			0.02						0					E105	E105	Enamine
148	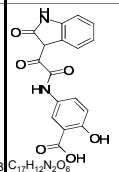 $C_{17}H_{12}N_2O_6$	340.287			0.13																							2E30	T0501-2159	Enamine
149	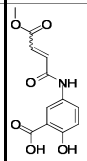 $C_{12}H_{11}NO_6$	265.219			0.01																							2E32	T0504-4852	Enamine

			DVL1PDZ			DVL3PDZ			PSD95-1			PSD95-2			PSD95-3			AF6PDZ			Shank3_PDZ			a-SynPDZ		Biological data IC50		Vendor & Ids		
CdId	Structure	Mol Weight	KD_NMR	KD_ITC	CSP	KD_NMR	KD_ITC	CSP	KD_NMR	KD_ITC	CSP	KD_NMR	KD_ITC	CSP	KD_NMR	ITC	CSP	KD_NMR	KD_ITC	CSP	KD_NMR	KI_FP	CSP	KD_NMR	CSP	Wnt3a_inhib	Cyto_tox	Nestor-ID	Vendor_ID	V_name
150	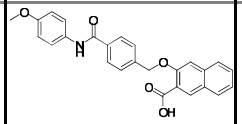 $C_{26}H_{21}NO_5$	427.449			0.01																							2E96	T5932894	Enamine
151	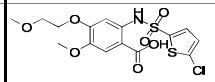 $C_{15}H_{16}ClNO_7S_2$	421.873			0.01																							3E43	T6539520	Enamine
152	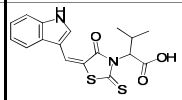 $C_{17}H_{16}N_2O_3S_2$	360.451			0.12			0									0.02											E010	E010	Enamine
153	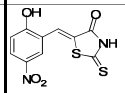 $C_{10}H_8N_2O_4S_2$	282.296						0													340.5		0.05					Cop28		Cop
154	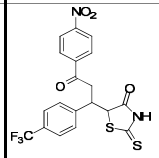 $C_{19}H_{13}F_3N_2O_4S_2$	454.443						0						0				95.8		0.22								KN78		
155	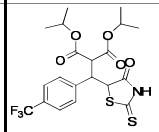 $C_{20}H_{22}F_3NO_5S_2$	477.518						0						0				88.4		0.2								KN79		
156	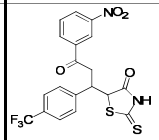 $C_{19}H_{13}F_3N_2O_4S_2$	454.443						0						0.17				62.2		0.3								KN80		
157	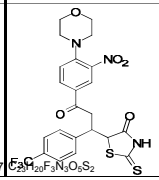 $C_{23}H_{20}F_3N_3O_5S_2$	539.547						0						0						0.12								KN97		

			DVL1PDZ			DVL3PDZ			PSD95-1			PSD95-2			PSD95-3			AF6PDZ			Shank3_PDZ			a-SynPDZ		Biological data IC50		Vendor & Ids		
CdId	Structure	Mol Weight	KD_NMR	KD_ITC	CSP	KD_NMR	KD_ITC	CSP	KD_NMR	KD_ITC	CSP	KD_NMR	KD_ITC	CSP	KD_NMR	ITC	CSP	KD_NMR	KD_ITC	CSP	KD_NMR	KI_FP	CSP	KD_NMR	CSP	Wnt3a_inhib	Cyto_tox	Nestor-ID	Vendor_ID	V_name
158	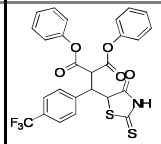 $C_{26}H_{16}F_3NO_9S_2$	545.55						0						0						0.04								KN98		
159	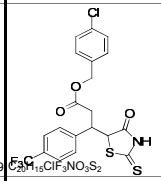 $C_{20}H_{15}ClF_3NO_3S_2$	473.916																		0.1								KN104		
160	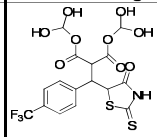 $C_{16}H_{14}F_3NO_9S_2$	485.409																221.4		0.2					0.03			KN105		
161	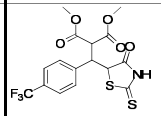 $C_{16}H_{14}F_3NO_6S_2$	421.411																192.3		0.2					0.04			KN106		
162	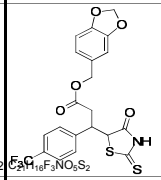 $C_{21}H_{16}F_3NO_5S_2$	483.481																		0.16								KN107		
163	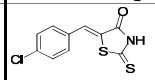 $C_{10}H_6ClNOS_2$	255.744						0.28			0			0									0					Cop37		Cop
164	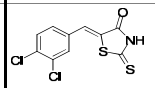 $C_{10}H_5Cl_2NOS_2$	290.189						0.4			0			0									0					Cop23		Cop
165	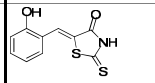 $C_{10}H_7NO_2S_2$	237.298						0.1			0			0							0							Cop11		Cop

			DVL1PDZ			DVL3PDZ			PSD95-1			PSD95-2			PSD95-3			AF6PDZ			Shank3_PDZ			a-SynPDZ		Biological data IC50		Vendor & Ids		
CdId	Structure	Mol Weight	KD_NMR	KD_ITC	CSP	KD_NMR	KD_ITC	CSP	KD_NMR	KD_ITC	CSP	KD_NMR	KD_ITC	CSP	KD_NMR	ITC	CSP	KD_NMR	KD_ITC	CSP	KD_NMR	KI_FP	CSP	KD_NMR	CSP	Wnt3a_inhib	Cyto_tox	Nestor-ID	Vendor_ID	V_name
166	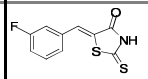 $C_{10}H_8FNOS_2$	239.289						0.01			0			0									0					Cop14		Cop
167	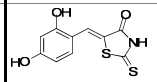 $C_{10}H_7NO_3S_2$	253.297						0.01			0			0									0					Cop12		Cop
168	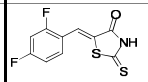 $C_{10}H_5F_2NOS_2$	257.28						0.01			0			0									0					Cop30		Cop
169	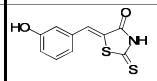 $C_{10}H_7NO_2S_2$	237.298						0.04			0			0									0.05					Cop10		Cop
170	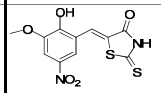 $C_{11}H_8N_2O_5S_2$	312.322						0			0	199.1		0.2									0					KN103		
171	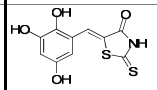 $C_{10}H_7NO_4S_2$	269.297						0			0			0.07									0.03					KN100		
172	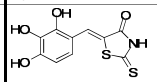 $C_{10}H_7NO_4S_2$	269.297						0			0			0.1			0.04											KN102		
173	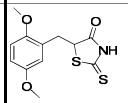 $C_{12}H_{13}NO_3S_2$	283.367						0						0.06														KN54		